DOCTORAL THESIS

Synthesis and Applications of Low Silica Zeolites from Bolivian Clay and Diatomaceous Earth

J. Gustavo García Mendoza

Chemical Technology

LULEÅ UNIVERSITY OF TECHNOLOGY

Synthesis and applications of low silica zeolites from Bolivian clay and diatomaceous earth

J. Gustavo García Mendoza

Chemical Technology

Department of Civil, Environmental and Natural Resources Engineering

Luleå University of Technology

SE - 971 87

Sweden

June 2017

Printed by Luleå University of Technology, Graphic Production 2017

ISSN 1402-1544
ISBN 978-91-7583-892-2 (print)
ISBN 978-91-7583-893-9 (pdf)

Luleå 2017

www.ltu.se

ABSTRACT

The aim of the present work was to develop synthesis routes to produce synthetic zeolites with industrial attractiveness from inexpensive Bolivian raw materials, such as clays and diatomite. The work was focused on the synthesis of low-silica zeolites with the LTA and FAU structures but some work was also devoted to the high silica zeolite ZSM-5. The raw materials as well as intermediate and final zeolite products were characterized by general techniques including scanning electron microscopy, X-ray diffraction, nitrogen adsorption and inductively coupled plasma mass spectrometry. In addition, the key properties for the intended applications, i.e. brightness for LTA zeolite and dynamic CO_2 adsorption data for FAU-type zeolite were evaluated for detergents and adsorbent applications, respectively.

The first part of this study deals with the synthesis of low silica zeolite A from Bolivian montmorillonite clay (Paper I). The clay was fused at high temperature with NaOH to render the material more reactive. Sodium aluminate was added to the mixture to decrease the SiO_2/Al_2O_3 ratio. An optimization of the synthesis time was performed. For the sake of comparison, the same treatment was applied to commercial kaolin. The final zeolite product from Bolivian montmorillonite exhibited high brightness despite the presence of iron in appreciable amount in the starting material and the final product. It was concluded that magnesium, present in the raw material, exerted a masking effect on iron. The latter was incorporated into extraneous magnesium aluminosilica compounds, thereby increasing brightness and strongly decreasing the yellowness of the final product. This simple method appears as a promising alternative to the complex and costly techniques suggested to reduce the iron content in natural raw materials, especially kaolin.

The second part of the study addresses the synthesis, characterization and evaluation of FAU-type zeolites from diatomite and chemical grade reagents, respectively. With regard to the synthesis of zeolite Y, the diatomite was leached in sulfuric acid to remove impurities prior to synthesis. This step also resulted in dealumination, which enabled the synthesis of the high silica zeolite ZSM-5 (Paper II). However, extra aluminum had to be added for the synthesis of zeolite Y (Paper III). In this case, the raw materials were reacted hydrothermally and parameters such as the Na_2O/SiO_2 ratio and synthesis time were investigated. The work

showed that it was possible to prepare micron-sized crystals of zeolite Y with a SiO_2/Al_2O_3 ratio of 3.9 at a Na_2O/SiO_2 ratio of 0.9. Also, zeolite Y with a SiO_2/Al_2O_3 ratio of 5.3 was achieved, however with low yield, at a Na_2O/SiO_2 ratio of 0.6. It was shown that diatomite behaved similarly to colloidal silica in traditional syntheses, both sources having in common a high degree of polymerization. Zeolite Y with a SiO_2/Al_2O_3 ratio of 5.3 might be useful for the production of ultra-stable zeolite Y for use as FCC catalyst. Addition of NaCl to this system was also found to completely inhibit the formation of zeolite P and to reduce the risk of overrunning by a synergic effect of Na and Cl ions (Paper IV).

Finally, zeolite X films were grown on steel nonporous monoliths and evaluated as adsorbent for CO_2 (Paper V). Adsorbents with film thicknesses of 3 and 11 μm supported on steel monoliths of 1600 cells per square inches were prepared. The structured adsorbents showed the expected CO_2 adsorption capacity and the CO_2 breakthrough fronts were very sharp. This illustrates the potential of zeolite NaX coated steel monoliths as promising alternatives to traditional adsorbents.

To summarize, zeolites with promising characteristics for detergents, catalysts and adsorbents were successfully synthesized from Bolivian raw materials in this thesis work. However, further characterization is required to qualify these products for industrial applications. This study might help the development of poor regions of the Bolivian Altiplano and open up for large scale production, since the methods developed in this work are simple and non-expensive.

ACKNOWLEDGMENTS

My sincere gratitude to my main supervisor Assoc. Prof. Johanne Mouzon, who expertly guided me through my graduate education, his unwavering enthusiasm for research as well as his personal generosity helped make my time in Luleå memorable. I would like to thank to Prof. Jonas Hedlund for giving me the opportunity to be part of his group and for his valuable recommendations and the contributions to this work. Also, I would like to express my deep gratitude to Dr. Saúl Cabrera, for his advice, guidance and friendship which have been priceless. Prof. Marta-Lena Antti, Dr. Rodny Balanza and Eng. Mario Blanco are also acknowledged for all their help during this time.

This dissertation would not have been possible without the collaboration from The Swedish International Development Cooperation Agency (SIDA).

I am also indebted to all friends and colleagues at Chemical Technology, not only for all their useful suggestions but also for the pleasant atmosphere, with special regard to the Zeolite group and the people who was part of the group as well including Ariana, Edgar, Wilson, Lidia and Edwin; I am taking a lot of priceless memories from all of you with me.

I would also like to thank all of my friends in Luleå and in La Paz with special regard to my research group IGN at my home University for their motivational words to strive towards my goal.

A mis papás y hermanos, por su aliento y apoyo incondicional en cada momento de mi vida. A mis segundos papás y hermano por cuidar de mi familia en mi ausencia. A mi amada esposa Laura por la inspiración, el apoyo y ánimo constante durante éste proceso. A mi personita favorita, mi pequeña Natalia, mi persona favorita y más amada, a ambas, gracias por su paciencia y amor, a quienes voy a dedicar mi vida.

LIST OF PAPERS

This doctoral thesis is based on the work reported in the following papers:

Paper I

Preparation of zeolite A with excellent optical properties from clay

Gustavo García, Wilson Aguilar, Ivan Carabante, Saúl Cabrera, Jonas Hedlund, Johanne Mouzon

Journal of Alloys and Compounds 619 (2015) 771–7

Paper II

Comparison between leached metakaolin and leached diatomaceous earth as raw materials for the synthesis of ZSM-5

Wilson Aguilar, Gustavo García, Johanne Mouzon, Jonas Hedlund

SpringerPlus 2014, 3:292

Paper III

Synthesis of zeolite Y from diatomite as silica source

Gustavo García, Saúl Cabrera, Jonas Hedlund, Johanne Mouzon

Microporous and Mesoporous Materials 219 (2016) 29 – 37

Paper IV

Influence of NaCl in the synthesis of FAU-type zeolites

Gustavo García, Saúl Cabrera, Jonas Hedlund, Johanne Mouzon

Submitted to Journal of Crystal Growth

Paper V

Zeolite coated steel monoliths for carbon dioxide separation

J. Mouzon, G. García, R.S. Luciano, E. Potapova, M. Grahn, D. Korelskiy, and J. Hedlund

To be submitted

My contribution to the papers included in the thesis:

PAPER I. Most of the experimental work and most of the evaluation and writing.

PAPER II. Some of the experimental work and little of the evaluation and writing.

PAPER III. All the experimental work and most of the evaluation and writing.

PAPER IV. All sample preparation and characterization of physical properties, most of the evaluation and writing.

PAPER V. Most of the experimental work, some of the characterization and evaluation.

Other publications from the author not included in the doctoral thesis:

Characterization and catalytic evaluation of aluminum oxides obtained by the atrane route

Gustavo García, Marisa Falco, Pedro Crespo, Saúl Cabrera, Ulises Sedrán

Catalysis Today 166 (2011) 60–66

The production of porous brick material from diatomaceous earth and Brazil nut shell ash

Escalera E., García G., Terán R., Tegman R., Antti M-L., Odén M.

Construction and Building Materials (2015) 98, 257–264.

CONTENTS

“I am as bad as the worst, but,

thank God, I am as good as the best.”

— Walt Whitman

CHAPTER 1 INTRODUCTION

1.1. Background

Non-metallic minerals, or industrial minerals that are not primarily a source of metal production, show great diversity in composition, property and physical/chemical behaviors, all of which are responsible for their tremendous range of industrial applications and end uses. Sand, limestone, marble, salt, clay and natural zeolites are some examples of non-metallic minerals.

Natural zeolites can be found as minerals in huge quantities. However, due to the high requirements on purity and uniformity of particle size, they have limited industrial applicability. On the other hand, synthetic zeolites are used in large quantities in many industrial applications [1]. Industrial methods for synthesizing zeolites usually involve use of chemical grade reagents as starting materials and crystallization from a gel or clear solution under hydrothermal conditions. Nevertheless, preparation of synthetic zeolites from chemical reagent-grade sources of silica and alumina is costly.

The cost-effect concern has called the attention of researchers to seek cheaper raw materials for zeolite synthesis; many studies have focused their attention to the use of low cost aluminosilicate raw materials in order to reduce costs of the final zeolite products. Non-metallic minerals such as clays and diatomites can serve as aluminosilica sources for the production of synthetic zeolites with an adapted pre-treatment procedure.

Zeolites are used in huge quantities in a large number of industrial applications. For instance, zeolite A is used as a softener in phosphate free detergents (20-25 % of detergent composition [2]). This is the largest application (in tons) of any zeolite and thus represents a huge market. Zeolite Y is used in the fluid catalytic cracking (FCC) process in oil refineries to convert heavy feedstock's to gasoline. This is the largest application of a zeolite as catalyst. Zeolites A and X are also used for gas drying in the industry.

Bolivia is a country with important non-metallic mineral resources distributed in the whole territory, but the most important geological provinces are the occidental mountain range and the Altiplano. However, the industrial use of these mineral resources has been limited and the

use of new technologies has not been implemented except some small factories of structural ceramics.

The conversion of Bolivian clays, feldspars and diatomaceous earth to the valuable zeolites A, Y and X consequently represents a potential major income for some regions of Bolivia.

1.2. Scope of the present work

In order to reach this objective, the scope of the present work was:

- To develop synthesis routes to obtain low silica zeolites (i.e. zeolite A, zeolite X and Y) from Bolivian raw materials (clay, diatomite).
- To evaluate the properties of the as-synthesized zeolites for intended future applications.
- To find innovative applications for future use of these zeolites, such as structured adsorbents for CO_2 removal.

The following introductory sections describe general aspects of the molecular sieve zeolites, focusing on zeolite structures, synthesis and properties. Also, particular emphasis on zeolite synthesis from natural raw materials is brought up. In addition, the various uses of zeolitic materials in industrial and potential innovative application are presented.

1.3. Zeolites

Zeolites are inorganic crystalline aluminosilicates with a network of pores classified as microporous materials (pore size < 2 nm). In recent years, the class of zeolites and related microporous materials has been greatly expanded. These materials are of particular interest, both in the industry and in academia, due to their large variety of properties and areas of applications. These applications are growing continuously spanning from adsorption and separation to heterogeneous catalysis, and, nowadays, also in green chemistry [3]. Considerable progress has been made in this dynamic field of research, with an emphasis on understanding the interplay of physicochemical properties, such as structure, composition, texture, and morphology, with the corresponding properties and behavior in the applications. Consequently, perspectives for new applications can be based on a rational material design.

Zeolites are highly porous and crystalline aluminosilicate compounds with different pore configurations comprising frameworks of $[SiO_4]^{4-}$ and $[AlO_4]^{5-}$ tetrahedrons with shared oxygen atoms. An empirical formula representative of a zeolite can be expressed in the following way:

$$M_{x/n}[(AlO_2)_x(SiO_2)_y] \cdot wH_2O$$

where M is an extra-framework cation (alkaline or alkaline earth metal) of valence n; y/x represents the SiO_2/Al_2O_3 ratio of the zeolite and w is the number of water molecules.

The physical and chemical properties of zeolites are influenced by the Si/Al ratio. A low ratio causes the surface to become more hydrophilic (having a strong affinity for water) as well as a stronger interaction with polar molecules. According to the International Zeolite Association (IZA) Structure Commission, zeolites can be categorized in relation to the Si/Al ratio; i.e. low silica zeolites (Si/Al = 1-2), medium silica zeolites (Si/Al = 3-10) and high silica zeolites (Si/Al = 10-∞) [4]. Zeolite structures are assigned a three-letter code by IZA Structure Commission, e.g. LTA for Linde Type A (Linde Division, Union Carbide) for zeolite A, FAU (Faujasite) for zeolite X and Y and MFI for ZSM-5, etc. The main structural difference between zeolites is the size of the pore openings that can vary in the micropore range from ~2 to 13 Å. Factors influencing the size of the pores are the location, coordination and size of the extra-framework cations, i.e. Na^+ substitution by either K^+ or Ca^{2+} cations causes a decrease or an increase of pore aperture in zeolite A, respectively.

In this work, synthesis paths leading to the low silica zeolites with sodium as the main extra-framework cation were studied, i.e. zeolite A and the zeolites X/Y having LTA and FAU framework type, respectively. In addition, high silica zeolite ZSM-5 was also prepared by taking advantage of the purified and dealuminated diatomite with increased SiO_2/Al_2O_3.

In Table 1.1, the main applications of the zeolites investigated in the present work are presented according to the Si/Al ratio.

Table 1.1 Major applications of zeolites of importance for the present work.

Framework code	Zeolite Type	Si/Al ratio	Major application
LTA	Zeolite A	1-1.7	Detergent builder, industrial gas dryer
FAU	Zeolite X	1-1.5	Industrial gas drying, O_2 enrichment of air
	Zeolite Y	1.5-5.6	Fluid catalytic cracking catalyst
MFI	ZSM-5	10-∞	Xylene isomerization
GIS	Zeolite P	~2.2	Cation exchanger

1.3.1. LTA zeolites

Zeolite A is one of the major components in detergents due to its ion exchange properties used to soften water [5]. Zeolite A (LTA) (Figure 1.1) defined by a Si/Al ratio of 1, is a low silica zeolite represented by the following formula: $Na_{12}[(AlO_2)_{12}(SiO_2)_{12}]\cdot 27H_2O$. The crystal structure is cubic with a lattice parameter of 12.32 Å. Zeolite A is characterized by a three-dimensional network consisting of cavities of 11.4 Å in diameter separated by circular openings of 4.2 Å in diameter [6]. It is composed of sodalite cages (Figure 1.1), which are linked via double four-membered rings forming a larger cage, the α-cage. In Figure 1.1, silicon and aluminum atoms are placed at the vertices and connected by lines. Zeolite A possesses excellent properties, such as non-toxicity, high porosity and surface area, relatively good thermal stability and environmental friendliness. Consequently, NaA zeolite (sodium form of zeolite A) is of great industrial importance due to its molecular sieving, ion exchange and water adsorption properties.

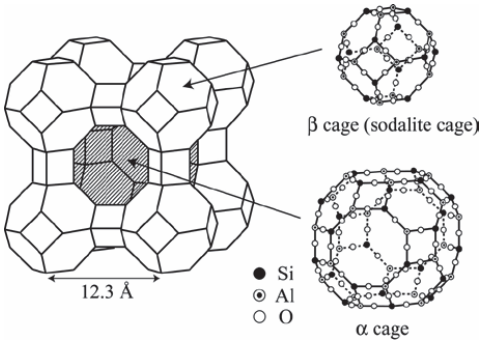

Figure 1.1 Schematic representation of LTA zeolite. Filled circles, open circles and circles with black dots represent Si, Al and O respectively [7].

1.3.2. FAU zeolites

The FAU-type zeolite (Figure 1.2) comprises zeolite X with a Si/Al ratio between 1-1.5 and zeolite Y with a ratio greater than 1.5 [1]. The basic structural units for this type of zeolite are sodalite cages (β-cages) which form supercages (α-cages) able to accommodate spheres up to 1.2 nm in diameter. β-cages are linked together by double six-membered rings (D6R) and form the supercages (Figure 1.2), which have a diameter of 13.0 Å. The structure is composed of perpendicularly intersected equidimensional channels. The openings to these large cavities are 12-membered oxygen rings with a free diameter of 7.4 Å. One of the faujasite-type zeolites is zeolite NaY, which has extensive industrial applications as a catalyst for a variety of reactions [8].

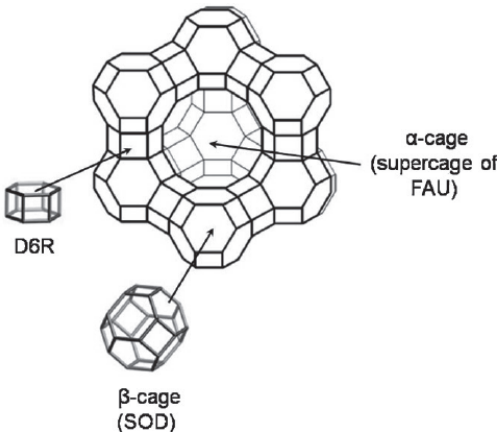

Figure 1.2 Schematic representation of FAU zeolite, the sodalite cages are linked to each other via double six-membered rings forming the supercage; silicon and aluminum atoms are placed at the vertices and connected by lines [9].

1.3.3. ZSM-5 as zeolites

ZSM-5 (MFI), a high silica zeolite, belongs to the pentasil family. It can be synthesized in a wide range of Si/Al ratio varying from 10 to infinity. The structure is composed of a three-dimensional pore system consisting of sinusoidal channels (5.1 x 5.5 Å) and straight channels (5.3 x 5.6 Å) made of 10 member rings, as depicted in Figure 1.3 [10].

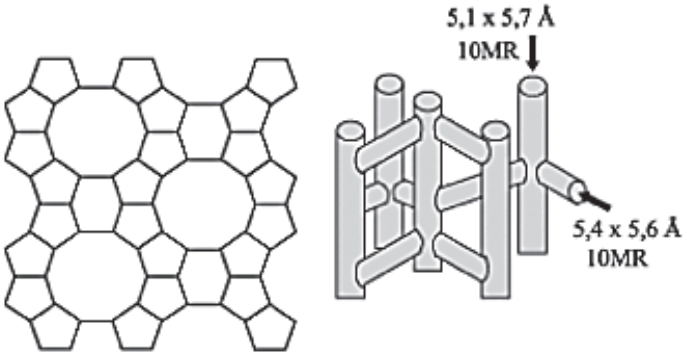

Figure 1.3 Sketch showing the three-dimensional pore system consisting of sinusoidal channels and straight channels in ZSM-5.

ZSM-5 is a well-known acid catalyst having a unique microporous structure that confers shape selectivity, good thermal stability and acidity. Thanks to these properties, ZSM-5 is used widely in the fuel-upgrading and production of petrochemicals [11].

1.4. Zeolite synthesis

Generally, the methods of zeolite production involve dissolving an aluminum source (source of AlO_4^{5-} in the structure) in alkaline media. A silica source (source of SiO_4^{4-} in the structure), and a template if required, is added to the initial solution, forming a slurry that is stirred until a homogeneous gel forms. After aging, the gel is transferred to an autoclave and usually heated to temperatures in the range of 353-473 K for a synthesis time varying from hours to days. Most of the zeolites can be obtained at temperatures < 373 K. However, in order to reduce synthesis time and control the size of the crystals, thermal treatments are often performed at temperatures > 373 K in autoclaves.

The role of each of the aforementioned reactants is summarized in the following table:

Table 1.2 Chemical sources and corresponding role in zeolite synthesis.

Source	Role
SiO_4^{4-}	Primary building unit(s) of the framework
AlO_4^{5-}	Primary building unit(s) of the framework, charge difference origin in the framework
OH^-	Mineralizer and provider of basic media
M (alkali cation), template	Counter-ion of the framework charge, guest molecule, pore stabilizer
H_2O	Solvent, guest molecule inside the framework

The properties of the starting materials used in the reaction mixture are of great importance and influence the properties of the resulting material. Pure chemical grade reagents are mostly used to produce materials which fulfill industrial requirements such as homogeneity and purity. The use of chemical grade reagents renders the synthesis of zeolites expensive. Concerns about energy consumption and production expenses have called the attention of researchers to seek cheaper raw materials for zeolite synthesis [12, 13] to reduce costs.

1.4.1. Natural raw materials

Many studies on the synthesis of zeolites from raw materials such as kaolin, diatomite, bentonite, fly ash, or smectite have been reported [14-16]. Also, additional treatments to improve the synthesis yield of zeolites from natural raw materials by using acid treatment and/or alkali fusion steps were reported. Kaolin is an ideal raw material for preparing NaA zeolite, because it possesses a Si/Al ratio of 1 as in the targeted zeolite. Kaolin has been one of the most versatile industrial minerals and was used extensively for many applications [17]. The synthesis of NaA zeolite from kaolin source has been developed since the 1970s [1, 18] by the hydrothermal reaction of dehydroxylated kaolin (metakaolin) in a sodium hydroxide solution. However, kaolin must be activated by calcination at high temperature to produce metakaolin, an amorphous material that can be easily digested during zeolite synthesis. Therefore, calcination is usually carried out in the temperature range of 773-1273K in order to convert kaolin to metakaolin [19]. However, these treatments increase the cost of zeolite production.

An attractive raw material with high silica content is diatomite, a siliceous biologic sedimentary rock. It contains mainly amorphous silicon oxide derived from biogenic siliceous sediments (unicellular algae skeletons, frustules) and is available in bulk quantities at low cost [20]. Being amorphous and silica rich, diatomite does not require any additional heat treatment or silica source, both of which representing additional costs for use in the synthesis of FAU-type zeolites [18].

Another interesting raw material rich in Si and Al is montmorillonite, a clay mineral in the sub-group of dioctahedral smectites. This natural aluminosilicate clay is a 2:1 phyllosilicate and has a sheet-type structure. There exist charge deficiencies originated by various Si^{4+} substitutions by Al^{3+} cations, which require the insertion of alkaline cations, alkaline earth cations and water in-between the lamellar interspace. However, natural clays of this type usually contain quartz and do not produce a reactive product such as metakaolin upon calcination.

The heat treatment usually required for metakaolinization can be used with advantage to fuse raw materials containing quartz under the action of the sodium required for zeolite synthesis. It is known that through alkali activation, large amounts of aluminosilicates can be transformed into more soluble species [21].

Diatomaceous earth as well as montmorillonite clay can be found in huge quantities in the Bolivian territory. Figure 1.4 shows the rough geographical location of the raw materials studied in this thesis.

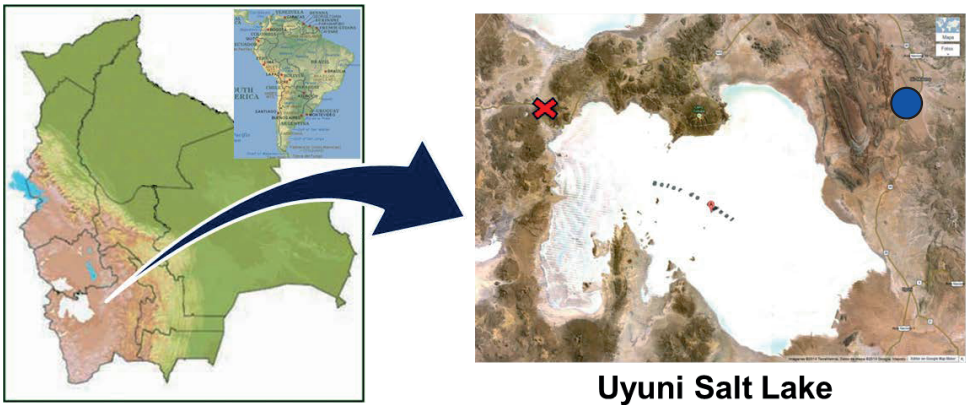

Figure 1.4 Bolivian map and sampling areas where diatomaceous earth (red cross) and montmorillonite clay (blue circle) were sampled.

However, impurities are usually present in natural raw materials. For instance, the occurrence of $CaCO_3$ and Fe as impurities is quite common in diatomite type materials and clays, respectively. Therefore, adequate treatments must be employed for purification [22]. Moreover, potassium, which is known to promote the formation of zeolite P [23], is also common in this kind of raw material meaning that a reduction in potassium content may be required.

1.5. Main applications of zeolites

1.5.1. Ion exchange

As aforementioned, zeolite structures possess negative charges that are compensated by cations and these cations are exchangeable. The use of low silica zeolites as water softener is mainly attributed to this property. Hard water contains Ca^{2+} and/or Mg^{2+} salts, which significantly decrease the surfactant effect of soaps and detergents. To soften the water, the Na^{+} ions present in the zeolite are exchanged with the calcium and magnesium ions present in the water, as described in Figure 1.5. Usually, phosphates are used as builder in household detergents. Due to the increasing awareness about the polluting effect of phosphates, many countries have banned or curtailed the use of phosphates in household detergents. Zeolite A is established as the most suitable substitute for phosphate builder in detergents.

With a molar ratio of Si/Al close to 1, zeolite A contains the maximum aluminum quantity in its framework. As a consequence, it contains the maximum number of cation exchange sites balancing the aluminum framework, and thus the highest cation content and exchange capacity.

$$Ca^{2+} + Na[zA] \longleftrightarrow Ca[zA] + 2Na^{+}$$

Figure 1.5 Schematic representation of the ion exchange process.

The application as detergent builder sets requirements on the zeolite A powder:

- The particle size has to be in the range of 1-10 μm [24] to prevent unacceptable particle deposition and to avoid particle retention in textile fibers.
- A proper morphology of the crystals is required to avoid incrustation; sharp edges in zeolite A crystals can be easily entangled in textile fibers and, in contrast, zeolite A with rounded corners and edges tend to decrease incrustation on textile materials.
- Brightness is another important property of a detergent builder; it has to be at least 90% of the ISO reflectance measured on $BaSO_4$ or MgO.
- Calcium exchange capacity (CEC) must be as high as possible with 510 meq Ca^{2+}/100 g of anhydrous solid being a recommended minimum [5] and 592 meq Ca^{2+}/100 g the highest achievable value at 294 K and for a 1000 ppm Ca^{2+} system [25].

The properties of zeolite A produced from kaolin in terms of CEC, particle size and morphology were found to be adequate for use as detergent builder in previously reported works. However problems associated with brightness and yellowness related to the iron content are usually encountered [26, 27]. Various techniques for removal of iron were investigated such as selective flocculation [28, 29], magnetic separation [30, 31] acid leaching [32, 33], optimum temperature for metakaolinization [34] and chemical treatments [35]. As an example, Chandrasekhar managed to reduce the amount of Fe_2O_3 in the final zeolite product from 0.59% to 0.04% starting with a Chinese kaolin containing 0.69 % Fe_2O_3 by a combination of several treatments, i.e. clay refining, control of alkali concentration, complexing and washing with alkaline water. Significant improvement of the color properties of the final zeolite A were reported, i.e. the brightness increased from 72.9 to 81.7% and yellowness reduced from 11.5% to 7.8% [36]. Nevertheless, these separation procedures represent additional costs to the general process. Simpler methods to achieve the color requirements of detergent builders are therefore needed in order to be able to use natural raw materials for the synthesis of zeolite A.

1.5.2. Catalysis

Zeolite catalysts may sometimes replace environmentally unfriendly catalysts. Typically, zeolite materials yield fewer impurities, have higher capacity, produce higher unit efficiency, and afford higher selectivity. Besides, for an industrial catalyst it is very important to exhibit outstanding thermal stability, which can be provided by the stable structures of zeolites. Unlike the more hazardous acid catalysts that have been used in the past, e.g. solid

phosphoric acid, hydrofluoric acid, etc., zeolites are non-hazardous and can be regenerated [37].

Zeolites may act as a catalyst support or be the functional catalyst themselves. In this way, they are extremely useful in several important reactions involving organic molecules, namely, alkylation, acylation, isomerisations, etc. The industrial sectors where zeolites have made substantial impact as catalysts include petroleum refining, synfuels production and petrochemical production. On the basis of molecular diameter, zeolites can act as shape-selective catalysts due to their ability to promote a diverse range of catalytic reactions including acid-base and metal induced reactions, either by transition state selectivity or by exclusion of competing reactants. The reactions can take place within the pores of the zeolite, which allows a greater degree of product control [38]. Particularly, FAU (Y) and MFI (ZSM-5) are widely used in petroleum refining and production of petrochemicals as catalysts.

Zeolite Y, with a framework topology like the rare zeolite mineral faujasite, has a higher thermal and acid stability over the similar zeolite X. The differences between zeolite X and Y in terms of composition and structure were found to have a striking and unpredicted effect on the properties. Hence, zeolite Y is the most widely employed zeolite catalyst due to its use in the FCC process for the conversion of heavy petroleum molecules into gasoline-range hydrocarbons because of its high selectivity, high concentration of active acid sites, and thermal stability [39, 40].

The properties of importance for the FCC processes, i.e. Si/Al ratio and crystal size of the Y zeolite, can be tailored by an appropriate variation of the synthesis parameters.

1.5.3. Adsorption

Adsorption is the adhesion of ions or molecules from a gas or liquid to a surface. The process creates a film of the adsorbate on the surface of the adsorbent. The adsorption process is commonly described through isotherms, which are the amount of adsorbate trapped by an adsorbent as a function of pressure (if gas) or concentration (if liquid) at a determined temperature.

The most common applications for gas separation by adsorption include H_2 purification, dehumidification of gas streams, hydrocarbon separation, natural gas upgrading and CO_2 removal. Zeolites are among the most widely reported physical adsorbents for CO_2 in the open literature, with zeolite X being the most extensively studied [41]. The structural

characteristics of zeolites for CO_2 adsorption have been extensively reviewed [42]. An important property that influences CO_2 adsorption is the Si/Al ratio, the lower this value is, the higher the adsorption of polar molecules [42]. The pore size of zeolites is another factor that influences the rate of CO_2 adsorption. Clearly, adsorbate molecules can penetrate the interior of the zeolite framework only if the pore size is sufficiently large. Moreover, there is a relationship between the CO_2 adsorption capacity and the zeolite pore size and dimensions of the cavity.

Zeolite NaX adsorbents in the form of pellets and granules (1-10 μm) are used in CO_2 adsorption processes. These zeolites adsorb CO_2 and high adsorption capacity for pellets has been reported for zeolite NaX in several works. At the experimental conditions used in the present work, i.e. a partial CO_2 pressure corresponding to 10% of atmospheric pressure and room temperature, Rodrigues et al. [41] reported a capacity of 2.5 mol CO_2/kg zeolite. However, a much higher capacity of 3.6 CO_2/kg zeolite at 304.4 °C for zeolite NaX powder was reported by Myers et al. [43].

Since the adsorption capacity of zeolite X is high, pellets of this material are used in cyclic gas separation processes, such as pressure swing adsorption (PSA) and temperature swing adsorption (TSA) processes for CO_2 separation. However, currently used adsorbents in the form of packed beds of beads or extrudates suffer from high internal mass transfer resistance in the beads or extrudates and pressure drop in the bed at the high gas velocities that occur at short cycle times. It is possible to reduce these limitations by using non-particulate adsorbent structures, i.e. structured adsorbents such as monoliths (Figure.1.6), laminates, foams and fabric structures [44].

1.5.4. Structured adsorbents

Structured adsorbents have been prepared in our group previously [45, 46]. In these works, zeolite X or ZSM-5 films were grown on cordierite monoliths and evaluated for CO_2 and NO_x adsorption, respectively. Zeolite NaX-coated cordierite monoliths displayed much sharper breakthrough fronts and lower pressure drop than zeolite NaX pellets [47]. A model showed that at very short cycle times, structured adsorbents could even reach higher productivity than pellets although the adsorption capacity was much lower [46]. It was also demonstrated by numerical modeling that the high porosity of the walls in cordierite monoliths had an adverse effect on the breakthrough front. The pores in the monolith result in dispersion by pore filling with CO_2 gas, not adsorption [48]. In contrast to cordierite

monoliths, metal monoliths offer many advantages, such as lower heat capacity and lower pressure drop. Additionally, steel monoliths are nonporous and therefore will display no unwanted pore filling with CO_2. Consequently, the preparation of structured NaX adsorbents using nonporous steel substrates was evaluated in the present work and the CO_2 separation was evaluated by breakthrough experiments. Although pure chemicals were used for the preparation, these structured adsorbents represent a potential future application, for which Bolivian natural raw materials might be used.

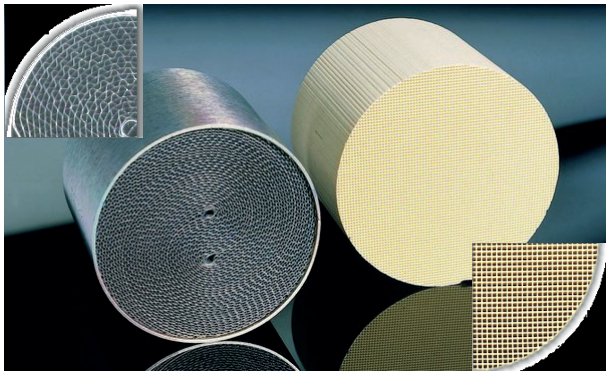

Figure 1.6 Metallic (left) and ceramic (right) substrates [49].

CHAPTER 2 MATERIALS AND METHODS

2.1. Preparation of zeolites synthesized from natural raw materials

2.1.1. Zeolite A synthesis (Paper I)

Montmorillonite clay from the Rio Mulatos (RMA) zone (Potosi, Bolivia) and commercial kaolin (KFA, Riedel de Haën, pro analysis) were used as aluminosilicate sources. Sodium hydroxide was employed in the form of pellets (NaOH, Sigma Aldrich, p.a., ≥ 98%). Anhydrous sodium aluminate in powder form ($NaAlO_2$, Riedel-de Haën, p.a.,) was used to adjust the SiO_2/Al_2O_3 ratio of the synthesis mixtures. Calcium nitrate ($Ca(NO_3)_2 \cdot 4H_2O$, Merck) and magnesium nitrate ($Mg(NO_3)_2 \cdot 6H_2O$, Merck) were utilized to investigate the influence of Ca and Mg on the color properties of alkali-activated kaolin, while ion exchange was carried out with sodium nitrate ($NaNO_3$, Merck). Commercial zeolite A powder (Akzo Nobel) was used as a reference. Barium sulfate ($BaSO_4$, Sigma Aldrich, p.a. 99%) was used as a standard for brightness and yellowness measurements.

The initial SiO_2/Al_2O_3 molar ratio of the RMA clay was 4.9 (see Table 3.1). Hence sodium aluminate was required to adjust this ratio to a suitable value for zeolite A synthesis. $NaAlO_2$ and NaOH provided the aluminum and sodium to set both the SiO_2/Al_2O_3 and Na_2O/SiO_2 ratios. RMA clay was added to sodium aluminate and sodium hydroxide and the mixture was carefully crushed in an agate mortar until a homogeneous powder was obtained. The crushed powder was placed in a platinum crucible and heated at 873 K for 1 hour using a heating rate of 10 K/min. The resultant mixture was crushed again, dispersed in distilled water and stirred for 6 h in an aging step. In the case of kaolin (KFA), the same procedure was used without the addition of sodium aluminate. The molar ratio of the components in the mixtures was $SiO_2/Al_2O_3 = X$, $Na_2O/SiO_2 = 2$ and $H_2O/Na_2O = 40$ with X varying between 2.0 and 1.15. After the aging period, the reaction mixture was transferred to Teflon-lined autoclaves and heated at 373 K for different times in order to identify the optimum time. Subsequently, the autoclave was quenched in cold water to stop the reaction. The solid products were repeatedly washed and filtered in distilled water until pH in the filtrate liquid reached 8-9. The products were dried at 373 K overnight. The prepared samples were denoted according to the type of clay that was used, namely RMA or KFA, followed by the molar SiO_2/Al_2O_3 ratio within brackets and synthesis time, e.g. RMA(2.0)-3h corresponds to a sample obtained

from a mixture with a molar SiO_2/Al_2O_3 ratio of 2.0 using montmorillonite clay from Rio Mulatos after 3 h of synthesis.

2.1.2. Synthesis of ZSM-5 (Paper II)

The raw diatomite was stirred in hydrochloric acid for 150 minutes at 388 K. Subsequently, the suspension was quenched and the acid leached product was filtered and washed with distilled water until the pH value was close to 7. The synthesis mixtures were prepared by mixing the aluminosilicate sources with distilled water, NBA and sodium hydroxide. The molar ratio in the synthesis mixtures were: $Na_2O/SiO_2 = 0.18$; $SiO_2/Al_2O_3 = 33$; $SiO_2/NBA = 7$; $H_2O/SiO_2 = 30$. The mixture was aged under stirring for 24 hours at room temperature and was thereafter hydrothermally heated in Teflon lined stainless steel autoclaves kept for different times in an oil bath at 438 K. After hydrothermal treatment, the solids were recovered by filtration and washed with distilled water until the pH reached a value close to 8. Drying at 373 K overnight and finally calcination at 823 K for 6 hours to remove the template were applied (see Figure 2.1).

2.1.3. Synthesis of FAU-type zeolites (Papers III, IV)

Diatomaceous earth originating from the Murmuntani zone (Potosi, Bolivia) was used as aluminosilicate source. Three different sampling locations were investigated. The corresponding diatomite samples are herein referred to as diatomite 1 (D1), diatomite 2 (D2) and diatomite 3 (D3). Aluminum sulfate octadecahydrate in powder form ($Al_2(SO_4)_3 \cdot 18H_2O$, Riedel-de Haën, p.a., > 99%) was employed to adjust the SiO_2/Al_2O_3 ratio to that of typical syntheses of zeolite Y. The alkalinity of the synthesis mixture was regulated with sodium hydroxide (NaOH, Sigma Aldrich, p.a., ≥ 98%).

The raw diatomites were crushed and dealuminated by two different methods: (a) with 3M HCl in a spherical glass container under reflux conditions in a thermo-stated oil bath maintained at 388 K for 150 min or (b) with 6M H_2SO_4 at 373 K for 24 hours in an autoclave under hydrothermal conditions; the leached products were rinsed with distilled water until the pH in the filtrate was close to 7 and dried overnight [50]. Acid treated diatomite (aD1, aD2, aD3), as well as a suitable amount of $Al_2(SO_4)_3$, were added to NaOH solutions of different concentrations whilst stirring. The molar ratios of the synthesis mixtures were: $Na_2O/SiO_2 = 0.4 – 2.0$; $SiO_2/Al_2O_3 = 11$; $H_2O/Na_2O = 40$. These solutions were aged with stirring at room temperature in glass beakers for 24 hours, and the reaction mixture was then transferred to

Teflon-lined autoclaves and placed in an oven at 373 K for different periods of time and subsequently quenched in cold water. The solid product was separated from the reaction mixture by suction filtering using filter paper grade with a pore size of 1 μm and repeatedly filtered and dispersed in distilled water until the pH of the filtrate liquid was 9. The final solid product was dried in an oven at 373 K overnight and weighed to estimate the yield. Samples were denoted according to the Na_2O/SiO_2 used and the synthesis time, e.g. S0.6-24h corresponds to a sample obtained from a mixture with a molar Na_2O/SiO_2 ratio of 0.6 after 24 h of synthesis.

Finally, the addition of NaCl to the aD1 synthesis system, as well as different salts containing either Na or Cl, was investigated. In this case, the molar composition of the synthesis mixture was: Na_2O/SiO_2 = 1.2; SiO_2/Al_2O_3 = 11; H_2O/Na_2O = 40 and X/Al_2O_3 = 40, where *X* = NaCl, $NaNO_3$, NaF, Na_2SO_4, KCl, NH_4Cl or NH_4OH. A schematic illustration of the zeolite A, ZSM-5 and Y preparation process is depicted in Figure 2.1.

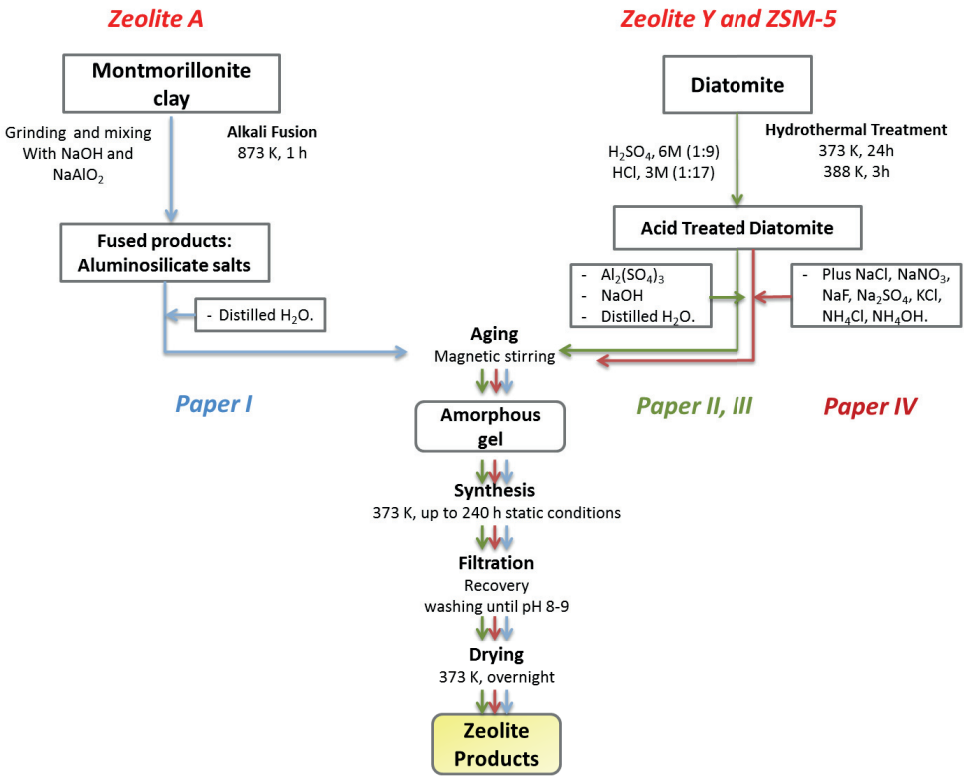

Figure 2.1 Schematic flux diagram of the zeolite synthesis process

2.2. Growth of zeolite NaX on steel monoliths (Paper V)

Cylindrical steel monoliths (Metalit, Emitec, Germany) with a cell density of 1600 cpsi were used as carriers for the structured adsorbents. Photographs of a monolith are shown in Figure 2.2. The weight of each steel monolith used for deposition of zeolite films was recorded prior to growth of zeolite films.

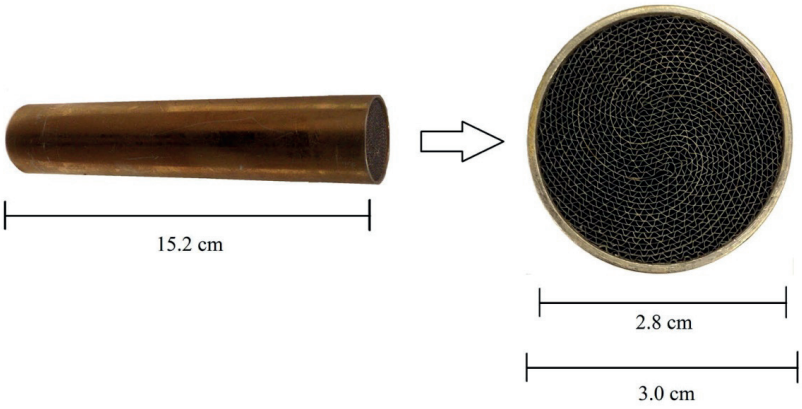

Figure 2.2 Characteristic dimensions of the steel monoliths.

Two types of NaX films with controlled thicknesses, 3 and 11 μm, were grown on the walls of steel monoliths by a seeding method, similarly as described previously by Öhrman et al. [51]. In brief, the monolith was first rinsed with 5% HF for a short time, then with a 0.1 M aqueous ammonia solution and subsequently treated with a 0.4 wt % aqueous solution of a cationic polymer (Redifloc 4150, EKA Chemicals, Sweden) at pH 8 to render the surface positively charged. A 1 wt % aqueous dispersion of zeolite NaX crystals with a diameter of 80 nm was used for seeding. The monolith was treated with the dispersion for 1 h to adsorb a monolayer of the crystals on the surface. The excess of seeds was removed by rinsing with a 0.1 M aqueous ammonia solution. After seeding, zeolite NaX films were grown on the monoliths by hydrothermal treatment in a clear synthesis solution with the molar composition: $73Na_2O:Al_2O_3:8SiO_2:4547H_2O$. The synthesis was performed in a glass reactor immersed in an oil bath kept at 363 K and connected to a reflux condenser. The synthesis was performed in 21 or 70 steps of 65 min each to reach a film thickness of 3 and 11 μm, respectively. After each step, the monolith was rinsed with a 0.1 M aqueous ammonia solution. After synthesis, the samples were rinsed and dried at 623 K in room air, cooled in vacuum and vented with dry nitrogen gas before the weights of the zeolite-coated monoliths

were recorded. The weights of the zeolite films were estimated from the difference of the weight after synthesis and the weight of the carrier material recorded before synthesis.

2.3. General characterization

The morphology of the raw materials and final zeolite products were studied by scanning electron microscopy using a XHR-SEM Magellan 400 instrument. The samples were investigated using a low accelerating voltage and no conductive coating was used. Energy dispersive spectroscopy (EDS, X-max detector 50 mm^2, Oxford Instruments) was also performed to establish the overall composition of the final products and to gain compositional information about individual zeolite crystals and extraneous phases.

The morphology of the zeolite X structured adsorbent was investigated using a Zeiss Merlin field emission scanning electron microscope. Cross sections of the samples were prepared by cooling the sample in liquid nitrogen and immediate fracturing to keep the film unaltered. EDS analysis was carried out at 10 kV using a microinjector in order to mitigate charging by blowing nitrogen gas close to the surface of the samples

In the same manner, to determine the Cation Exchange Capacity (CEC) of the zeolite A samples, the concentration of Na, Mg, Al and Si was measured with the beam scanning a large area of the sample at low magnification (100 times) to avoid diffusion of Na, while the concentration of Ca was measured locally in 10 individual crystals. The number of equivalents-gram was calculated for Ca^{2+} in each case. The total exchange equivalents for Ca^{2+} was assessed by subtracting the amount of equivalents of Ca^{2+} present initially in the powder to the final number of equivalents of Ca^{2+} after the exchanged process.

To determine the chemical composition of the raw materials, final products and the structured adsorbents, inductively coupled plasma-sector field mass spectrometry (ICP-SFMS) analysis was carried out. For this purpose, 0.1 g sample was melted with 0.375 g of $LiBO_2$ and dissolved in HNO_3. Loss on ignition (LOI) was determined by heating the sample to 1273 K.

The mineralogical composition of the raw materials, final zeolite powders, as well as the zeolite X films, were determined by X-ray diffraction (XRD) using a PANalytical Empyrean X-ray diffractometer, equipped with a PixCel3D detector and a graphite monochromator. CuKα1 radiation with λ = 1.540598 Å at 45 kV and 40 mA was used in the 2θ range 5-50° at a scanning speed of 0.026°/s. The diffractograms were compared with the powder diffraction files (PDF) database. Silicon (Merck, p.a., > 99) was used to calibrate the peak position during XRD experiments. The unit cell dimension was determined from the data and used to

estimate the SiO_2/Al_2O_3 ratio in the crystals by assessing the lattice parameter from the (555) reflection of faujasite and using the empirical relationship proposed by Rüscher et al. [52].

$$x = 5.348a_0 - 12.898 \quad (1)$$

where x = Al molar fraction and a_0 = lattice parameter (Å).

Crystallinity of the zeolite products was assessed by calculating the area under the peaks in the 2Θ region after background removal and comparing it to that recorded for commercial zeolite powders; for zeolite Y, the peaks in the 2Θ region *30°* – *32.5°* were used and *6.5°* – *7.5°* for zeolite A. The following formula was used:

$$X - ray\ crystallinity\ (\%) = \frac{\sum Area\ peaks\ sample}{\sum Area\ peaks\ standard} * 100 \quad (2)$$

For zeolite A, brightness and yellowness of the final products were measured on a spectrometer using an integrating sphere (Perkin Elmer Lambda 2SUV/VIS). The results were expressed in percentage of the reflectance obtained for the Ba_2SO_4 powder [53]. Brightness was measured at 457 nm, while the difference between the reflectance measured at 570 and 457 nm yielded a measure for yellowness.

For zeolite Y, nitrogen adsorption data at 77 K was recorded using a Micromeritics ASAP 2010 instrument. Specific surface area was determined by using the Brunauer–Emmett–Teller (BET) method. The micropore volume of the low silica zeolite products was determined by the t-plot method.

$$t = \sqrt{\frac{13.9900}{0.0340 - log\left(\frac{P}{Po}\right)}} \quad (3)$$

A commercial powder of zeolite Y (Akzo Nobel, CBV100L-T) was used as reference sample for comparison of the results obtained by nitrogen gas adsorption and X-ray diffraction.

2.4. Breakthrough profiles

CO_2 breakthrough experiments were carried out using several experimental configurations as illustrated in Figure 2.3. In these experiments, two steel monoliths were mounted in series in a steel column with an inner diameter of 3.2 cm. Graphite tape (Aesseal, Sweden) was

wrapped around the column to seal the gap between the monolith and the column. Glass beads were placed in the bottom of the column, to reduce the dead volume of the conical column entrance. Prior to the experiment, the column was kept at a temperature of 573 K for three hours, with a nitrogen (Linde Gas, 99.99%) flow of 0.2dm^3/min. After cooling, CO_2 breakthrough experiments were conducted at atmospheric pressure and room temperature. For this purpose, a feed comprised of 10% CO_2 in nitrogen (AGA Gas AB, 99.990% CO_2/99.9990% N_2) with a flow rate of 1.00, 0.50 or 0.25 dm^3/min was used. The carbon dioxide concentration in the effluent from the column was measured by an IR 1507 fast response carbon dioxide infrared transducer (CA-10 Carbon Dioxide Analyzer - Sable Systems International, response time 0.5 s). Regeneration of the adsorbent between the adsorption steps was carried by heating the column to 393 K, with a nitrogen flow of 0.2 dm^3/min. Heating rates during activation and regeneration of the adsorbent were 2 K/min and the cooling rates were lower (self-cooling).

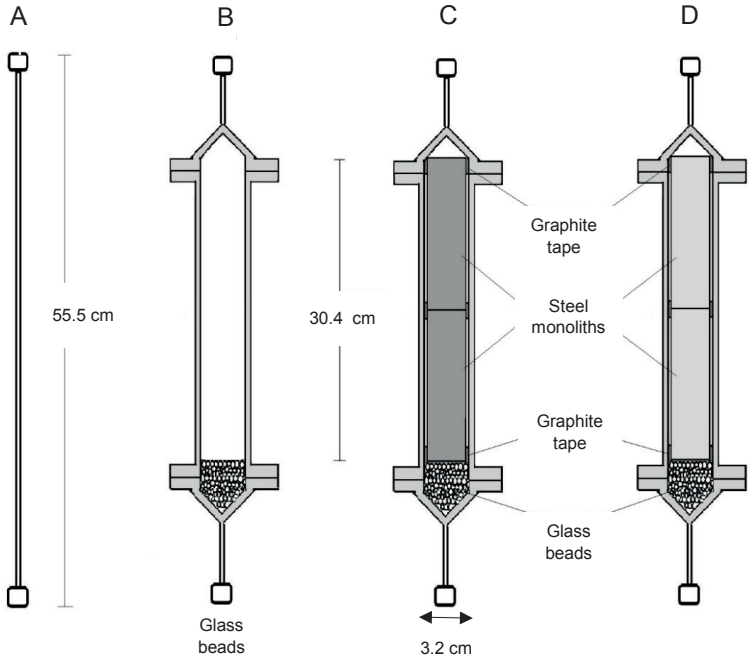

Figure 2.3 Schematic illustrations of the different experimental configurations evaluated for breakthrough experiments: (A) Tube (ID 1.5 mm) with a total length of 555 mm connected to the breakthrough apparatus, (B) column (ID 3.2 cm) with glass beads, (C) column with 2 steel monoliths, graphite tape and glass beads and (D) column with 2 zeolite coated steel monoliths, graphite tape and glass beads.

The experimental setup for breakthrough experiments consisted of a gas feed section, an adsorption column and a gas analysis section, and is schematically shown in Figure 2.4. At time zero, the feed was switched from N_2 to a 0.2, 0.5 or 1 l/min flow of 10% CO_2 in N_2 using a pneumatic actuator (switching time of less than 0.1 s) and the CO_2 concentration was logged by the computer software.

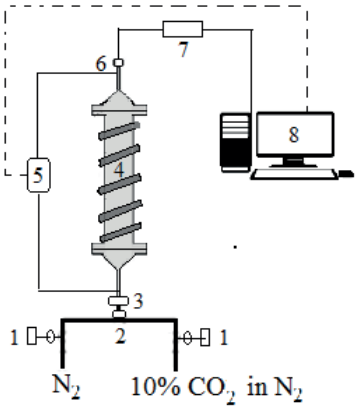

Figure 2.4 Experimental rig for the adsorption experiments; (1) mass flow controller, (2) three-way valve, (3) pneumatic actuator, (4) adsorption column with resistive heating, (5) differential pressure gauge, (6), mass flow meter, (7) CO_2 analyzer, (8) computer.

The CO_2 adsorption capacity q of the zeolite on the monoliths was estimated from the breakthrough data from the time t to reach $C/C_0 = 0.5$ for the coated monoliths and the time t to reach $C/C_0 = 0.5$ for the uncoated monoliths using the simple equation:

$$q = \frac{p_{CO_2} F \left(t^{coated}_{C/C_0=0.5} - t^{uncoated}_{C/C_0=0.5} \right)}{R\, T\, m} \tag{4}$$

In this relation, p_{CO_2} is the partial pressure of CO_2, F is the flow rate, R is the ideal gas constant, T is the temperature of the gas and m is the mass of zeolite in the breakthrough experiment.

CHAPTER 3 RESULTS AND DISCUSSION

3.1. Zeolites synthesized from Bolivian raw materials

3.1.1. LTA from Montmorillonite (Paper I)

3.1.1.1. Montmorillonite and kaolin characterization

The diffractogram of montmorillonite clay (RMA) is presented in Figure 3.1A. The characteristic peaks of montmorillonite at 2θ = 5.9, 19.8 and 35^{o} as compared with PDF patterns can be noticed, but also the occurrence of quartz in low content. Raw kaolin (KFA in Figure 3.1C) contains mostly kaolinite as evidenced by reflections at 2θ = 12.33, 19.80, 20.40, 21.40, 24.81 and 35.11º, but also traces of quartz and muscovite (2θ = 8.83; 35.06). The elemental composition of both clays was determined by ICP-SFMS analysis (Table 3.1). Besides silica and alumina, calcium and magnesium were present in considerable amounts in the montmorillonite in comparison to kaolin. However, both clays contained similar amounts of iron, i.e. 0.79-0.82 wt. % Fe_2O_3.

Table 3.1 Main components of the raw materials.

Material	Main components (wt. %)								Molar ratio
	SiO_2	Al_2O_3	Fe_2O_3	Na_2O	CaO	K_2O	MgO	LOI	SiO_2/Al_2O_3
RMA	63.75	21.95	0.82	0.71	3.19	0.46	4.64	7.20	4.90
KFA	54.43	42.87	0.79	0.13	0.07	1.41	0.30	12.20	2.20

During alkali fusion, montmorillonite and kaolin suffered a structural reorganization. Fused RMA resulted in formation of different sodium aluminosilicates, i.e. Na_2SiO_3, Na_4SiO_4, $NaAlSiO_4$, $Na_2(Si_3O_7)$, $Na_{1.95}Al_{1.95}Si_{0.05}O_4$, as shown in Fig.3.1B and Fig.3.1D, respectively.

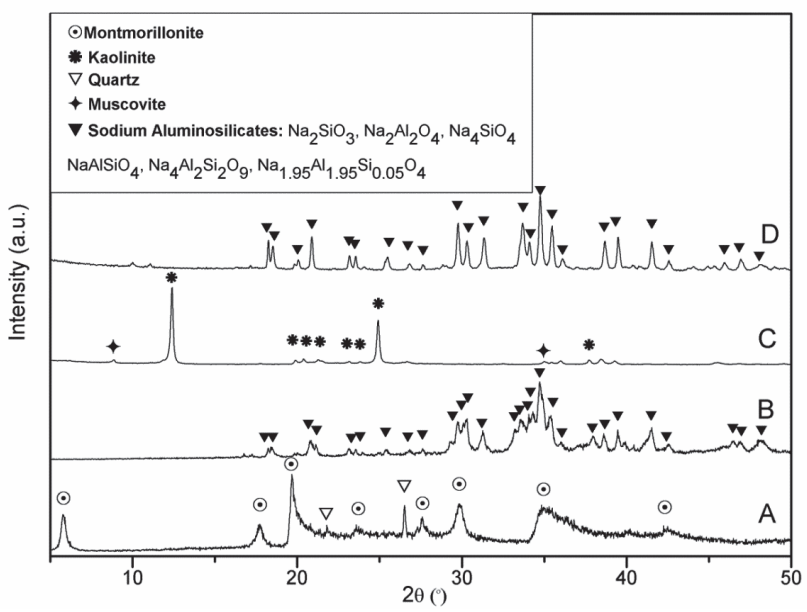

Figure 3.1 XRD diffractograms of: (A) RMA; (B) fused RMA; (C) KFA and (D) fused KFA.

3.1.1.2. Synthesis optimization

Figure 3.2 shows the XRD diffractograms of the final products after hydrothermal treatment at 373 K at different synthesis times. When a molar SiO_2/Al_2O_3 ratio of 2 was used, 3-4 hours of hydrothermal treatment were required to obtain zeolite A as a unique product with high crystallinity for the RMA and KFA clays (see RMA(2.0)-3h and KFA(2.0)-4 in Figure 3.2). Significant amounts of amorphous material in the samples were present if shorter synthesis times were used (RMA(2.0)-2h and KFA(2.0)-3h in Figure 3.2). Table 3.2 shows the overall SiO_2/Al_2O_3 ratios of the final products determined by EDS. RMA(2.0)-3h was found to contain an excess of silica with a SiO_2/Al_2O_3 ratio of 2.36 compared to the ideal ratio of 2.0. Therefore, the molar SiO_2/Al_2O_3 ratio in the RMA synthesis mixture was varied in the range 1.15-2.0. Decreasing this ratio from 2 to 1.8 resulted in a slight decrease of the SiO_2/Al_2O_3 ratio in the product to 2.22, see RMA(1.8)-3h in Table 3.2 and also Figure 3.2. However, it was not possible to lower the ratio in the product further by increasing the amount of aluminum in the synthesis mixture. Instead, this resulted in a steady decrease in crystal size, while the SiO_2/Al_2O_3 ratio in the product was almost constant. The RMA sample prepared with a molar SiO_2/Al_2O_3 ratio of 1.8 were also mainly amorphous for synthesis times shorter than 3 h, e.g. RMA(1.8)-2h in Figure 3.2.

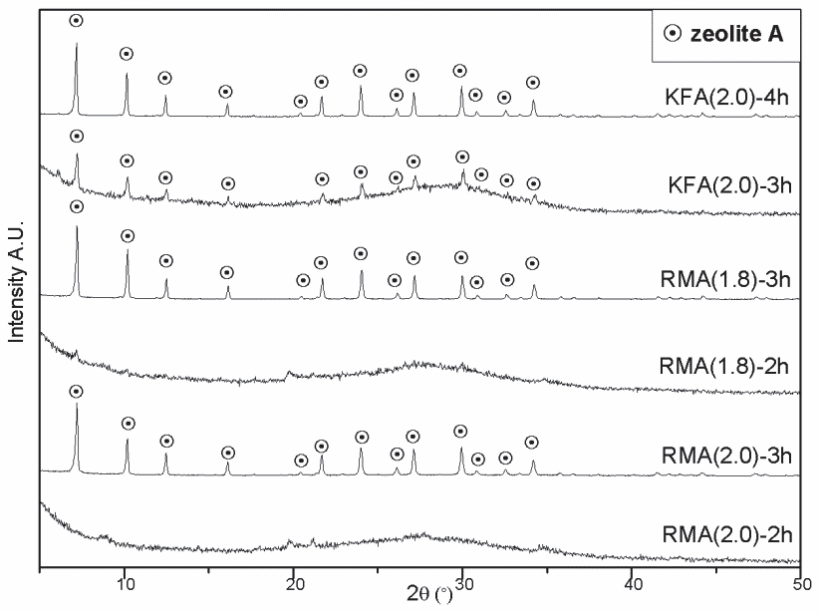

Figure 3.2 XRD diffractograms of the following samples: RMA(2.0)-2h; RMA(2.0)-3h; RMA(1.8)-2h; RMA(1.8)-3h; KFA(2.0)-3h and KFA(2.0)-4h.

Table 3.2 Compositional ratios in the final products determined by EDS.

Sample	Ion exchange	SiO_2/Al_2O_3	Na/Al	2Ca/Al	2Mg/Al	(Na+2Ca)/Al
commercial	-	2.08	0.99	n.d.	n.d.	0.99
RMA(2.0)-3h	-	2.36	0.87	0.11	0.18	0.98
RMA(1.8)-3h	-	2.22	0.90	0.12	0.19	1.02
RMA(1.8)-3h	Na	2.28	0.93	0.03	0.18	0.96
KFA(2.0)-4h	-	2.22	0.97	0.01	0.01	0.98
KFA(2.0)Mg-4h	-	2.16	0.99	n.d.	0.16	0.99
KFA(2.0)Mg-4h	Na	2.28	0.98	0.01	0.16	0.99

n. d. (non-detected)

3.1.1.3. Size and morphology of the final zeolite products

SEM micrographs of RMA(1.8)-3h, KFA(2.0)-4h and commercial zeolite A are shown in Figure 3.3.

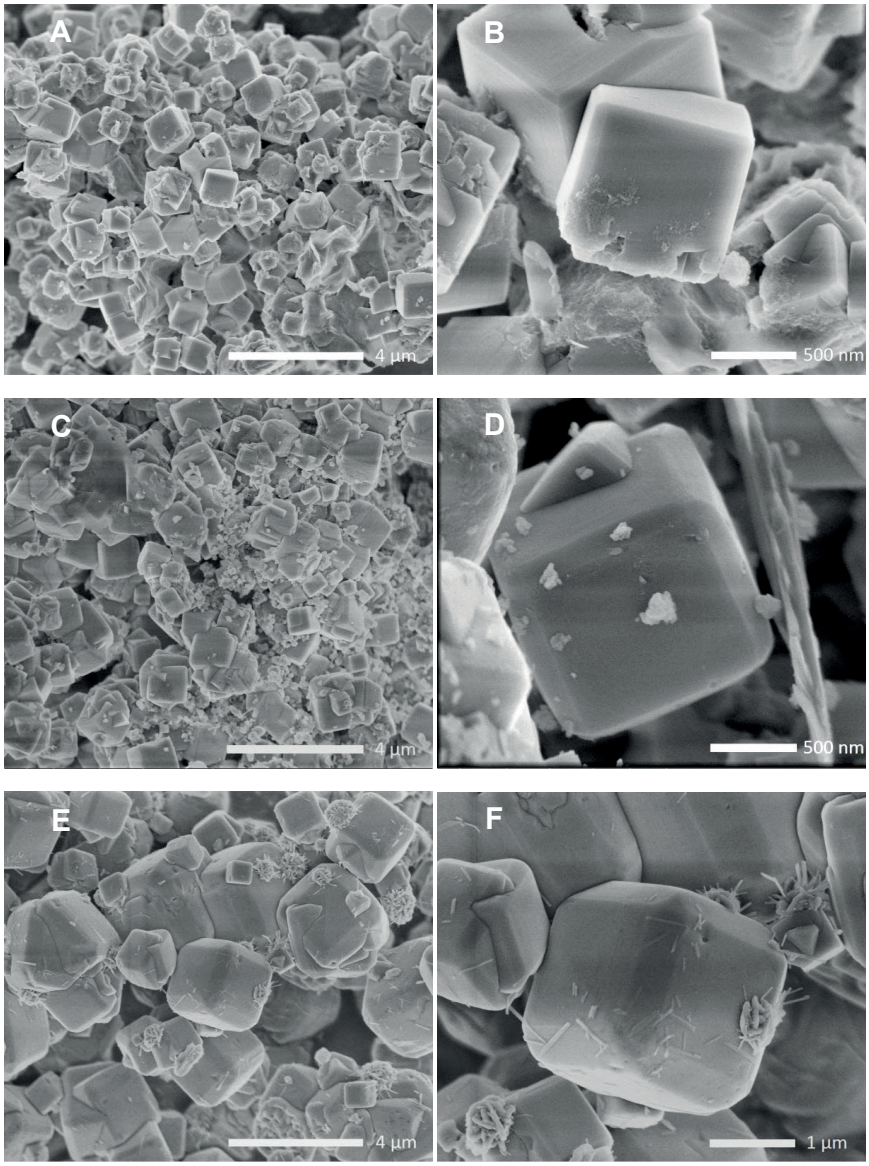

Figure 3.3 SEM micrographs of: (A)-(B) RMA(1.8)-3h; (C)-(D) KFA(2.0)-4h; (E)-(F) commercial zeolite A.

As shown in Figure 3.3A, RMA(1.8)-3h consisted of cubic crystals ranging between 0.5-1.5µm in length. Some crystals exhibited intergrowth, which is usually rationalized by a high concentration of nuclei [54]. Figure 3.3B reveals that the largest crystals possessed chamfered edges, which is favorable for detergent grade zeolites. KFA(2.0)-4h zeolite crystals showed similar characteristics, except for a slight increase in length to approximately 1-2 µm (Figure 3.3 C and D). Comparatively, the crystals in the commercial powder were found to measure between 1 and 7 µm in length and to be relatively intergrown (Figure 3.3 E and F).

3.1.1.4. Brightness measurements

Brightness and yellowness measurements performed on RMA(1.8)-3h, KFA(2.0)-4h and commercial zeolite A are shown in Table 3.3. With 94.5% brightness and 3.0% yellowness, the sample obtained from montmorillonite after optimal synthesis time (RMA(1.8)-3h) exhibited outstanding optical properties, which were superior to those of the commercial powder (92.6% brightness and 3.8% yellowness). In contrast, the sample obtained from kaolin was slightly orange to the naked eye. Accordingly, low brightness and relatively high yellowness values were obtained for KFA(2.0)-4h (Table 3.3), i.e. 76.4% and 14.4%, respectively. These values are typical of zeolite A powder synthesized from metakaolin. Therefore, the alkali fusion method to activate kaolin did not seem to influence the final color of the zeolite A powder.

Table 3.3 Brightness and yellowness properties.

Sample	Brightness	Yellowness
Commercial powder	92.6	3.8
RMA(1.8)-3h	94.5	3.04
KFA(2.0)-4h	76.4	14.4
KFA(2.0)Ca-4h	73.7	11.5
KFA(2.0)Mg-4h	82.1	5.4
KFA(2.0)MgCa-4h	85.6	5.2

Usually, the poor brightness and yellowness of zeolite A powders synthesized from kaolin are attributed to the formation of colored iron precipitates (e.g. iron(III) hydroxide) during the aging step and the crystallization process [55]. The iron content

was found to be 0.44 and 0.54 wt. % by ICP-SFMS in the RMA(1.8)-3h and KFA(2.0)-4h samples, respectively. Although these amounts were similar and both samples were synthesized by the same method, the corresponding final zeolite products showed very different optical properties in terms of brightness and yellowness.

According to the values given in Table 3.1, the major compositional difference between the two raw materials investigated in this work was the high content in calcium and magnesium in montmorillonite clay. These elements were still present in appreciable amounts in the final products as shown by the EDS results in Table 3.2. Therefore, the difference in optical properties was first attributed to a positive effect of one of these (or both) elements. In order to test this hypothesis, amounts of calcium and magnesium similar to those present in montmorillonite clay were added to the synthesis mixture based on kaolin clay before alkali fusion using nitrates. Three new products were obtained and denoted KFA(2.0)Ca-4h, KFA(2.0)Mg-4h and KFA(2.0)MgCa-4h depending on whether only calcium or magnesium or both elements were added, respectively. According to the XRD patterns (Figure 3.4A), these new products consisted of zeolite A with minor contents of sodalite (~ 5%). Based on the SEM results in Figure 3.4B, C and D, these samples exhibited similar morphologies and consisted of cubic crystals with rounded edges ranging between 0.75-1.5µm in length with a few intergrown crystals. The presence of small amounts of flower shaped crystals was attributed to sodalite. The results in Table 3.3 showed that the addition of solely calcium slightly improved yellowness. Interestingly, addition of magnesium to kaolin before alkali fusion remarkably enhanced the optical properties of the final powder, independently of whether calcium was added or not. The corresponding brightness and yellowness values were higher than those obtained by Chandrasekhar and colleagues [22], who employed a complex combination of chemical treatments to reduce the amount of Fe_2O_3 in the final zeolite product to 0.04 wt. %.

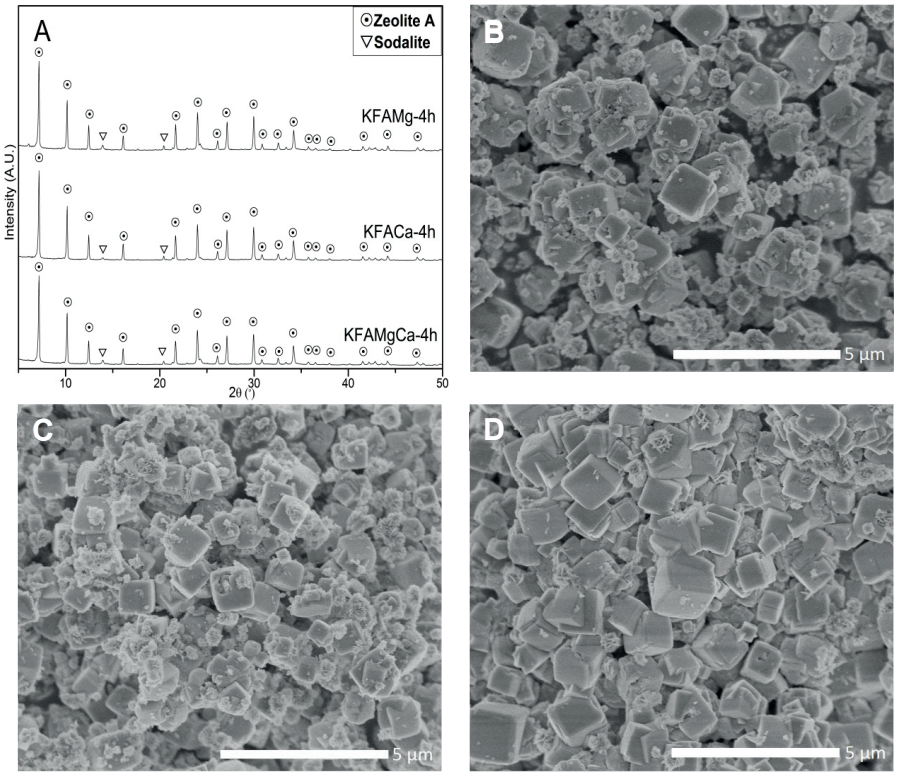

Figure 3.4 (A) XRD diffractograms of the final products obtained from KFA after 4 h of synthesis with addition of Ca, Mg and Ca-Mg and SEM micrographs showing: (B) KFA(2.0)Ca-4h; (C) KFA(2.0)Mg-4h and (D) KFA(2.0)MgCa-4h.

3.1.1.5. Cation Exchange Capacity

As shown in Table 3.2, the commercial zeolite A and KFA(2.0)-4h samples were completely in sodium form, as evidenced by the Na/Al ratios, which were estimated to be 0.99 and 0.97, respectively. However, the as-synthesized samples obtained by alkali fusion of montmorillonite clay were not completely in sodium form but also contained calcium ions that occupied approximately 11-12% of the sites. With regard to cation exchange capacity (CEC), 84% of the exchangeable sites of zeolite A can be compensated by Ca^{2+}cations at 294 K, which represents 592 meq Ca^{2+}/100g anhydrous solid. Considering the final SiO_2/Al_2O_3 and 2Ca/Al ratios measured by EDS on the RMA(2.0)-3h and RMA(1.8)-3h samples, maximum CEC values of 480-487 meq

Ca^{2+}/100g anhydrous solid could be anticipated for these samples. As a matter of fact, loss-on-ignition and ICP-SFMS measurements on the calcium ion exchanged RMA(2.0)-3h sample yielded a value of 487 meq Ca^{2+}/100g anhydrous solid. The RMA(1.8)-3h sample was ion exchanged with sodium nitrate to verify that the calcium ions were exchangeable. As shown in Table 3.2, the 2Ca/Al ratio was reduced from 0.12 to 0.03, which showed that this was the case.

To reflect the validity of the quantitative EDS method developed in the current work, it is important to remark that all samples investigated in Table 3.2 showed (Na+2Ca)/Al ratios very close to 1.0. This reflects the validity of the quantitative EDS method developed in this work. It was found to be more reliable than ICP-SFMS because of the large error margin of the latter, which brought too much uncertainty on the elements present in large amounts.

The results in Table 3.2 indicate that, in contrast to calcium, magnesium was not ion-exchanged by sodium when exposed to a solution of sodium nitrate, which was consistent with the fact that solvated magnesium ions can barely diffuse into zeolite A. In addition, the fact that all values of the (Na+2Ca)/Al ratio were close to 1 strongly suggest that magnesium was not located inside zeolite A. As a matter of fact, Mg could not be detected by local EDS inside zeolite A crystals. This is illustrated by the EDS spectrum of Figure 3.5B, which was obtained by point analysis in a zeolite A crystal, i.e. the encircled region in Figure 3.5A. Instead, Mg and Fe were found to be concentrated in the extraneous material consisting of platelets and finely divided matter as revealed in the region delimited by the rectangle in Figure 3.5A and the corresponding EDS spectrum in Figure 3.5C. Consequently, our data demonstrate that magnesium exerts a masking effect on iron by incorporating the latter inside magnesium aluminosilicate compounds with low coloration. This simple method appears as a promising alternative to complex and costly techniques developed in order to reduce the iron content in natural raw materials.

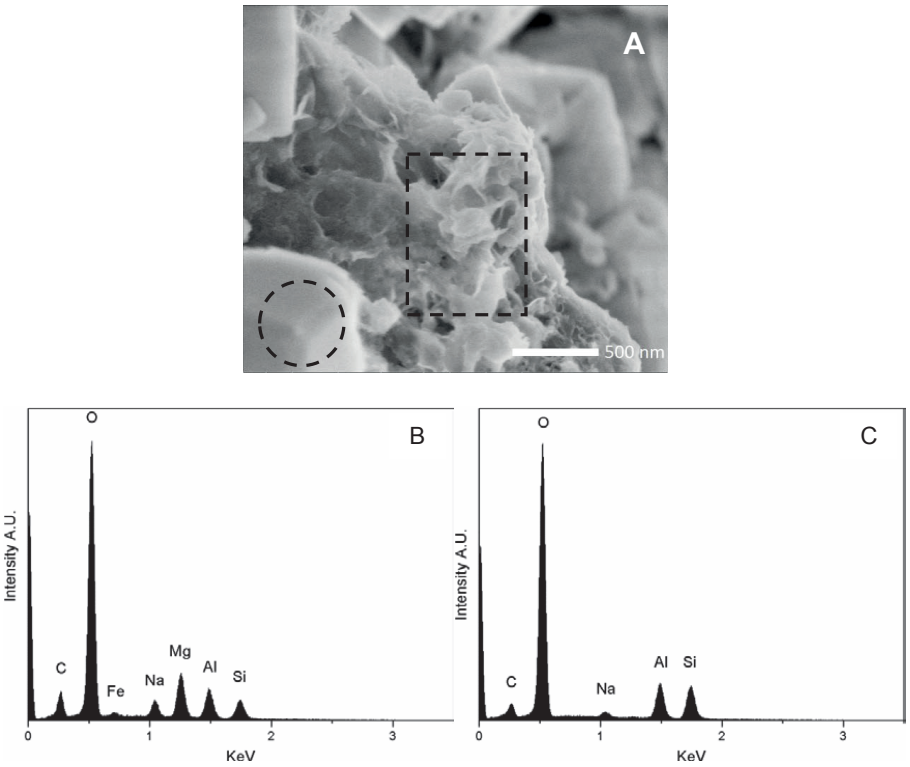

Figure 3.5 (A) SEM micrograph showing the extraneous matter in RMA(1.8)-3h; EDS analysis of: (B) extraneous matter (dotted square in A) and (C) a zeolite A crystal (dotted circle in A).

3.1.2. ZSM-5 synthesis from diatomaceous earth (Paper II)

To enable controlled synthesis of ZSM-5 and FAU-type zeolite from diatomite, a purification and dealumination process of diatomite using a mineral acid was performed. The effect of sulfuric and hydrochloric acids was compared. The ICP results for the dealumination process of diatomite with sulfuric acid and hydrochloric acid are presented in Table 3.4. It is evident that the differences in concentration of the main components do not differ appreciably with the exception of Ca. Removal of potassium was particularly desirable, as it is known to favor the formation of zeolite P, as a secondary phase. The high amount of Ca can be attributed to the sampling location and the occurrence of calcium minerals.

Table 3.4 Compositions (in mol %) of diatomaceous earth and leached diatomaceous earth by ICP-SFMS.

	SiO_2	Al_2O_3	Fe_2O_3	Na_2O	CaO	K_2O	MgO	SiO_2/Al_2O_3
D2	78.59	5.21	0.22	6.76	4.43	1.28	3.29	15.1
aD2 H_2SO_4	93.92	2.05	0.03	0.30	2.14	0.27	0.24	45.7
aD2 HCl	96.40	2.17	0.06	0.35	0.49	0.33	0.19	44.0

The aD2 HCl raw material was successfully used for the synthesis of ZSM-5 without the addition of extra source of neither silica nor alumina, since the SiO_2/Al_2O_3 ratio obtained after acid leaching was appropriate for ZSM-5 synthesis (SiO_2/Al_2O_3 = 44). The SEM image in Figure 3.6A shows the morphology of the reaction products obtained from acid treated diatomite. The ZSM-5 crystals obtained from leached diatomite were rounded with an average diameter around 7-8 μm and an aspect ratio close to 1. This sample also contained smaller particles and particularly small slabs as those encircled in Fig. 3.6A, which were attributed to mordenite. The diffractogram of the final reaction product obtained after 12 hours is presented in Figure 3.6 B, where the main characteristic peaks correspond to the MFI structure (2θ = 7.9; 8.7; 23.0 etc.) in good agreement with the reference pattern PDF-042-0024. The intensities of the main peak of quartz was similar and of the same order of magnitude as in the leached material. Consequently, the quartz content originated from the raw material. However, the final zeolite product obtained from acid treated diatomite contained traces of mordenite, approximately 5% when compared with the intensity of the main peak of ZSM-5. The residual calcium is suspected to have caused the formation of mordenite as a side-product.

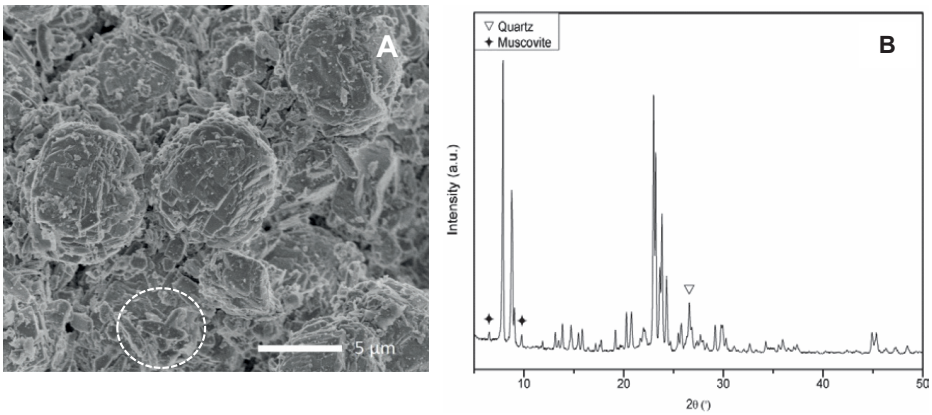

Figure 3.6 (a) XRD diffractogram and (b) SEM image of ZSM-5 crystals obtained after 12 hours of synthesis from diatomite.

The purification process with sulfuric acid was employed for the synthesis of FAU-type zeolites.

3.1.3. FAU from diatomaceous earth (Paper III and IV)

3.1.3.1. Diatomite Characterization

The XRD diffractograms of the raw diatomites are shown in Figure 3.7A. Depending on the sampling location, different amounts of halite (NaCl, PDF 01-071-4661), calcite ($CaCO_3$, PDF 01-078-4614), quartz (SiO_2, PDF 01-085-0457), muscovite ($KAl_2(Si,Al)_4O_{10}(OH)_2$, PDF 00-058-2034), montmorillonite ($Ca_{0.5}((Al_2Si_4O_{11})(OH))$, PDF 01-076-8291), chlorite (chamosite $Fe_3Si_2O_5(OH)_4$, PDF 00-010-0404), plagioclase ($Na_{0.499}Ca_{0.491}(Al_{1.488}Si_{2.506}O_8)$, PDF 01-079-1149) and gypsum ($Ca(SO_4)(H_2O)_2$, PDF 01-070-0982) were found to be present in addition to the amorphous background attributed to the amorphous silica structure of diatomite. The identified secondary phases are typical of diatomites of this type [56].

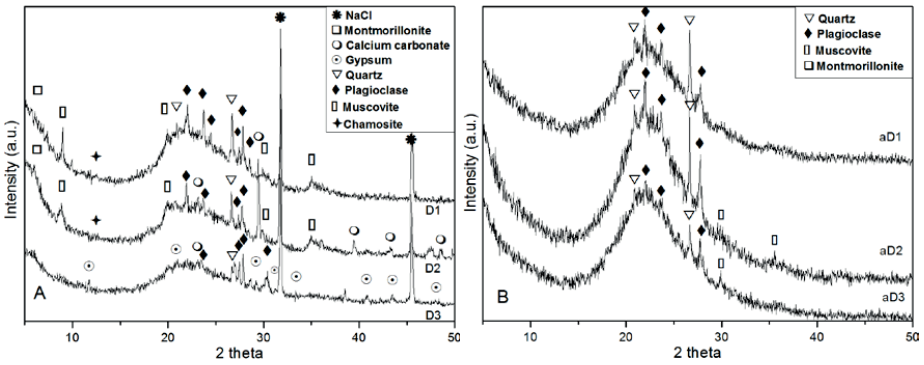

Figure 3.7 XRD diffractograms of the different diatomites: (A) D1 (plagioclase-rich), D2 (calcium carbonate-rich) and D3 (calcium sulfate-rich) before acid treatment; (B) acid-treated diatomites aD1, aD2 and aD3.

The occurrence of halite was expected, since the raw material originated from Llica, a region near the Uyuni salt lake. The composition of the original diatomites and corresponding acid leached diatomites was obtained by ICP-AES and the results are given in Table 3.5. The main elements in the raw diatomites D1, D2 and D3 were silicon and aluminum with SiO_2/Al_2O_3 ratios ranging between 15.1 and 20.1. However, Fe, Na, Ca, K, S and Mg were also present as impurities with variable contents depending on the sampling location and attributed to the minerals chamosite, muscovite montmorillonite in accordance with XRD results in the three diatomites investigated in this work. The high concentration in calcium in sample D2 (i.e. 4 wt.% CaO) is undoubtedly due to the presence of calcium carbonate in addition to the plagioclase corresponding to calcian albite and consisting approximately of a 50-50 at.% solid solution of sodium and calcium. The latter was also identified in the other diatomites D1 and D3. However, the diatomite D3 was the purest raw material containing comparatively less amounts of quartz, plagioclase and muscovite. It is noteworthy that sulfur was present in the original diatomites and particularly in sample D3 (i.e. 1.68 wt.% SO_4). This was found to be related to the presence of gypsum (calcium sulfate dihydrate) crystals as identified by XRD.

Comparison between the XRD (Figure 3.7) and ICP-AES results (Table 3.5) of the original materials and the acid treated counterparts (aD) shows that sodium chloride and calcium carbonate were removed by rinsing and dissolution by the acid, respectively. The acid leaching step was also successful in decreasing the iron and magnesium

content. Sulfur was almost completely washed away by the acid treatment in sample aD3 due to the dissolution of the gypsum crystals [57].

A dark sedimented layer containing large particles of quartz and plagioclase was discarded after the first washing step with water. As a result, calcium represented the main impurity after acid leaching of the three diatomites with aD2 containing as much as 2 wt% CaO, whereas aD1 and aD3 only contained 0.79 and 0.40 wt% CaO. Another direct consequence of the acid treatment was that the SiO_2/Al_2O_3 ratio was increased to values ranging between 42.9 and 52.8. Therefore, aluminum sulfate, an inexpensive salt, was added to the synthesis mixture in order to adjust the SiO_2/Al_2O_3 ratio to suitable levels for the synthesis of zeolite Y.

Table 3.5 Chemical composition of the raw diatomites (D1, D2 and D3) and the corresponding acid treated diatomites (aD1, aD2 and aD3) determined by ICP-AES.

Material	Weight (%)								Ratio
	SiO_2	Al_2O_3	Fe_2O_3	Na_2O	CaO	K_2O	MgO	SO_3	SiO_2/Al_2O_3
D1	77.30	8.01	1.49	7.17	1.84	1.64	1.72	0.35	16.4
aD1	94.07	3.73	0.11	0.31	0.79	0.48	0.16	0.34	42.9
D2	75.83	8.54	0.56	6.74	3.99	1.94	2.12	0.29	15.1
aD2	92.27	3.43	0.09	0.30	1.97	0.42	0.15	1.37	45.7
D3	75.66	6.39	0.77	10.34	0.98	1.73	2.45	1.68	20.1
aD3	95.51	3.08	0.12	0.32	0.40	0.38	0.18	0.01	52.8

SEM micrographs of the three diatomite samples and their acid treated counterparts indicated that little morphological changes occurred during the acid treatment. Figure 3.8 shows the morphology of D1 and aD1. Diatomite exhibits large particles with typical shapes of diatomaceous biogenic sediments. Some diatomite particles were partially broken in smaller pieces by the mechanical action of stirring during the acid treatment but their typical shapes could still be distinguished (Figure 3.8B).

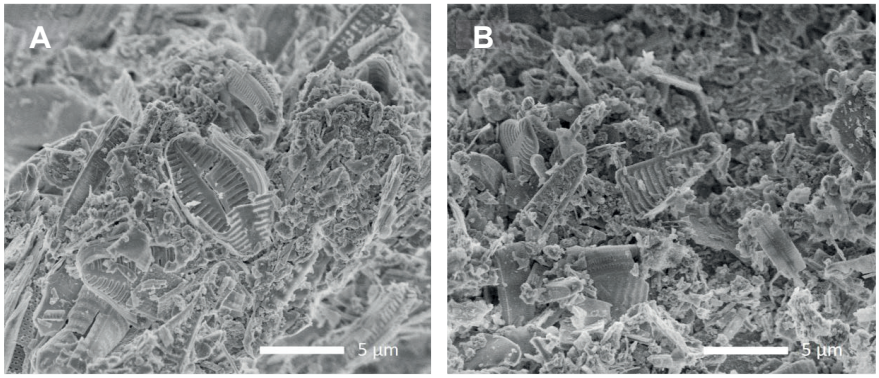

Figure 3.8 SEM images of (A) diatomite and (B) leached diatomite.

3.1.3.2. Synthesis optimization

Optimization of the synthesis of zeolite Y at different compositions was carried out at fixed conditions (Table 3.6) with aD2 as aluminosilica source.

Table 3.6 Composition and synthesis conditions for sample aD2-S0.4 to aD2-S2.0.

Sample	Molar composition			Ageing		Heating		Main product (secondary product within brackets)
	SiO_2/Al_2O_3	Na_2O/SiO_2	H_2O/Na_2O	Time (h)	Temperature (K)	Time (h)	Temperature (K)	
aD2-S2.0	11.6	2.0	40	24	298	48	373	P
aD2-S1.2	11.1	1.2	40	24	298	48	373	P
aD2-S0.9	11.1	0.9	40	24	298	48	373	FAU, (P)
aD2-S0.8	11.1	0.8	40	24	298	48	373	FAU, (P)
aD2-S0.7	11.1	0.7	40	24	298	48	373	FAU, (P)
aD2-S0.6	11.6	0.6	40	24	298	48	373	FAU, (P)
aD2-S0.5	11.6	0.5	40	24	298	48	373	Amorphous
aD2-S0.4	11.5	0.4	40	24	298	48	373	Amorphous

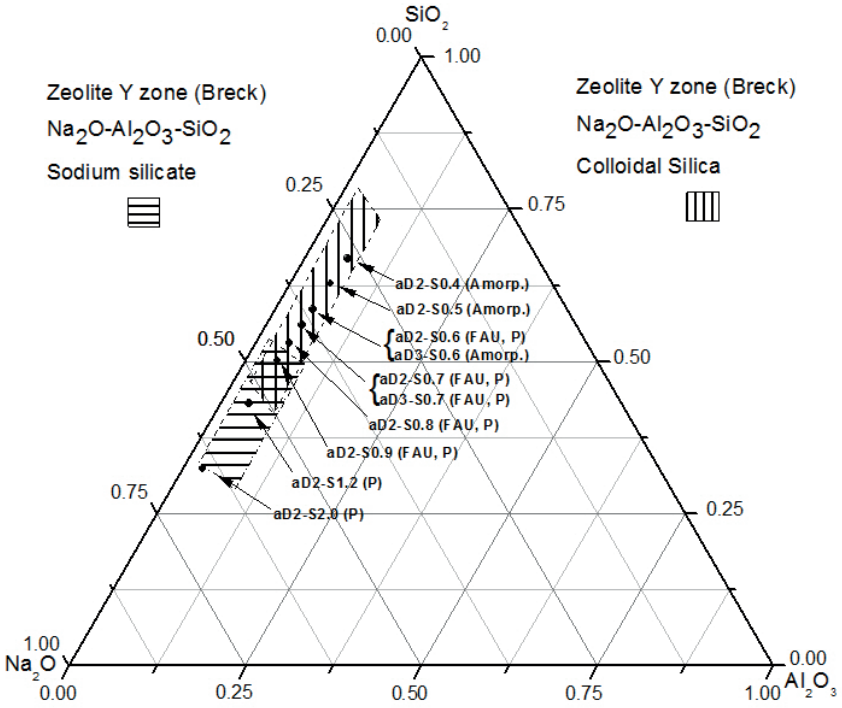

Figure 3.9 SiO_2–Al_2O_3–Na_2O phase diagram showing the distribution of the samples synthesized and products at different Na_2O/SiO_2 ratios [1].

Breck and Flanigen [1] identified two different compositional regions depending on whether sodium silicate or colloidal silica was used as silica source (Figure 3.9). Using aD2 as starting material, only amorphous material was obtained as products for Na_2O/SiO_2 ratios < 0.6 (aD2-S0.4 and aD2-S0.5 in Table 3.6 and Figure 3.9), while mixtures consisting of zeolite FAU and P were obtained for Na_2O/SiO_2 ratio between 0.6 and 0.9. By further increasing the Na_2O/SiO_2 ratio, only zeolite P was obtained (samples aD2-S1.0, aD2-S1.2 and aD2-S2.0). It was possible to reproduce these results by using aD1. Unexpectedly, the purest diatomite aD3 did not yield faujasite for Na_2O/SiO_2 ratios below 0.7.

Sample aD2-S0.6 obtained after 48 hours of synthesis time showed evident signs of overrunning (Figure 3.10). Zeolite P crystals (tetragonal) appear to grow on dissolving FAU zeolite crystals. Both zeolites showed comparable SiO_2/Al_2O_3 ratios, namely 4.36 for FAU and 4.30 for P as determined by XRD and EDS, respectively. Hansen *et al*. reported tetragonal zeolite P with similar characteristics and SiO_2/Al_2O_3 ratio of 6.9

(PDF 40-1464) [58]. Such nucleation and growth of zeolite P on dissolving faujasite has already been observed by SEM and TEM [59, 60]. It is well-known that zeolite P is a more stable phase than zeolite FAU and that the former can nucleate before complete formation of the latter [18]. Therefore, to maximize the yield of the FAU zeolite and to limit the formation of zeolite P, synthesis time was reduced below 48 h for Na_2O/SiO_2 ratios between 0.6 and 2.0 using aD1 as starting material.

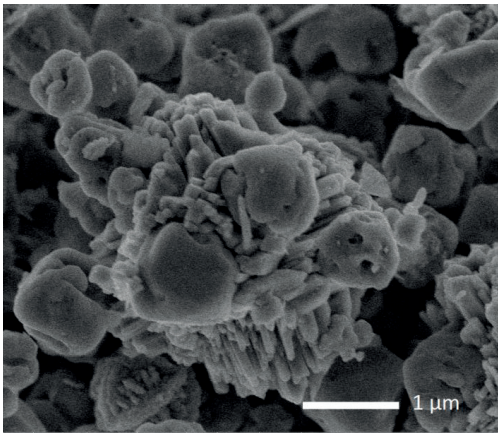

Figure 3.10 SEM of aD2-S0.6 for 48 h.

For a sample prepared from a gel with a Na_2O/SiO_2 ratio of 0.6 and 30h of hydrothermal treatment, XRD shows that zeolite P was absent. Instead amorphous material is observed (Figure 3.11A). Consequently it was not suitable to obtain pure FAU zeolite for this composition. Similar behavior was observed for a ratio of 0.7 (Figure 3.11B), for which 28 h was the optimal time to avoid the presence of zeolite P. For a Na_2O/SiO_2 ratio of 0.8, FAU zeolite nearly free from zeolite P was obtained after 15 h (Figure 3.11C); however, the background indicated the presence of a small amount of amorphous material. Reducing time to 13, 6 and 6h for Na_2O/SiO_2 ratios of 0.9, 1.2 and 2.0, respectively, prevented the formation of zeolite P and resulted in FAU zeolite with high crystallinity as the only product, as shown in Figure 3.11 (D), (E) and (F), respectively.

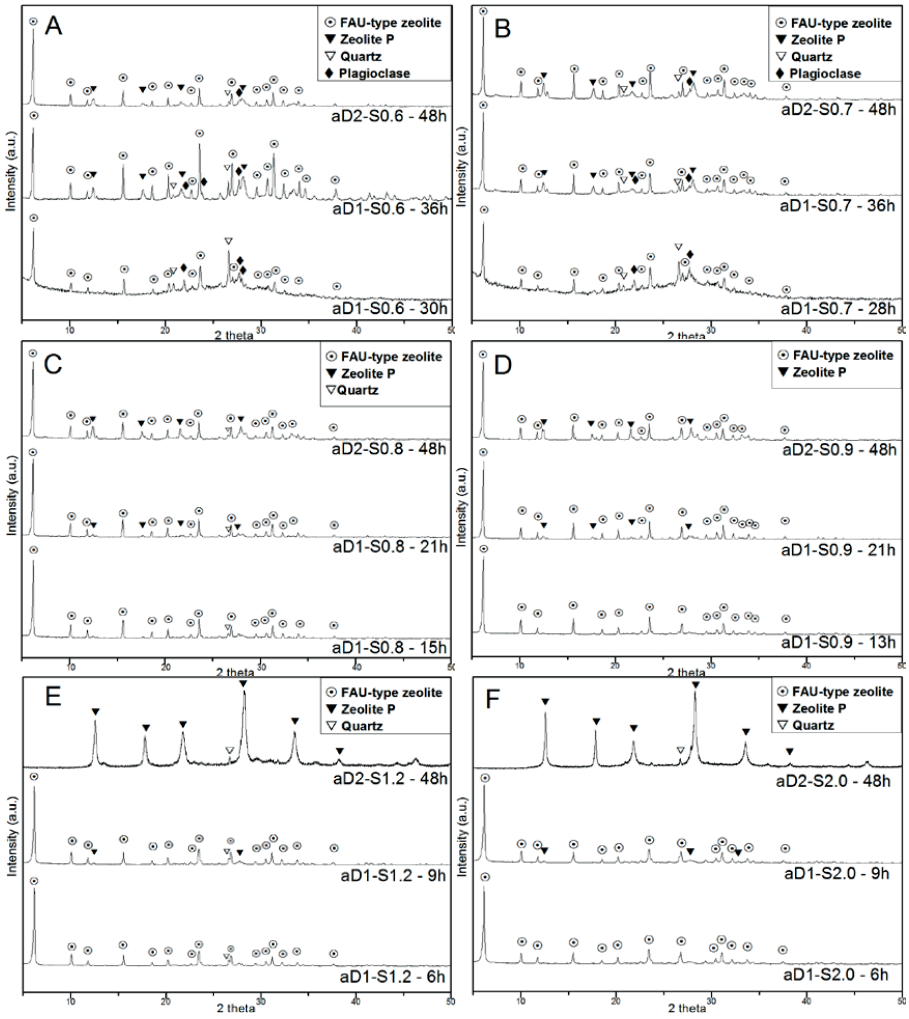

Figure 3.11 XRD diffractograms of the solid products obtained after different synthesis times for Na_2O/SiO_2 ratios of: (A) 0.6; (B) 0.7; (C) 0.8; (D) 0.9; (E) 1.2; and (F) 2.0.

Interestingly, although no FAU could be synthesized for Na_2O/SiO_2 ratios below 0.7 when aD3 was used, a well-crystallized FAU product was obtained when this ratio was set to 0.85 and synthesis time to 13 h (Figure 3.12).

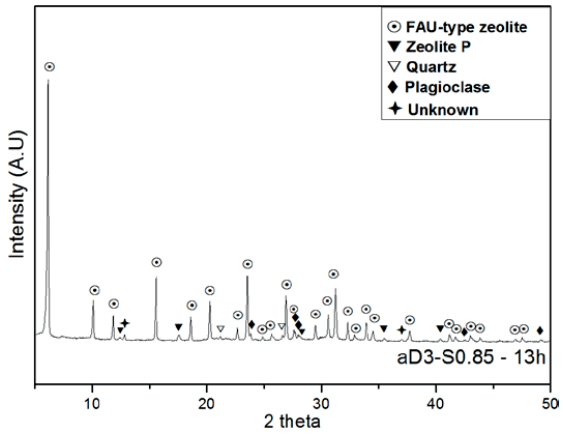

Figure 3.12 XRD diffractogram of the sample aD3-S0.85-13h.

3.1.3.3. Characteristics of the final product

Optimal synthesis time

Table 3.7 gives the SiO_2/Al_2O_3 ratio in the FAU crystals determined by X-ray diffraction for the different Na_2O/SiO_2 ratios tested, as a function of synthesis time and type of raw material used. For each Na_2O/SiO_2 ratio except 0.6, the observed values are constant within deviations of ± 0.2, which was found to be the precision of the method. As shown above, after passing an optimal synthesis time, zeolite P appeared in all cases and the FAU particles started to dissolve. Therefore, the nucleation of zeolite P and subsequent dissolution of FAU-zeolite resulted in a rather constant measured SiO_2/Al_2O_3 ratio in the dissolving FAU crystals, except for a Na_2O/SiO_2 ratio of 0.6 which showed a strong decrease of this parameter along with dissolution of the FAU crystals. This suggests that the shell of the FAU crystals is Si-rich and the core Al-rich in aD2-S0.6. This has already been observed experimentally on large FAU-crystals by energy dispersive spectroscopy [61] or on Ce^{3+} exchanged zeolite Y by X-ray photoelectron spectroscopy [62].

Table 3.7 SiO_2/Al_2O_3 composition determined by XRD of the FAU products from optimal synthesis time and further on.

Starting material	Na_2O/SiO_2	SiO_2/Al_2O_3										
		6h	9h	12h	13h	14h	15h	28h	30h	33h	36h	48h
	0.6								5.3	4.8	4.7	4.6
	0.7							4.7			4.6	4.7
aD1,	0.8						4.1					4.0
aD2	0.9			3.9	3.6							3.7
	1.2	3.0	3.2	3.4								
	2.0	3.4	3.0	3.2								
aD3	0.85				3.9	3.9	4.0					

Particle size

Figure 3.13 shows scanning electron micrographs of all samples obtained at optimal synthesis time. All samples contained euhedral particles consisting of more or less intergrown crystals with octahedral symmetry. Particle size clearly increased as alkalinity was decreased by lowering the Na_2O/SiO_2 ratio from 2.0 to 0.7 (Figure 3.13 A-E), specifically from 0.5 μm for aD1-S2.0-6h to 2.3 μm for aD1-S0.7-28h. The degree of intergrowth also clearly diminishes with lowering the Na_2O/SiO_2 ratio in the same range, more well-defined crystals with octahedral symmetry formed as the Na_2O/SiO_2 ratio was gradually decreased. However, particle size was found to decrease and the degree of intergrowth to increase again for aD1-S0.6-30h (Figure 3.13 F). For Na_2O/SiO_2 ratios less than or equal to 0.8, the presence of unreacted materials becomes obvious (Figure 3.13 D-F). Large non-reacted diatomite skeletons were still present in aD1-S0.6 after 30h of synthesis, as shown in Figure 3.14A.

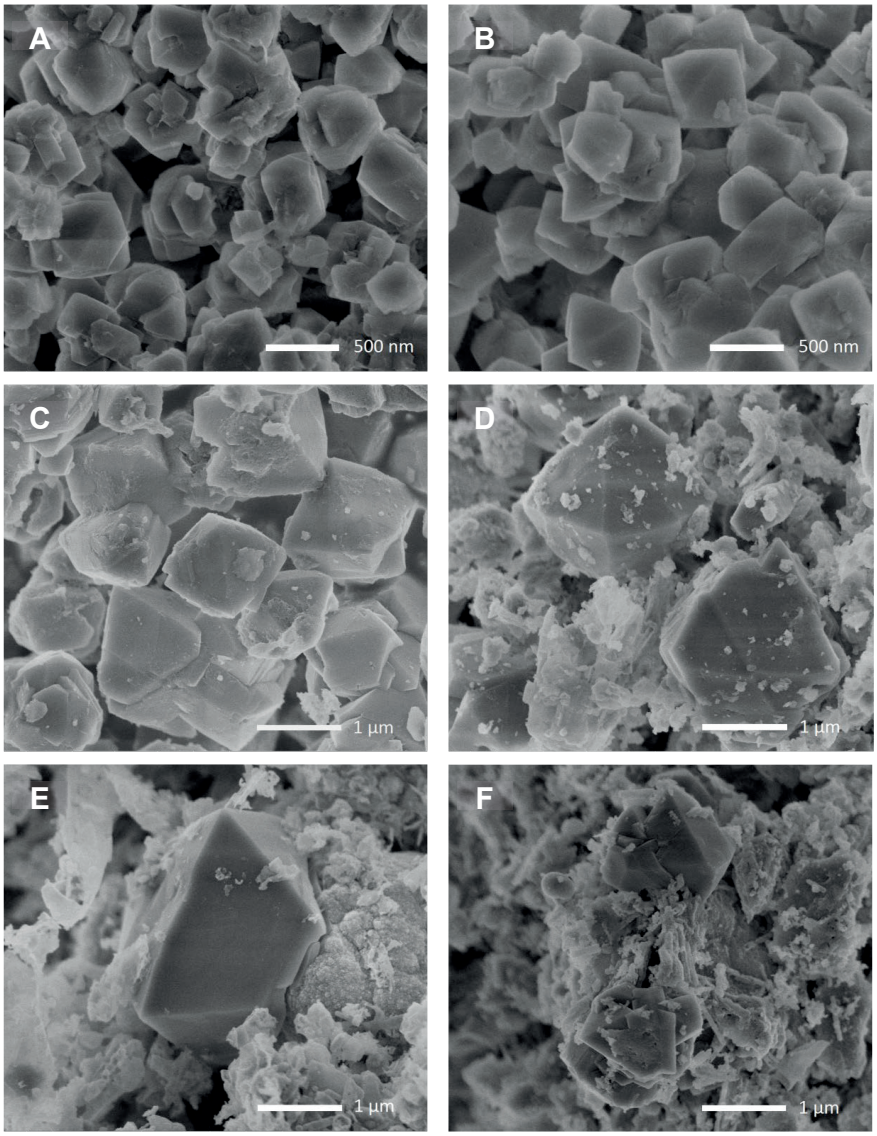

Figure 3.13 Scanning electron micrographs of all zeolite Y samples obtained from aD1 at optimal synthesis time: (A) aD1-S2.0-6h; (B) aD1-S1.2-6h; (C) aD1-S0.9-13h; (D) aD1-S0.8-15h; (E) aD1-S0.7-28h; (F) aD1-S0.6-30h.

Although the reactivity process window with respect to alkalinity was narrower on the low alkalinity side for aD3 in comparison with the other leached diatomites, the well-crystallized final product obtained for aD3-S0.85-13h (Figure 3.14 B) exhibited particles with morphology and size consistent with aD1-S0.8 and aD1-S0.9.

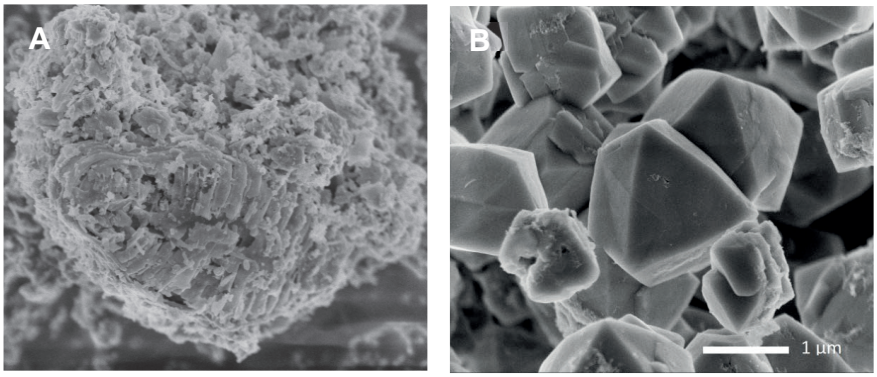

Figure 3.14 Scanning electron micrographs showing: (A) a large fragment of diatomite remaining in aD1-S0.6 after 30 h of synthesis; (B) aD3-S0.85 -13h.

Yield of FAU crystals

The amount of FAU zeolite produced can be approximately estimated from the measured microporosity yield and X-ray crystallinity, which are reported in comparison to the values of a commercial zeolite Y powder in Table 3.8. High values of the microporosity yield and X-ray crystallinity were obtained for Na_2O/SiO_2 ratios in the range 0.85-2.0, which shows that FAU crystals could be produced from diatomite at a high yield. However, the unreacted remaining minerals e.g. quartz and plagioclase identified by XRD in Figure 3.7, most likely influenced the values of the microporosity yield that could be achieved. The increase of the crystallinity values as the Na_2O/SiO_2 ratio was decreased from 2.0 to 0.85 was attributed to textural effects due to particle size. However, the microporosity yield and X-ray crystallinity values dropped dramatically as alkalinity was decreased for Na_2O/SiO_2 ratios below 0.85 due to non-dissolved fragments of diatomite.

Formation of zeolite P

Table 3.8 also shows the yield in terms of aluminum (η_{Al}) calculated from gravimetric measurements and ICP-AES. Interestingly, this value oscillates around 1, between 0.87 and 1.36. Since yield values cannot be higher than 1, indicating that all aluminum introduced in the synthesis mixture is present in the final solid product, the results are influenced by the error of the ICP-AES method. Considering that high microporosity yield and X-ray crystallinity values were obtained for Na_2O/SiO_2 ratios in the range 0.85-2.0 and that these results corresponded to the longest allowed synthesis time for obtaining FAU zeolite as the sole product, it can be concluded that it is the

depletion in aluminum that triggered the formation of zeolite P in these samples. It is well known that aluminum is preferentially consumed over silicon in the beginning of the growth of FAU zeolites and that growth ceases as aluminum is depleted, which renders the synthesis of high silica FAU difficult. This is usually assigned to the fact that aluminate ions are necessary for the formation of sodalite cages, which are part of the FAU structure [63].

Table 3.8 Yield, SiO_2/Al_2O_3 ratios and porous properties of the final products of the optimized syntheses.

Sample	Yield in terms of Al (η_{Al})	EDS SiO_2/Al_2O_3 ratio (R_{EDS})	XRD SiO_2/Al_2O_3 ratio (R_{XRD})	X-ray crystallinity	Surface area BET (m^2/g)	External surface area (m^2/g)	Micropore volume (cm^3/g)	Microporous yield
aD1-S0.6-30h	0.97	4.6	5.3	0.18	94.4	29.61	0.030	0.10
aD1-S0.7-28h	0.92	4.4	4.7	0.22	107.7	44.88	0.029	0.09
aD1-S0.8-15h	0.99	4.0	4.1	0.48	466.6	44.55	0.197	0.63
aD3-S0.85-13h	0.99	4.1	3.9	0.94	584.5	35.84	0.255	0.82
aD1-S0.9-13h	0.87	3.8	3.6	0.81	618.4	51.76	0.264	0.85
aD1-S1.2-6h	1.13	3.2	3.1	0.73	611.0	60.51	0.256	0.83
aD1-S2.0-6h	1.36	3.5	3.4	0.69	646.2	56.57	0.276	0.89
zY com	-	5.2	5.2	1.00	717.1	51.21	0.311	1.00

SiO_2/Al_2O_3 ratio

The SiO_2/Al_2O_3 ratio in the zeolite (R_{XRD} in Table 3.8) increased steadily as alkalinity decreased in our system using diatomite as silica source reaching values of 3.9 or higher for Na_2O/SiO_2 ratios ≤ 0.85. It has been shown by different research groups that the SiO_2/Al_2O_3 ratio increases in various zeolites as the excess alkalinity decreases [64, 65]. However, the synthesis of high silica faujasite usually requires the use of colloidal silica as silica source, since FAU crystals with SiO_2/Al_2O_3 ratios larger than 3.9 cannot be obtained in the SiO_2-Al_2O_3-Na_2O-H_2O system by utilizing sodium silicate [1]. The use of diatomite also allowed SiO_2/Al_2O_3 ratios larger than or equal to 3.9 to be reached in the compositional field identified for colloidal silica by Breck and Flanigen (see Figure 3.9). Hence, our results suggest that the higher polymerized state of silica in colloidal

silica and diatomite seems to play a role in the formation of high silica faujasite. It might be due to the release of larger silica species [64] or by further decrease of alkalinity during depolymerization of the starting silica source [66], or a combination thereof. However, diatomite was too bulky to be completely consumed under the investigated synthesis conditions.

Potential use as FCC catalyst

According to Breck and Flanigen's definition, zeolite X is formed when the faujasite structure contains aluminum such as the SiO_2/Al_2O_3 ratio is below 3 [3]. This definition was confirmed by Rüscher *et al.* who argued that both domains of zeolite X and Y exist above this ratio and that pure zeolite Y can only be claimed if ratio is greater than or equal to 5.4 [39]. This limitation was based on the resistance against amorphization during dealumination by steaming. In light of these definitions, all final products obtained in this work can be denominated zeolite Y. However, syntheses aD1-S2.0-6h and aD1-S1.2-6h produced FAU crystals with SiO_2/Al_2O_3 ratios close to 3 (see Table 3.8), which therefore can be said to mainly consist of zeolite X with very few zeolite Y domains. Breck and Flanigen's and Rüscher's studies showed that crystals with a SiO_2/Al_2O_3 ratio higher than 3.8 possessed hydrothermal stability only inferior by approximately 10% to that obtained for high-silica zeolite Y after steaming at 410°C for 3 h or 500°C for 5 h, respectively. Therefore, the product of synthesis aD3-S0.85-13h, which showed a SiO_2/Al_2O_3 ratio of 3.9 and high crystallinity, may be a stable and inexpensive alternative for FCC catalysts.

Influence of impurities in the starting materials

The ions released in solution during dissolution of the minerals and clays were not found to affect the course of reaction particularly. The only observation that can be made is that calcium and sulfate ions might favor the nucleation of FAU crystals under low alkalinity conditions (Na_2O/SiO_2 ratio of 0.6). In fact, Mg and Ca were found to be located inside the FAU crystals by local EDS measurements [67].

Interestingly, the two-fold difference in CaO content between the leached diatomites aD1 and aD3 (i.e. 0.79 and 0.40 wt% CaO, respectively, in Table 3.5) resulted in twice as less uptake of calcium inside sample aD3-S0.85-13h as compared with FAU zeolites prepared from aD1, as indicated by the Ca/Al ratios of 0.05 and 0.09 given in Table 3.9 for aD3-S0.85-13h and the average value of the aD1 samples, respectively. These

observations underpin the fact that improved methods must be developed to purify diatomite in order to use the latter as aluminosilica source for producing FCC-grade zeolite Y.

Table 3.9 Relative equivalents with respect to aluminum of the cations located in the zeolite of the final products. The values were determined by EDS.

Sample	Na/Al	2Ca/Al	2Mg/Al	(Na+2Ca+2Mg)/Al
zY com	1.00	n.d.	n.d.	1.00
aD1 samples*	0.90	0.09	0.02	1.00
aD3-S0.85- 13h	0.97	0.05	0.03	1.05

n. d. (non-detected)

* Average values for aD1-S2.0-6h, aD1-S1.2-6h and aD1-S0.9-13h

3.1.3.4. Addition of NaCl (Paper IV)

The acid treated diatomite aD1 was used to study the influence of the addition of NaCl on the synthesis of FAU-type zeolites. The composition with a Na_2O/SiO_2 ratio of 1.2 and $x = 0$ (x = NaCl) was studied as a function of synthesis time. This series is hereafter referred to as S1.2-0NaCl. Figure 3.15A shows that FAU zeolite starts to crystallize after 1 h and reach maximum crystallinity between 4 and 6h of synthesis time. For longer synthesis times (> 6h), a decrease of XRD crystallinity due to dissolution of FAU crystals is attained. Instead, the more thermodynamically stable zeolite P forms (Figure 3.15B). SEM micrographs of S1.2-0NaCl at different synthesis times are shown in Figure 3.16. After 5h (Figure 3.16A), the sample consists mainly of FAU-type crystals with octahedral shape and a high degree of intergrowth. Extending synthesis time causes the FAU zeolite crystals to be completely replaced by tetragonal crystals of zeolite P after 48h (Figure 3.16B).

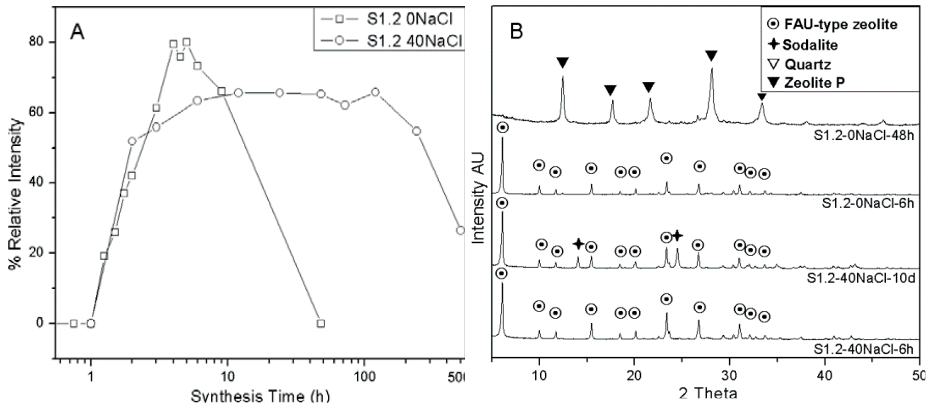

Figure 3.15 (A) Relative XRD crystallinity for the S1.2 system with $x = 0$ and 40 as a function of synthesis time. (B) XRD diffractograms for selected samples showing either maximum faujasite crystallinity or high degree of overrun.

By addition of NaCl ($x = 40$, i.e. S1.2-40NaCl) the crystallization rate barely changes (Figure 3.15A). Similarly, crystallization also starts after 1h and its rate is similar until 2 h before slowing down during the following 4 h to reach maximum crystallinity after approximately 6 h. This time to reach maximum crystallinity is comparable with that obtained without the addition of NaCl. However, the presence of NaCl causes crystallinity to remain constant over a long period of time, i.e. the FAU XRD crystallinity decreases only after 120 h of synthesis. As a matter of fact, the formation of zeolite P was completely inhibited and instead another secondary product was identified after 240 h of synthesis, namely sodalite (Figure 3.15B).

These results for S1.2-40NaCl were confirmed by SEM observations. It is evident by comparing Figure 3.16C and D that no morphological changes occur to the faujasite crystals between 6 and 120 h. However, sodalite crystals (white arrows in Figure 3.16E) with rounded shape started to grow after 240 h and are more evident after 504 h (Figure 3.16F). Besides, FAU-type crystals size increased even further, probably by Ostwald ripening (white circles).

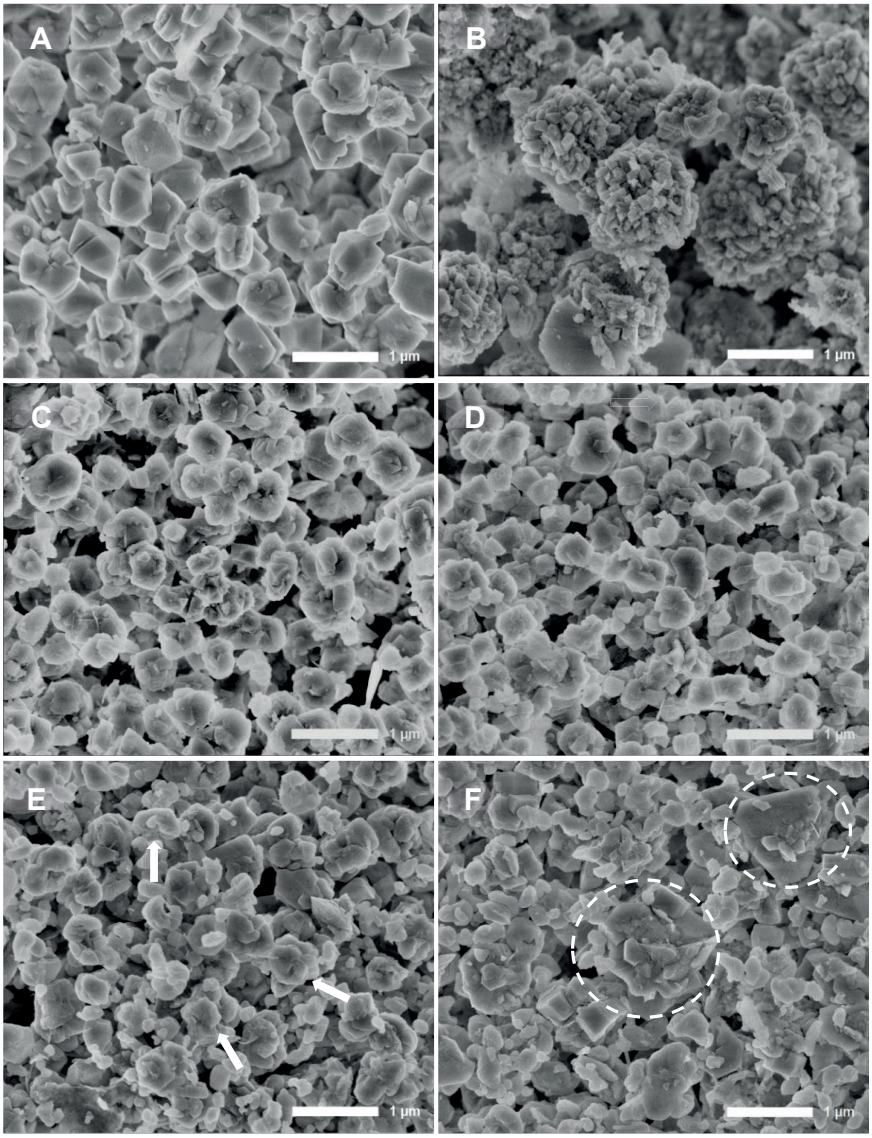

Figure 3.16 SEM micrographs showing: S1.2-0NaCl after (A) 5 h and (B) 48h of synthesis time; and S1.2-40NaCl after different synthesis times: (C) 6h, (D) 120h, (E) 240 h and (F) 504h.

Table 3.10 Data on silicon partition, relative XRD crystallinity, SiO_2/Al_2O_3 ratio, microporous yield and external surface area.

Sample	**Si in final solid** (% of all Si)	**Relative XRD crystallinity** (%)	**XRD SiO_2/Al_2O_3**	**Microporous yield** (%)	**External surface area** (m^2/g)
S1.2-0NaCl-5h	50	87.7	2.91	79	42.5
S1.2-40NaCl-6h	52	63.3	2.71	93	65.0
S1.2-40NaCl-120h (5d)	48	65.8	2.66	92	81.2
S1.2-40NaCl-240h (10d)	-	54.9	2.66	68	43.5
Commercial zeolite Y	-	100	5.16	100	49.5

Although the relative XRD crystallinity was lower for S1.2-40NaCl-6h than for S1.2-0NaCl-5h with 63.3 and 87.7 respectively, the sample with NaCl addition showed a higher crystallinity from microporous yield, i.e. 93% to be compared with 79% in the absence of NaCl (Table 3.10). Interestingly, both samples consisted mostly of FAU crystals and were produced at comparable yield as indicated by the partition of silicon between the liquid and the final product for the corresponding syntheses, i.e. 50 and 52% of the total silicon present in the final solid product in S1.2-0NaCl-5h and S1.2-40NaCl-6h, respectively. By measuring crystal size in SEM micrographs on a large number of crystals, the corresponding size distribution for both samples was obtained, as shown in Figure 3.17. A median size of 600 nm was measured on S1.2-0NaCl-5h. The 10% decrease in size for S1.2-40NaCl-6h, i.e. 540 nm, might have caused a decrease in intensity of the diffracted peaks used for calculating crystallinity, while it contributed to expose more external surface area for probing the microporous volume, as shown in Table 3.10 by the higher value of the specific external surface area for S1.2-40NaCl-6h compared with S1.2-0NaCl-5h.

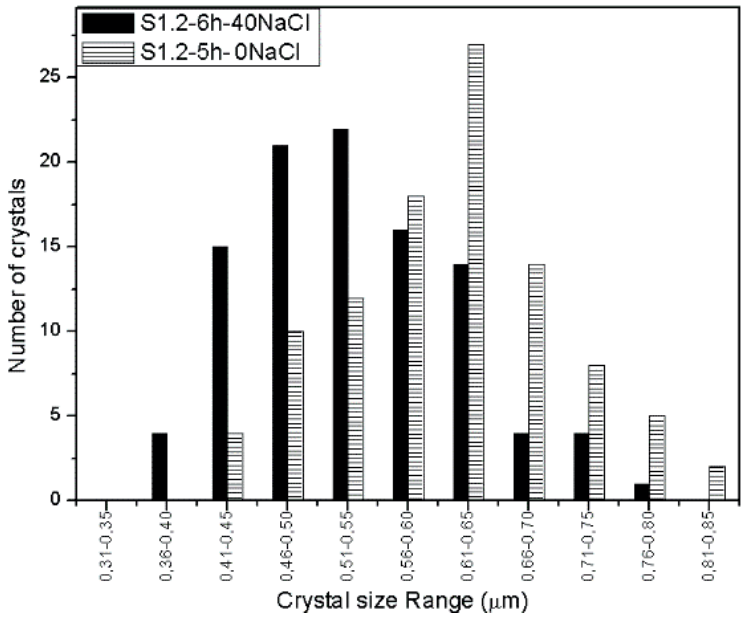

Figure 3.17 Crystal size distribution in S1.2-40NaCl-6h (black) and S1.2-0NaCl-5h (striped pattern).

Table 3.10 also gives information about the SiO_2/Al_2O_3 ratio in the FAU crystals determined by X-ray diffraction for the samples with x = 0 or 40. Samples synthesized in the presence of a large amount of NaCl exhibit a lower SiO_2/Al_2O_3 ratio of approximately 2.7 compared with 2.9 without NaCl addition. Previously, it was shown that all the aluminum was present in the final solid product. Therefore, the addition of NaCl must have promoted incorporation of Al from plagioclase or an intermediate product into the framework of the zeolite which might also be responsible for the higher microporous yield of the S1.2-40NaCl samples (93 and 92% for 6 and 120 h, respectively) compared with S1.2-0NaCl (79% for 5 h). The same trend was reported in Paper III, in which higher Na_2O/SiO_2 ratios by addition of NaOH led to lower SiO_2/Al_2O_3 ratios in the FAU-type zeolite. A higher incorporation of aluminum in the zeolite framework is expected in the case of high availability of charge balancing Na^+ cations.

Furthermore, the addition of NaOH and NaCl influenced the crystal size obtained by increasing the Na_2O/SiO_2 ratio. Since the S1.2-0NaCl-5h and S1.2-40NaCl-6h samples reached maximum crystallinity with similar yields according to the final partition of

silicon (Table 3.10), NaCl clearly influenced nucleation, probably by increasing the number of nuclei, resulting in smaller final crystals. Classical theories usually interpreted this behavior as an increase of supersaturation [68]. Recently, Liu *et al*. [69] reached a similar conclusion based on inorganic salts that were introduced to the synthesis mixture under controlled synthesis parameters, such as alkalinity and crystallizing temperature. The results showed that the particle size of zeolite Y could be apparently decreased by introduction of NaCl. Also, Zhan *et al*. [70] showed that particle size is reduced by the addition of NaCl at low concentration (down to Na/Si = 0.001). Zhan et al. also suggested that the formation of FAU zeolite is favored over LTA by NaCl promoting the formation of more building units of 6 membered rings (6R and D6R) over 4 membered rings (4R and 4DR), the latter being the precursors for zeolite A and zeolite P (only 4R). This seems to be caused by the transformation of 4R and D4R to 6R and D6R. As a result, there probably exist a higher number of 6-membered rings for connecting sodalite cages to form FAU-type zeolite crystals than 4-membered rings for connection of sodalite cages in the configuration leading to LTA-type crystals. This may be also the reason why the formation of zeolite P is inhibited and that FAU-type zeolite directly forms sodalite (composed by sodalite cages) at very long synthesis time in the presence of NaCl.

In addition, Na^+ ions could be responsible for these observations, since it is known as a "structure-directing agent" for sodalite cages. However, considering the findings of Zhang et al. [70], Cl^- was demonstrated to strongly promote the formation of FAU-type zeolites. To test this hypothesis, NaCl was substituted with different salts in the aD1-S1.0-40NaCl-120h system. The ratio x = salt/Al_2O_3 was set to 40 with respect to Na^+ or Cl^- contained in the salt. XRD of the resulting products are presented in Figure 3.18. As discussed earlier, the addition of NaCl results in pure FAU even after 120 h of synthesis. Interestingly, the addition of $NaNO_3$ resulted in almost pure sodalite. The formation of sodalite at higher Na_2O/SiO_2 ratio is similar to the addition of NaOH, apart from being triggered earlier herein. However, other anions were also found to play an important role on the outcome of the syntheses. As a matter of fact, addition of NaF or Na_2SO_4 resulted in a mixture of zeolite P and analcime. As analcime is known to be an overrun product of zeolite P [71], the reaction kinetics seems to have been increased by these salts. This can be understood by the fact that fluorine ions F^- are known to act as mineralizer as OH^-. Our results suggest that it might also be the case of sulfate ions. To

investigate the effect of Cl^- ions, both KCl and NH_4Cl were evaluated resulting in the formation of almost exclusively zeolite P, which can be related to potassium ions [23]. Surprisingly, zeolite crystallization was completely inhibited by addition of NH_4Cl. Addition of NH_4OH resulted in the formation of montmorillonite-type clay. Therefore, our results suggest that chlorine ions inhibit crystallization of zeolite P and analcime and that the beneficial effect of NaCl addition on the synthesis of FAU zeolite is due to a synergic effect of Na^+ and Cl^- ions.

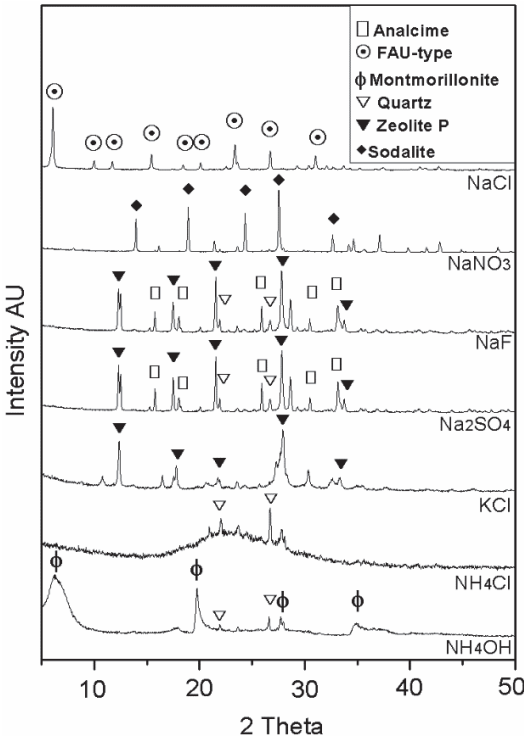

Figure 3.18 XRD diffractograms of S1.0-40X-120h, where X = NaCl, $NaNO_3$, NaF, Na_2SO_4, KCl, NH_4Cl or NH_4OH.

Finally, in order to determine the necessary quantity of NaCl, the amount of added NaCl was reduced to x = 1. Figure 3.19 shows the XRD results of samples S1.2-0NaCl-12h and S1.2-1NaCl-12h. Obviously, this lower amount of NaCl was still successful in inhibiting the formation of zeolite P until at least 12 h of synthesis.

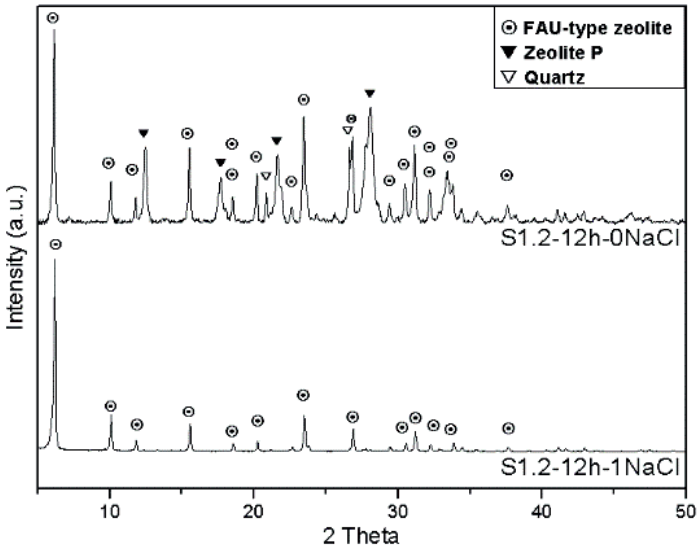

Figure 3.19 XRD diffractograms of S1.2-0NaCl-12h and S1.2-1NaCl-12h.

3.2. Structured zeolite NaX adsorbent for CO_2 adsorption (Paper V)

3.2.1. Physical characterization of the structured adsorbent

Based on results from an earlier work [46], films with a thickness of about 10 μm on nonporous monoliths would be close to an ideal adsorbent with low pressure drop, good adsorption capacity and low dispersion. Therefore, in the present work, NaX zeolite films were grown on the walls of steel supports, having 1600 cells per square inch, using a seeding technique and using clear synthesis solutions in a multiple step synthesis procedure.

Figure 3.20 shows representative SEM images of the structured adsorbents prepared in the present work. The images of the cross sections illustrate that walls of the steel monolith were smooth and nonporous, as opposed to the cordierite monoliths used in earlier work [46]. The plan view images show that the crystals in the film have typical FAU morphology. There are no other crystals with morphologies representative of other phases. Furthermore, the zeolite film was continuous, even, and appeared to be comprised of well-intergrown crystals. As illustrated in Figure 3.20, the film thickness was about 3 μm for the sample grown in 21 steps and 11 μm for the sample grown in 70 steps, see Table 3.11. Consequently, the film thickness is almost linearly proportional to

the number of growth steps, as expected, and increased with about 0.15 μm per step. For the sake of simplicity, the samples are hereafter referred to as the 3 μm and 11 μm films, respectively.

Table 3.11 Film thickness, Si/Al and Na/Al ratios determined by EDS and zeolite mass of the adsorbents.

Number of growth steps	Film thickness (μm)	Molar Si/Al ratio	Molar Na/Al ratio	Zeolite mass (g)
21	3	1.09	0.97	5.6
70	11	1.10	0.98	19.8

The results of the EDS analysis of the 3 and 11 μm films are given in Table 3.11. The Si/Al and Na/Al ratios are in the range 1.09-1.10 and 0.97-0.98, respectively. This shows that the FAU crystals in the films are the sodium form of zeolite X. The weights of the zeolite films, determined from the difference in weight before and after film growth on the two monoliths used for breakthrough experiments were 5.6 g and 19.8 g for the 3 μm and 11 μm films, respectively. The weight of the films is linearly proportional to the film thickness as expected.

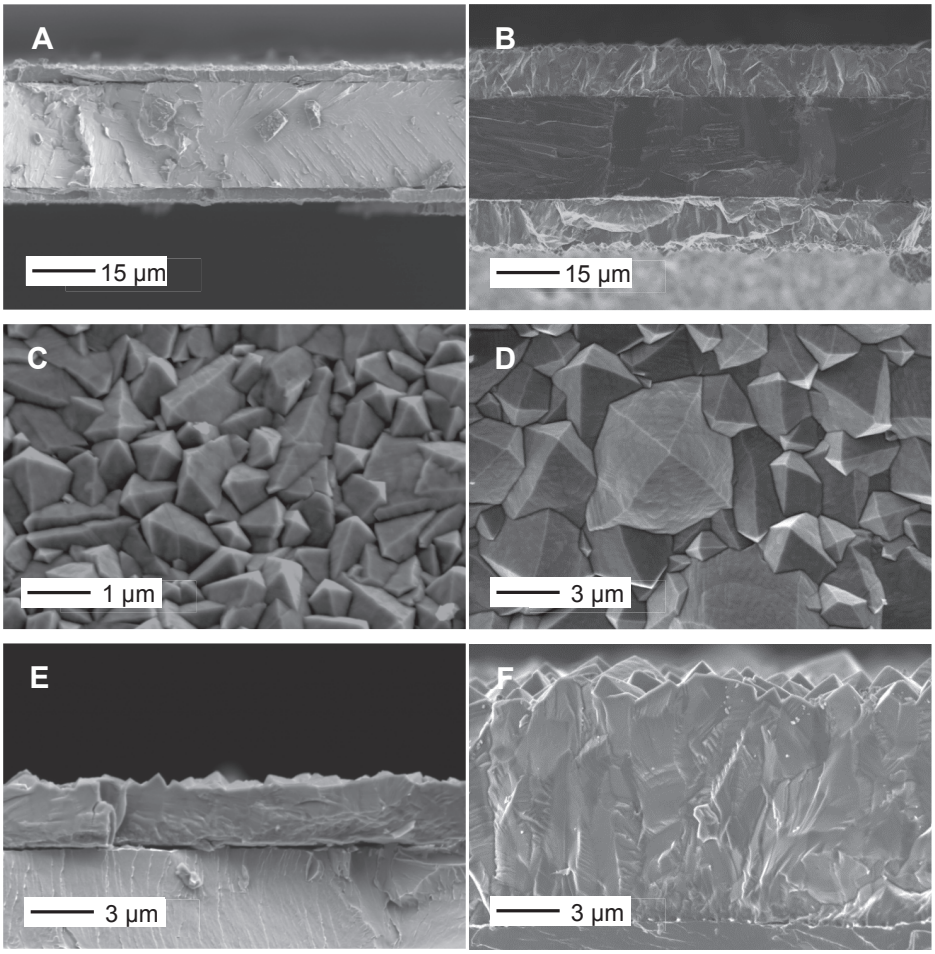

Figure 3.20 SEM images of the structured adsorbent, 3 µm (A-C-E) and 11 µm films (B-D-F).

Figure 3.21 shows XRD data recorded for a sample cut from the structured adsorbent with the 3 µm film after removal of the background signal. The vertical bars represent the ICDD reference pattern 01-070-2168 for randomly oriented zeolite NaX crystals. No other reflections apart from those typical zeolite NaX and stainless steel were observed for the sample. In addition, the intensities of the measured reflections agree well with those of the database pattern for randomly oriented crystals. This shows that the film is comprised of randomly oriented zeolite NaX crystals in concert with SEM and EDS observations.

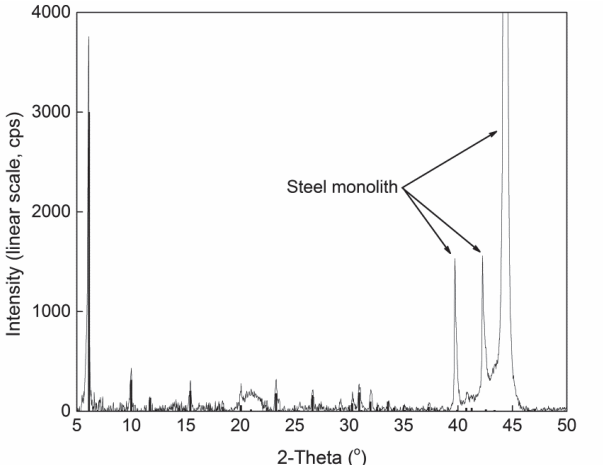

Figure 3.21 XRD pattern of steel monolith coated with a 3 μm zeolite film. The vertical bars represent the ICDD reference pattern 01-070-2168 for randomly oriented zeolite NaX crystals. Reflections originating from steel are indicated with arrows.

3.2.2. CO_2 breakthrough experiments

Figure 3.22 shows breakthrough data recorded for a steel tube (illustrated in Figure 2.3A) connected to the breakthrough apparatus for a flow rate of 1.00 dm^3/min. The volume of the steel tube is as small as about 4 ml, corresponding to a delay of only 0.2 s at this flow rate. Consequently, this experiment measures the response time and dispersion created by the breakthrough apparatus and the CO_2 analyser. Breakthrough of CO_2 (i.e. $C/C_0 > 0.05$) is detected after less than 1 s, which illustrates that the response time of the system is very low. A concentration of about 10% CO_2, i.e. $C/C_0 \approx 1$ is reached after about 10 seconds and this time corresponds to the dispersion created by the system.

The breakthrough data recorded for the column with some glass beads (illustrated in Figure 2.3B) connected to the breakthrough apparatus for a flow rate of 1.00 dm^3/min is also shown in Figure 3.22. Due to the much larger void volume of the column with glass beads (251 ml) as compared to the steel tube (4 ml), the breakthrough front is now shifted about 17 seconds in time. This shift matches very well with the expected delay of 15 seconds due to filling of the larger volume. However, the dispersion of the breakthrough front for the column is quite similar to that for the tube, and consequently,

the observed dispersion is only an effect of dispersion in the breakthrough apparatus and not in the column itself.

Figure 3.22 also shows the breakthrough curve recorded when the column was loaded with two steel monoliths (as illustrated in Figure 2.3C) for a flow rate of 1.00 dm^3/min. In this case, the breakthrough front is shifted 4 s earlier in time, which precisely matches the expected shift due to the reduced dead volume of the system (4.5 s). Again, the dispersion of the breakthrough front is about 10 s, as a result of dispersion in the breakthrough apparatus. The time t to reach C/C_0=0.5 for the uncoated monoliths is 13 seconds at this flow rate (average for 5 runs), see Table 3.12.

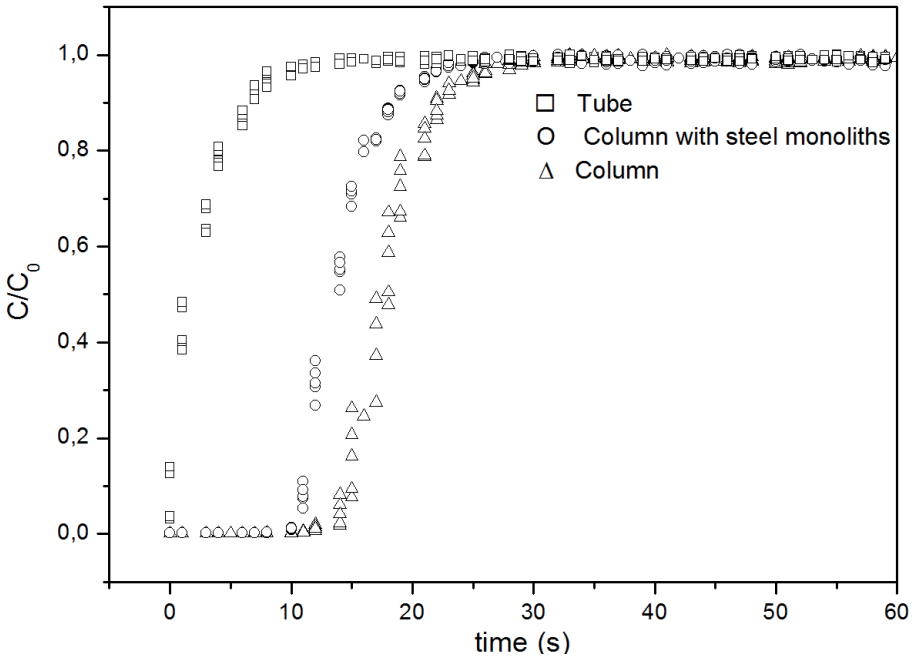

Figure 3.22 Experimental breakthrough profiles (points) for a flow rate of 1.00 dm^3/min recorded for tube (ID 1.5 mm), column (ID 3.2 cm) with glass beads and column with steel monoliths, graphite tape and glass beads as illustrated in Figure 2.3 A-C, respectively. Each breakthrough experiment is carried out 5 times and lines indicate the fitted model.

Breakthrough data for the steel monoliths coated with a 3 μm zeolite film are illustrated in Figure 3.23. Sharp and overlapping breakthrough profiles were obtained after regeneration of the adsorbent at 393 K. The breakthrough front is still quite sharp, but is broadened slightly as compared to the front recorded for the column with steel

monoliths without zeolite due to mass and heat transfer effects in the zeolite film. This will be discussed below. The times t to reach $C/C_0 = 0.5$ and the CO_2 adsorption capacity q estimated using equation 1 for the steel monoliths coated with a 3 µm zeolite film are given in Table 3.12. The average adsorption capacity q is 2.7 mol CO_2/kg zeolite for the 3.0 µm zeolite film. The standard deviation is as small as 0.1 mol CO_2/kg zeolite, which illustrates good precision for the breakthrough experiments.

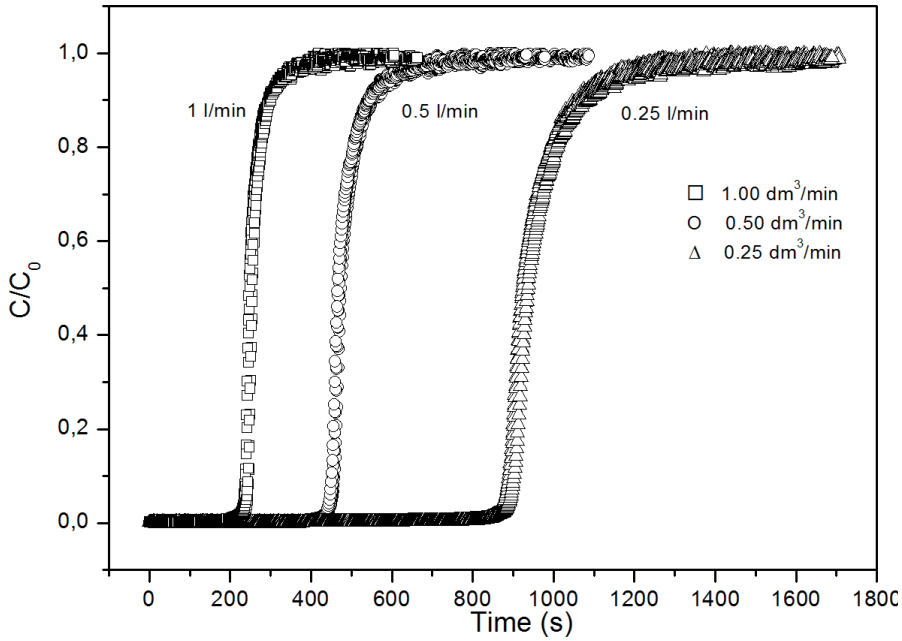

Figure 3.23 Experimental CO_2 breakthrough profiles (points) for steel monolith coated with a 3 µm zeolite film for flow rates of 1.00, 0.50 and 0.25 dm^3/min. Each breakthrough experiment was performed 5 times and the adsorbent was regenerated at 393 K between the adsorption cycles.

Breakthrough data for the steel monoliths coated with an 11 µm zeolite film are illustrated in Figure 3.24. Again, sharp and overlapping breakthrough profiles were obtained, but in this case, breakthrough of carbon dioxide occurs much later due to much higher adsorption capacity of the much thicker zeolite film. The time t to reach $C/C_0 = 0.5$ and the CO_2 adsorption capacity q estimated using equation 1 for the steel monoliths coated with a 11 µm zeolite film is given in Table 3.12. The average adsorption capacity q is 2.8 mol CO_2/kg zeolite, i.e. very similar to that observed for the

monoliths coated with a 3 μm zeolite film (Table 3.12). However, in this case the standard deviation is slightly larger, i.e. 0.3 mol CO_2/kg zeolite.

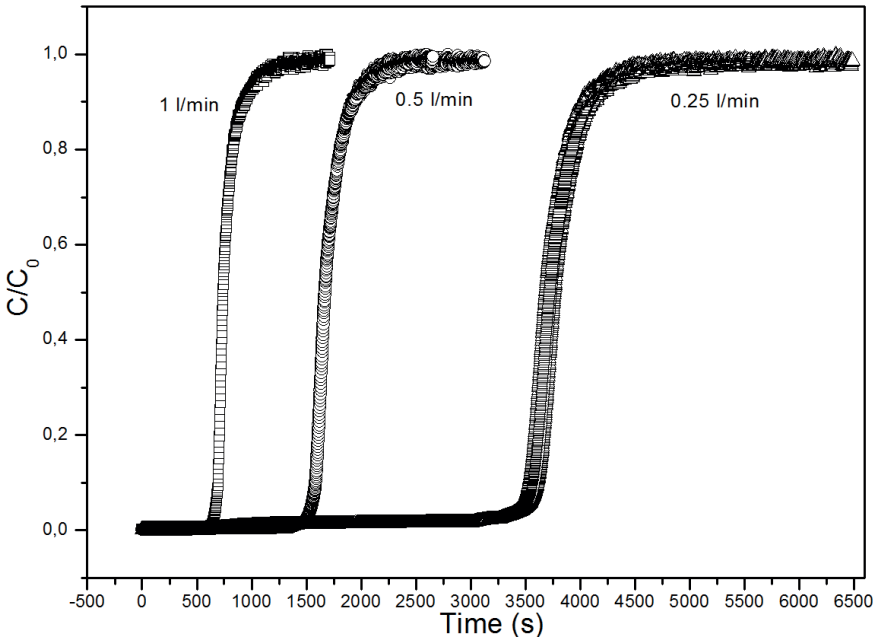

Figure 3.24 Experimental CO_2 breakthrough profiles (points) for steel monolith coated with a 11 μm zeolite film for flow rates of 1.00, 0.50 and 0.25 dm^3/min. Each breakthrough experiment was performed 5 times and the adsorbent was regenerated at 393 K between the adsorption cycles.

Table 3.12 Breakthrough data for the time to reach C/Co=0.5 and CO_2 adsorption capacity of the 3 and 11 μm films.

Structured Adsorbent	**Flow rate (dm^3/min)**		
	0.25	**0.50**	**1.00**
	time *t* to reach $C/C_0 = 0.5$		
Uncoated monolith	52.7	25.2	13.0
3 μm zeolite film	876	445	238
11 μm zeolite film	3659	1639	723
	CO_2 adsorption capacity *q* (mol CO_2/kg zeolite)		
3 μm zeolite film	2.6	2.7	2.9
11 μm zeolite film	3.1	2.8	2.5

The average adsorption capacity for the 3 and the 11 μm monoliths estimated using equation 4 is 2.8 mol CO_2/kg zeolite with a standard deviation of 0.2 mol CO_2/kg zeolite. This adsorption capacity is in-between the values of 2.5 and 3.6 reported by Rodrigues et al. [72] and Myers et al. [73], respectively. Furthermore, the adsorption capacity 2.8 mol CO_2/kg zeolite corresponds to 0.3 mmol CO_2/cm^3 adsorbent for the 11 μm monolith. This can be compared to the adsorption capacity for zeolite NaX beads, which is about 2.3 mmol CO_2/cm^3 adsorbent [46], i.e. about 8 times larger. Consequently, an 8 times larger column with an 11 μm film coated monolith will have the same adsorption capacity as a column filled with beads. Alternatively, an 8 times shorter cycle time may be used to separate the same amount of CO_2 per time.

In Figure 3.25, the breakthrough profile of the 11 μm film is compared with that of traditional NaX pellets filled in the same column. The column is now holding as much as 177 g pellets with approximately 10% binder material. The column is consequently loaded with about 159 g zeolite, i.e. 8 times larger mass of zeolite in line with the discussion above, It is clear that for the 11 μm film, the profile was very sharp compared to that for the pellets, that display a very dispersed breakthrough front. The times t to reach $C/C_0 = 0.5$ for the 11 μm film and the NaX pellets were 723 and 3256 s, respectively. Although the column holds an 8 times larger mass of NaX adsorbent, the time to reach $C/C_0 = 0.5$ is only 4.5 times longer. This is a result of the non-ideal adsorption performance of the pellets resulting in a very much dispersed breakthrough front. The column with pellets has not reached saturation even after 6000 s.

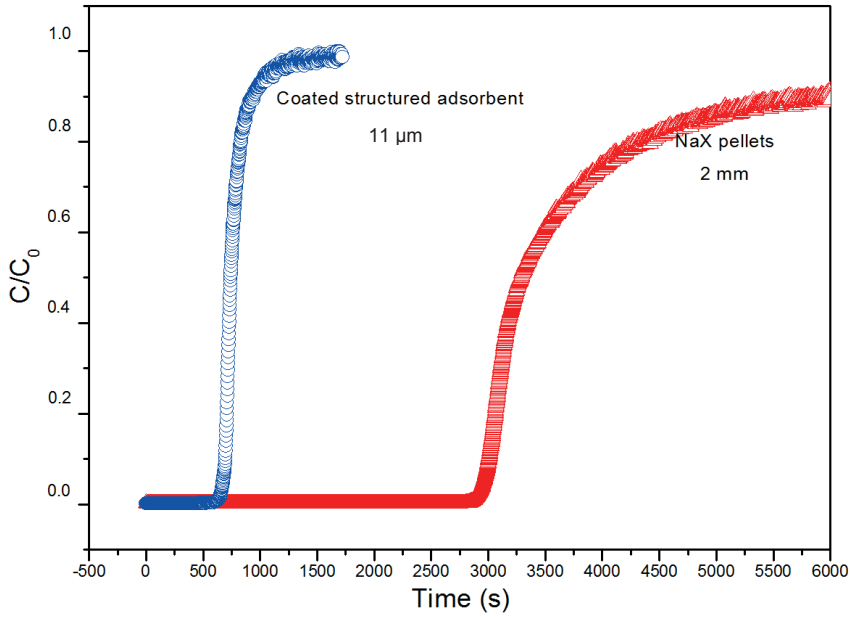

Figure 3.25 Experimental CO_2 breakthrough profiles for steel monolith coated with an 11 µm zeolite film (blue) and NaX pellets (red) for a flow rate of 1.00 dm^3/min. The column is the same but it holds an 8 times larger mass of zeolite when it is loaded with pellets.

The very sharp breakthrough fronts observed here confirms that nonporous steel monoliths are more suitable than porous cordierite monoliths to be used as a support for the zeolite films as suggested in earlier work [44]. The work also clearly shows that zeolite coated steel monoliths are promising alternatives to traditional adsorbents such as beads in processes with short cycle times.

Finally, the collected information regarding the synthesis protocols developed for FAU synthesis from diatomite (or montmorillonite) could be applied in the preparation of NaX films on structured adsorbents, also by using a natural alumina source, e.g. bohemite, bauxite.

CHAPTER 4 CONCLUSIONS

In this work, it was shown that Bolivian raw materials could be used as aluminosilica sources for the synthesis of zeolite A and zeolite Y with high yield and crystallinity. The main findings regarding each zeolite can be summarized as follows:

Zeolite A

- Zeolite A crystals with satisfactory size, morphology and cation exchange capacity were synthesized from Bolivian montmorillonite clay and commercial kaolinite.
- Addition of magnesium to the synthesis mixture was shown to mask the detrimental effect of Fe impurities on the whiteness and yellowness of the powder. This simple method might contribute to allow the use of natural raw materials to synthesize detergent-grade zeolite A.

Purification of diatomite

- As a purification step of diatomite, leaching with sulfuric or hydrochloric acid was shown to reduce the content of the main impurities comparatively to the same level, except for calcium.
- Diatomite leached by HCl was successfully used for the synthesis of ZSM-5 without the addition of extra source of neither silica nor alumina.

Synthesis of FAU zeolites

- Zeolite Y powders with different SiO_2/Al_2O_3 ratios were successfully synthesized from Bolivian diatomite, which was shown to behave closely as colloidal silica in traditional syntheses, both sources having in common a high degree of polymerization.
- It was possible to synthesize almost pure zeolite Y with a SiO_2/Al_2O_3 ratio of 5.3 suitable for FCC application. However, the yield was low, as the diatomite frustules were too bulky to be completely dissolved under the required low alkalinity.

- Overrun of all investigated compositions resulted in the formation of zeolite P nucleating and growing onto dissolving zeolite Y crystals.
- Addition of NaCl to the synthesis mixture of FAU-zeolites was found to completely inhibit the formation of zeolite P. This new finding may be used in order to speed up the synthesis process by increasing temperature of crystallization.

Additionally, zeolite NaX films were grown on nonporous steel monoliths as structured adsorbent and CO_2 separation was evaluated by breakthrough experiments:

- Steel monoliths coated with a zeolite film thickness of 11 μm were prepared for the first time. The films exhibited well intergrown zeolite NaX crystals free of sediments and undesirable secondary phases, e.g. hydroxysodalite.
- The CO_2 breakthrough fronts were very sharp and the mass transfer resistance was very low compensating the low zeolite loading, which should lead to reduced cycle time and higher cycle frequency and thereby increase throughput.
- This makes zeolite NaX coated steel monoliths a promising alternative to traditional adsorbents for CO_2 removal, which might constitute a future application for the use of Bolivian non-metallic raw materials.

CHAPTER 5 FUTURE WORK

This work has shown the feasibility of preparing valuable zeolites from non-costly Bolivian raw materials. However, there are still many challenges remaining to achieve the original goals of this project. Therefore, it would be necessary to:

- Tailor the synthesis procedure of zeolite A in order to achieve a SiO_2/Al_2O_3 ratio closer to 1.
- Test the catalytic and adsorption properties of the zeolites synthesized by the different procedures in order to assess their performances in the targeted applications.
- Investigate the technical-economical possibility of producing these zeolites on an industrial scale in order to contribute to the development of the poor regions in Bolivia.

The present work has also shown the promising characteristics of NaX structured adsorbents. Therefore, the following future work is recommended:

- A modeling study of the process is required for a better understanding of the parameters associated to the adsorption process (i.e. thermal effects).
- To develop an automated synthesis reactor in order to grow thicker films (i.e. 30 μm) and thereby approach the performance of the traditional beads in terms of adsorption capacity.
- Determining experimentally the maximum zeolite film thickness, at which the diffusion resistance starts to reduce the adsorption performance of a steel monolith.
- To test the feasibility of preparing NaX structured adsorbents from the Bolivian raw materials studied in this thesis work.

REFERENCES

[1] D.W. Breck, Synthesis and Properties of Union Carbide Zeolites L, X and Y, in: Conference at University of London, 1967, pp. 47-61.

[2] U. Zoller, P. Sosis, Handbook of Detergents: Part F, in: Handbook of Detergents, CRC Press 2008.

[3] J. Liu, J. Yu, Chapter 1 - Toward Greener and Designed Synthesis of Zeolite Materials A2 - Sels, Bert F, in: L.M. Kustov (Ed.) Zeolites and Zeolite-Like Materials, Elsevier, Amsterdam, 2016, pp. 1-32.

[4] S.M. Csicsery, Pure & Appl. Chem. 58 (1986) 841-856.

[5] R.A. Llenado, Use of sodium type A zeolite in laundry detergents, in: D. Olson, A. Bisio (Eds.), Proceedings of The Sixth International Zeolite Conference, Butterworths, Reno, Usa, 1984, pp. 940-956.

[6] Broni, Josip, Pal, Ana, Suboti, Boris, L. Itani, V. Valtchev, Materials Chemistry and Physics 132 (2012) 973-976.

[7] T. Nakano, Y. Nozue, Journal of Computational Methods in Sciences and Engineering 7 (2007) 443-462.

[8] C.A. Ríos R, J.A. Oviedo V, J.A. Henao M, M.A. Macías L, Catalysis Today 190 (2012) 61-67.

[9] C.A. Ríos, C.D. Williams, O.M. Castellanos, Ingeniería y competitividad 14 (2012) 125-137.

[10] S.B.C. Pergher, L.C.A. Oliveira, A. Smaniotto, D.I. Petkowicz, Química Nova 28 (2005) 751-755.

[11] L. Zhang, H. Liu, X. Li, S. Xie, Y. Wang, W. Xin, S. Liu, L. Xu, Fuel Processing Technology 91 (2010) 449-455.

[12] T. Li, H. Liu, Y. Fan, P. Yuan, G. Shi, X.T. Bi, X. Bao, Green Chemistry 14 (2012) 3255-3259.

[13] M. Mezni, A. Hamzaoui, N. Hamdi, E. Srasra, Applied Clay Science 52 (2011) 209-218.

[14] D. Boukadir, N. Bettahar, Z. Derriche, Annales de Chimie - Science des Matériaux 27 (2002) 1-13.

[15] B. Ghosh, D.C. Agrawal, S. Bhatia, Industrial and Engineering Chemistry Research 33 (1994) 2107-2110.

[16] K. Abdmeziem-Hamoudi, B. Siffert, Applied Clay Science 4 (1989) 1-9.
[17] H. Murray, Clay Minerals 34 (1999) 39-49.
[18] R.M. Barrer, Hydrothermal Chemistry of Zeolites, London, 1982.
[19] S. Chandrasekhar, Clay Minerals 31 (1996) 253-261.
[20] S.É. Ivanov, A.V. Belyakov, Glass and Ceramics (English translation of Steklo i Keramika) 65 (2008) 48-51.
[21] V.S. Fajnor, K. Jesenak, Journal of Thermal Analysis and Calorimetry 46 (1996) 489-493.
[22] X. Liu, C. Yang, Y. Wang, Y. Guo, Y. Guo, G. Lu, Chemical Engineering Journal 243 (2014) 192-196.
[23] M. Murat, A. Amokrane, J.P. Bastide, L. Montanaro, Clay Minerals 27 (1992) 119-130.
[24] P. Fruijtier, ouml, C. lloth, C. lloth, Archives of Toxicology 83 (2009) 23-35.
[25] R.P. Denkewicz, Jr., A. Monino, D. Russ, H. Sherry, J Am Oil Chem Soc 72 (1995) 31-35.
[26] S. Chandrasekhar, P.N. Pramada, Journal of Porous Materials 6 (1999) 283-297.
[27] E. Costa, A. De Lucas, M.A. Uguina, J.C. Ruiz, Industrial and Engineering Chemistry Research 27 (1988) 1291-1296.
[28] R. Asmatutu, Turkish Journal of Engineering & Environmental Sciences 26 (2002) 447-453.
[29] R.J. Pruett, Minerals and Metallurgical Processing 29 (2012) 27-35.
[30] C. Poole, H. Prijatama, N.M. Rice, Minerals Engineering 13 (2000) 831-842.
[31] R.B. Scorzelli, L.C. Bertolino, A.B. Luz, M. Duttine, F.A.N.G. Silva, P. Munayco, Clay Minerals 43 (2008) 129-135.
[32] P. Sengupta, N.J. Saikia, D.J. Bharali, P.C. Saikia, P.C. Borthakur, Current Science 91 (2006) 86-90.
[33] V.R. Ambikadevi, M. Lalithambika, Applied Clay Science 16 (2000) 133-145.
[34] F.K. Sutili, N. Miotto, E. Rigoti, S.B.C. Pergher, F. Penha, aacute, G. bio, Química Nova 32 (2009) 879-883.
[35] E.l. Basaldella, R.M.T. Sanchez, J.C. Tara, Clays and Clay Minerals 46 (1998) 481-486.
[36] S. Chandrasekhar, P. Raghavan, G. Sebastian, A.D. Damodaran, Applied Clay Science 12 (1997) 221-231.
[37] K. Smith, G.A. El-Hiti, Green Chemistry 13 (2011) 1579-1608.

[38] P. Morales-Pacheco, J.M. Domínguez, L. Bucio, F. Alvarez, U. Sedran, M. Falco, Catalysis Today 166 (2011) 25-38.
[39] G. García, M. Falco, P. Crespo, S. Cabrera, U. Sedran, Catalysis Today 166 (2011) 60-66.
[40] Q. Tan, X. Bao, T. Song, Y. Fan, G. Shi, B. Shen, C. Liu, X. Gao, Journal of Catalysis 251 (2007) 69-79.
[41] S. Cavenati, C.A. Grande, A.E. Rodrigues, Journal of Chemical & Engineering Data 49 (2004) 1095-1101.
[42] S.-T. Yang, J. Kim, W.-S. Ahn, Microporous and Mesoporous Materials 135 (2010) 90-94.
[43] J.A. Dunne, R. Mariwala, M. Rao, S. Sircar, R.J. Gorte, A.L. Myers, Langmuir 12 (1996) 5888-5895.
[44] F. Rezaei, P. Webley, Separation and Purification Technology 70 (2010) 243-256.
[45] A. Mosca, Structured Zeolite Adsorbents for PSA Applications, in: LTU, Lulea, 2009.
[46] F. Rezaei, A. Mosca, J. Hedlund, P.A. Webley, M. Grahn, J. Mouzon, Separation and Purification Technology 81 (2011) 191-199.
[47] A. Mosca, J. Hedlund, P.A. Webley, M. Grahn, F. Rezaei, Microporous and Mesoporous Materials 130 (2010) 38-48.
[48] F. Rezaei, A. Mosca, P. Webley, J. Hedlund, P. Xiao, Industrial & Engineering Chemistry Research 49 (2010) 4832-4841.
[49] http://www.emitec.com/en/emitec/, in.
[50] K. Rangsriwatananon, A. Chaisena, C. Thongkasam, Journal of Porous Materials 15 (2008) 499-505.
[51] A. Mosca, J. Hedlund, P.A. Webley, M. Grahn, F. Rezaei, Microporous and mesoporous materials 130 (2010) 38-48.
[52] C.H. Rüscher, J. -Chr. Buhl, W. Lutz, in: A. Galarneau, F.D. Renzo, F. Fajula, J. Vedrine (Eds.), Zeolites and Mesoporous Materials at the Dawn of the 21 st Century, Stud. Surf. Sci. Cat., vol 135, Elsevier, Amsterdam, 2001, pp. 1, 13-P15.
[53] J.S. Udhoji, A.K. Bansiwal, S.U. Meshram, S.S. Rayalu, Journal of Scientific and Industrial Research 64 (2005) 367-371.
[54] L. Gora, K. Streletzky, R.W. Thompson, G.D.J. Phillies, Zeolites 18 (1997) 119-131.

[55] A. Zegeye, S. Yahaya, C.I. Fialips, M.L. White, N.D. Gray, D.A.C. Manning, Appl Clay Sci 86 (2013) 47-53.
[56] S. Mendioroz, M.J. Belzunce, J.A. Pajares, Journal of Thermal Analysis 35 (1989) 2097-2104.
[57] X. Wang, L. Yang, X. Zhu, J. Yang, Particuology 17 (2014) 42-48.
[58] S. Hansen, U. Håkansson, A.R. Landa-Canovas, L. Falth, Zeolites 13 (1993) 276-280.
[59] F.G. Dwyer, P. Chu, Journal of Catalysis 59 (1979) 263-271.
[60] H.W. Zandbergen, D. van Dyck, The Use of High Resolution Electron Microscopy in Fundamental Zeolite Research, in: vol 49, 1989, pp. 599-608.
[61] T.J. Weeks Jr, D.E. Passoja, Clays and Clay Minerals 25 (1977) 211-213.
[62] J.F. Tempere, D. Delafosse, J.P. Contour, Chemical Physics Letters 33 (1975) 95-98.
[63] C.H. Rüscher, N. Salman, J.C. Buhl, W. Lutz, Microporous and Mesoporous Materials 92 (2006) 309-311.
[64] S.P. Zhdanov, Molecular Sieves, Society of Chemical Industry, London, 1968.
[65] H. Lechert, H. Kacirek, H. Weyda, Molecular Sieves, Van -Nostrand Reinhold, New York, 1992.
[66] F. Delprato, L. Delmotte, J.L. Guth, L. Huve, Zeolites 10 (1990) 546-552.
[67] G. García, W. Aguilar-Mamani, I. Carabante, S. Cabrera, J. Hedlund, J. Mouzon, Journal of Alloys and Compounds 619 (2015) 771-777.
[68] B. Subotic, J. Bronic, R.v. Ballmoos, J.B. Higgins, M.M.J., in: Proc. 9th Int. Zeolite Conf., Butterworth-Heinemann, Treacy (Eds.), 1993, p. 321.
[69] X. Liu, L. Li, T. Yang, Z. Yan, Shiyou Xuebao, Shiyou Jiagong/Acta Petrolei Sinica (Petroleum Processing Section) 28 (2012) 555-560.
[70] Y. Zhan, X. Li, Y. Zhang, L. Han, Y. Chen, Ceramics International 39 (2013) 5997-6003.
[71] S.N. Azizi, A. Alavi Daghigh, M. Abrishamkar, Journal of Spectroscopy 2013 (2013) 5.
[72] S. Cavenati, C.A. Grande, A.E. Rodrigues, J. Chem. Eng. Data 49 (2004) 1095-1101.
[73] J.A. Dunne, M. Rao, S. Sircar, R.J. Gorte, A.L. Myers, Langmuir 12 (1996) 5896-5904.

Paper I

Preparation of zeolite A with excellent optical properties from clay

Gustavo García, Wilson Aguilar, Ivan Carabante, Saúl Cabrera, Jonas Hedlund, Johanne Mouzon

Journal of Alloys and Compounds 619 (2015) 771–7

Journal of Alloys and Compounds 619 (2015) 771–777

Contents lists available at ScienceDirect

Journal of Alloys and Compounds

journal homepage: www.elsevier.com/locate/jalcom

Preparation of zeolite A with excellent optical properties from clay

Gustavo García [a,b,*], Wilson Aguilar-Mamani [a,c], Ivan Carabante [a], Saúl Cabrera [b], Jonas Hedlund [a], Johanne Mouzon [a]

[a] Chemical Technology, Luleå University of Technology, 971 87 Luleå, Sweden
[b] Chemistry Research Institute IIQ, Higher University of San Andrés, La Paz, Bolivia
[c] Department of Chemistry, Faculty of Science and Technology, San Simon University, Cochabamba, Bolivia

ARTICLE INFO

Article history:
Received 27 May 2014
Received in revised form 1 September 2014
Accepted 8 September 2014
Available online 16 September 2014

Keywords:
Oxide materials
Amorphous material
Chemical synthesis
Exchange
Optical properties
Scanning electron microscopy

ABSTRACT

Discoloration of zeolite A powder is a common problem when natural raw materials such as kaolin clay are used because of the formation of colored iron compounds. In this study, we report on a novel method to produce zeolite A with excellent optical properties, from clays. The brightness is as high as 94.5 and the yellowness is as low as 3.0. The product is comprised of intergrown zeolite A crystals with cubic habit and a length ranging between 0.5 and 2 μm. Good optical properties are obtained when the raw material contains magnesium, as some natural raw materials do, or alternatively, when a magnesium compound is added to the raw material. Magnesium probably forces iron inside colorless extraneous magnesium aluminosilicate compounds. This simple process appears very promising for the preparation of zeolite A with good optical properties from inexpensive natural raw materials.

1. Introduction

Zeolite A, LTA (Linde Type A) or 4A is a synthetic sodium aluminosilicate. It is a low silica zeolite represented by the formula: $Na_{12}[(AlO_2)_{12}(SiO_2)_{12}]\cdot 27H_2O$. The crystal structure is cubic with a lattice parameter of 12.32 Å. Zeolite A is characterized by a 3-dimensional network consisting of spherical cavities of 11.4 Å in diameter separated by circular openings of 4.2 Å in diameter [1]. It has a high cation exchange capacity as each alumina tetrahedral in the framework introduces a negative charge that must be compensated by a cation. This property confers to zeolite A water softening abilities by ion exchanging Ca^{2+} and to a lesser extent Mg^{2+} for Na^{+}, thereby preventing precipitation of calcium compounds. Therefore, the most important application of zeolite A is as a detergent builder [2,3].

For zeolite to be used as a detergent grade builder, there are various requirements set on the size of the particles, crystal shape, cation exchange capacity (CEC) and brightness. The optimal range for particle size is 1–10 μm [4]. Crystal sizes smaller than 1 μm may be retained in damaged textile fibers, while particles over 10 μm in size cause unacceptable deposition in textile materials, fabric and machine parts [5]. Incrustation of textiles can be reduced by achieving appropriate morphology of the crystals. Zeolite A crystals with sharp edges can be entangled in textile fibers. In contrast, zeolite A with rounded corners and edges tend to decrease incrustation on textile materials. Besides, the CEC of detergent builders must be as high as possible with 510 meqCa^{2+}/100 g of anhydrous solid being a recommended minimum [6] and 592 meqCa^{2+}/100 g the highest achievable value at 294.1 K and 1000 ppm [7]. Another important property of a detergent builder is the optical brightness which has to be at least 90% of the ISO reflectance measured on $BaSO_4$ or MgO.

Pure chemical grade reagents are mostly used to produce materials which fulfill all the aforementioned requirements. Concerns about energy consumption, carbon economy and production costs have called the attention of researchers to seek cheaper raw materials for zeolite synthesis [8,9]. Many studies have been published on the synthesis of zeolite A from raw materials such as kaolin, diatomite, bentonite, fly ash, or smectite [10–14]. Kaolin is of particular interest because it possesses the appropriate SiO_2/Al_2O_3 ratio that matches the composition of zeolite A [15]. Kaolin has been widely investigated for the synthesis of zeolites and the effect of different factors affecting the synthesis process was extensively reported [16,17]. However, kaolin must be activated in the form of metakaolin by calcination at high temperature in the range 773–1273 K in order to produce an amorphous material that can be easily digested during zeolite synthesis [18,19].

* Corresponding author at: Chemical Technology, Luleå University of Technology, 971 87 Luleå, Sweden. Tel.: +46 0920 49 25 02; fax: + 46 0920 49 13 99.
E-mail addresses: gustavo.garcia@ltu.se, gusygarmen@hotmail.com (G. García).

http://dx.doi.org/10.1016/j.jallcom.2014.09.080
0925-8388/

The properties of zeolite A produced from metakaolin in terms of CEC, particle size and morphology were found to be adequate for use as detergent builder. However, problems associated with brightness and yellowness and related to the iron content are usually encountered when using kaolin for zeolite production [20,21]. Various techniques for removal of iron have been investigated [22] such as selective flocculation [23,24], magnetic separation [25,26], acid leaching [27,28], optimum temperature for metakaolinization [18] and chemical removal treatments [29]. As an example, Chandrasekhar [22] managed to reduce the amount of Fe_2O_3 in the final zeolite product from 0.59% to 0.04% starting with a Chinese kaolin containing 0.69% Fe_2O_3 by a combination of treatments, i.e. clay refining, control of alkali concentration, complexing and washing with alkaline water. Dramatic improvement of the optical properties of the final zeolite A product were observed, the brightness increased from 72.9% to 81.7% and yellowness reduced from 11.5% to 7.8%. However, these separation procedures represent additional costs to the general process.

Use of other types of clays than kaolin as raw materials for the synthesis of zeolite A might result in brightness improvement. However, natural clays based on 2:1 phyllosilicate clays usually contain quartz and do not produce a reactive product such as metakaolin upon calcination. The energy used for the metakaolinization heat treatment can be used with advantage to fuse raw materials containing quartz under the action of the sodium required for zeolite synthesis. It is known that through alkali activation, large amounts of aluminosilicates can be transformed into more soluble species [30,31].

In this study, we report on a novel method to improve brightness in zeolite A prepared by alkali fusion from natural clays, namely Bolivian montmorillonite and commercial kaolinite clays.

2. Experimental section

2.1. Materials

Montmorillonite-type clay sampled from the Rio Mulatos zone (Potosi, Bolivia) and commercial kaolin (Riedel de Haën, pro analysis) were used as aluminosilicate sources. Sodium hydroxide was employed in the form of pellets (NaOH, Sigma Aldrich, p.a., ⩾98%). Anhydrous sodium aluminate in powder form ($NaAlO_2$, Riedel-de Haën, p.a., Al_2O_3 50–56%, Na_2O 40–45%) was used to adjust the SiO_2/Al_2O_3 ratio to that of typical synthesis mixtures for zeolite A. Calcium nitrate ($Ca(NO_3)_2 * 4H_2O$, Merck) and magnesium nitrate ($Mg(NO_3)_2 * 6H_2O$, Merck) were utilized to investigate the influence of Ca and Mg on the color properties of alkali-activated kaolin, while ion exchange was carried out with sodium nitrate ($NaNO_3$, Merck). Commercial zeolite A powder (Akzo Nobel) was used as a reference. Barium sulfate ($BaSO_4$, Sigma Aldrich, p.a. 99%) was used as a standard for brightness and yellowness measurements.

2.2. Synthesis procedure

The initial SiO_2/Al_2O_3 molar ratio of the Rio Mulatos clay (RMA) was 4.9 (see Table 1). Hence an additional amount of sodium aluminate was required to decrease this ratio to the proper value. $NaAlO_2$ and NaOH provided the aluminum and sodium to set both the SiO_2/Al_2O_3 and Na_2O/SiO_2 ratios to 2. RMA clay was added to sodium aluminate and sodium hydroxide in calculated proportions and the mixture was carefully crushed in an agate mortar until a homogeneous powder was obtained. The crushed powder was placed in a platinum crucible and heated at 873 K for 1 h using a heating rate of 10 K/min. The resultant mixture was crushed again, dispersed in distilled water and stirred for 6 h in an aging step. In the case of kaolin (KFA), the same procedure was used without the addition of sodium aluminate. The molar ratio of the components in the mixtures was $SiO_2/Al_2O_3 = X$, $Na_2O/SiO_2 = 2$ and $H_2O/Na_2O = 40$ with X varying between 2.0 and 1.15. After the aging period, the reaction mixture was transferred to Teflon-lined autoclaves and heated at 373 K for different times in order to perform optimization of the hydrothermal treatment. Subsequently, the autoclave was quenched in cold water to stop the reaction. The solid products were repeatedly washed and filtered in distilled water until pH in the filtrate liquid reached 8–9. The products were dried at 373 K overnight. The prepared samples were denoted according to the type of clay that was used, namely RMA or KFA, followed with the molar SiO_2/Al_2O_3 ratio within brackets and synthesis time, e.g. RMA(2.0)-3 h corresponded to a sample obtained from a mixture with a molar SiO_2/Al_2O_3 ratio of 2.0 using Rio Mulatos clay after 3 h of synthesis.

2.3. Apparatus

To determine the chemical composition of the clays, fused clays and synthetic zeolite products, inductively coupled plasma-sector field mass spectrometry (ICP-SFMS) was used. For the analysis, 0.1 g sample was digested with 0.375 g of $LiBO_2$ and dissolved in HNO_3; LOI (loss on ignition) was performed at 1273 K. The mineralogical composition of the raw materials and products were determined by X-ray diffraction (XRD) using a PANalytical Empyrean X-ray diffractometer, Cu Kα1 radiation with $\lambda = 1.540598$ Å at 45 kV and 40 mA in the range of $2\theta = 5–50°$ at a scanning speed of 0.026°/s. The peaks observed in the diffractograms were compared with the existing pattern of known materials from the powder diffraction files (PDF). The morphology of the raw materials, intermediate products and final products were studied by extreme high resolution-scanning electron microscopy

Table 1
Main components of the raw materials.

Material	Main components (wt.%)								Molar ratio
	SiO_2	Al_2O_3	Fe_2O_3	Na_2O	CaO	K_2O	MgO	LOI	SiO_2/Al_2O_3
RMA	63.75	21.95	0.82	0.71	3.19	0.46	4.64	7.20	4.90
KFA	54.43	42.87	0.79	0.13	0.07	1.41	0.30	12.20	2.20

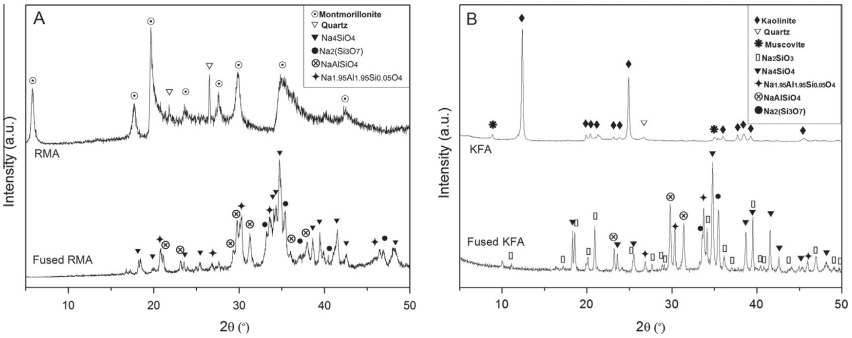

Fig. 1. XRD diffractograms of (A) RMA and fused RMA and (B) KFA and fused KFA samples.

(XHR-SEM Magellan 400, the FEI Company) at low accelerating voltage without conductive coating. Energy dispersive spectroscopy (EDS, X-max detector 50 mm^2, Oxford Instruments) was also performed to establish the overall composition of the final products and to gain compositional information about individual zeolite A crystals and extraneous phases. EDS analysis was carried out at 10 kV on a SEM equipped with a microinjector (Merlin SEM, Carl Zeiss) in order to mitigate charging by blowing nitrogen gas close to the surface of samples. The concentration of Na, Mg, Al and Si was measured at low magnification (100 times) to avoid diffusion of Na, while the concentration of Ca was measured locally in 10 individual crystals. Brightness and yellowness were measured on a spectrometer using an integrating sphere (Perkin Elmer Lambda 2SUV/VIS). The results were expressed in percentage of the reflectance obtained for the Ba_2SO_4 powder [32]. Brightness was measured at 457 nm, while the difference between the reflectance measured at 570 and 457 nm yielded a measure for yellowness.

The number of equivalents-gram was calculated for Ca^{2+} in each case. The total exchange equivalents for Ca^{2+} was assessed by subtracting the amount of equivalents of Ca^{2+} present for the initial to the final number of equivalents of Ca^{2+} after the exchanged process.

3. Results

3.1. Synthesis of zeolite A by alkali fusion

The diffractogram of the raw RMA clay (Fig. 1A) shows the characteristic peaks of montmorillonite at $2\theta = 5.9$, 19.8 and 35° as compared with PDF patterns, but also the occurrence of quartz in low content. Raw kaolin (KFA in Fig. 1B) contains mostly kaolinite as evidenced by reflections at $2\theta = 12.33$; 19.80; 20.40; 21.40; 24.81 and 35.11, but also traces of quartz and muscovite ($2\theta = 8.83$; 35.06). The elemental compositions of the RMA and KFA clays obtained by ICP-SFMS are given in Table 1. Apart from silica and alumina, calcium and magnesium were present in appreciable amounts in the Bolivian montmorillonite in comparison to kaolin. However, both clays contained similar amounts of iron, i.e. 0.79–0.82 wt.% Fe_2O_3.

During alkali fusion at 873 K montmorillonite and quartz, as well as kaolin, suffered a structural reorganization. Fused RMA and fused KFA resulted in formation of various sodium aluminosilicates, i.e. Na_4SiO_4, Na_2SiO_3, $Na_2(Si_3O_7)$, $NaAlSiO_4$, $Na_{1.95}Al_{1.95}Si_{0.05}O_4$ by the XRD data shown in Fig. 1A and B. All compounds formed after alkali fusion of the starting clays could be readily dissolved in water and serve as reactants for zeolite synthesis in combination with sodium aluminate and sodium hydroxide.

Fig. 2 shows the XRD diffractograms of the final products after hydrothermal treatment at 373 K after different synthesis times. When a molar SiO_2/Al_2O_3 ratio of two was used, 3 and 4 h of hydrothermal treatment was required to obtain zeolite A as a unique product with high crystallinity for the RMA and KFA clays, respectively (RMA(2.0)-3 h and KFA(2.0)-4 h in Fig. 2A and C respectively). Samples obtained at longer times did not exhibit appreciable changes either in intensity or morphology (RMA(2.0)-4 h and RMA(1.8)-4 h in Fig. 2A and B, respectively). Samples obtained after shorter synthesis times still contained appreciable amounts of amorphous material, which can be attributed to geopolymers [33] (RMA(2.0)-2 h in Fig. 2A; KFA(2.0)-3 h and KFA(2.0)-2 h in Fig. 2C). In sample KFA(2.0)-3 h, a small amount of zeolite *X* was found. However, it was barely noticeable at longer times (KFA(2.0)-4 h). Table 2 shows the overall SiO_2/Al_2O_3 ratios of the final products determined by EDS. RMA(2.0)-3 h was found to contain an excess of silica with a SiO_2/Al_2O_3 ratio of 2.36 compared to the ideal ratio of 2.0 in terms of cation exchange capacity. Therefore, the molar SiO_2/Al_2O_3 ratio in the RMA synthesis mixture was varied in the range 1.15–2.0. Decreasing this ratio from 2 to 1.8 resulted in a slight decrease of the SiO_2/Al_2O_3 ratio in the product to 2.22, see RMA(1.8)-3 h in Table 2 and also Fig. 2B. However, it was not possible to lower the ratio in the product further by increasing the amount of aluminum in the synthesis mixture. Instead, this resulted in a steady decrease in crystal size, while the SiO_2/Al_2O_3 ratio in the product was almost constant.

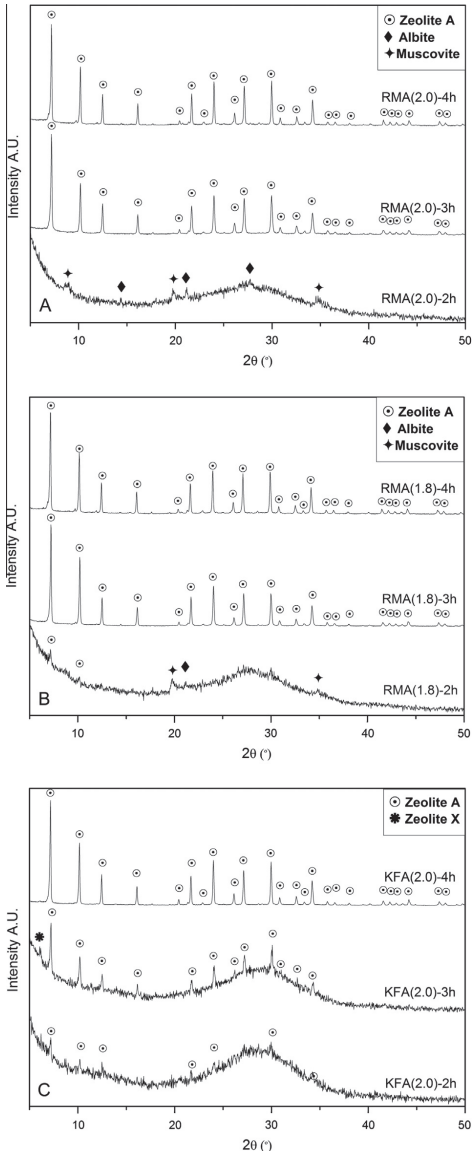

Fig. 2. XRD diffractograms of the (A) RMA(2.0); (B) RMA(1.8) and (C) KFA(2.0) series.

The RMA sample prepared with a molar SiO_2/Al_2O_3 ratio of 1.8 were also mainly amorphous for synthesis times shorter than 3 h, e.g. RMA(1.8)-2 h in Fig. 2B.

3.2. Size and morphology of the particles

Fig. 3 shows SEM micrographs of RMA(1.8)-3 h, KFA(2.0)-4 h and the commercial powder.

Table 2
Compositional ratios in the final products determined by EDS.

Sample	Ion exchange	SiO_2/Al_2O_3	Na/Al	2Ca/Al	2 Mg/Al	(Na + 2Ca)/Al
Commercial	–	2.08	0.99	n.d.	n.d.	0.99
RMA(2.0)-3 h	–	2.36	0.87	0.11	0.18	0.98
RMA(1.8)-3 h	–	2.22	0.90	0.12	0.19	1.02
RMA(1.8)-3 h	Na	2.28	0.93	0.03	0.18	0.96
KFA(2.0)-4 h	–	2.22	0.97	0.01	0.01	0.98
KFA(2.0)Mg-4 h	–	2.16	0.99	n.d.	0.16	0.99
KFA(2.0)Mg-4 h	Na	2.28	0.98	0.01	0.16	0.99

n.d. (non-detected).

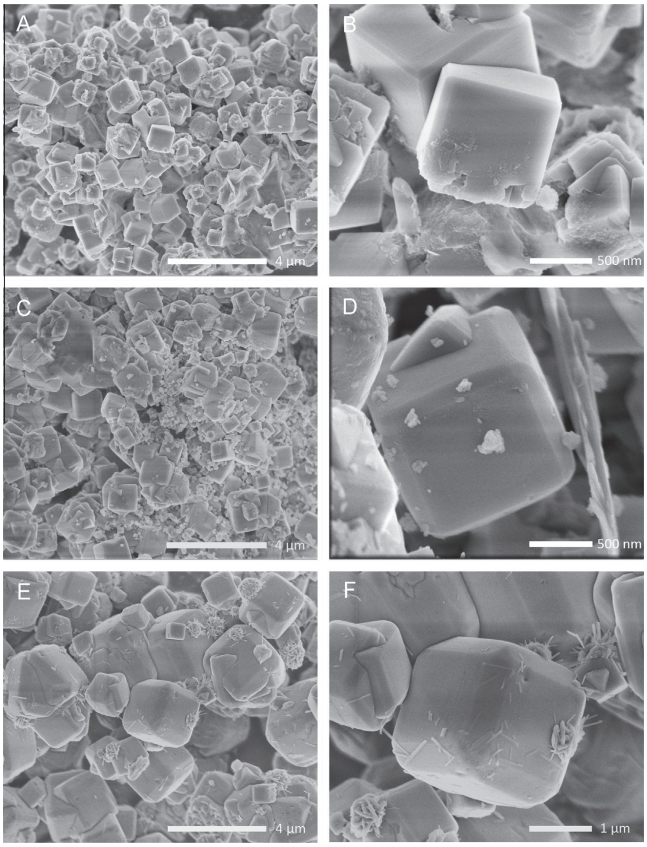

Fig. 3. SEM micrographs of: (A)–(B) RMA(1.8)-3 h; (C)–(D) KFA(2.0)-4 h; (E)–(F) commercial zeolite A.

Table 3
Brightness and yellowness properties.

Sample	Brightness	Yellowness
Commercial powder	92.6	3.8
RMA(1.8)-3 h	94.5	3.04
KFA(2.0)-4 h	76.4	14.4
KFA(2.0)Ca-4 h	73.7	11.5
KFA(2.0)Mg-4 h	82.1	5.4
KFA(2.0)MgCa-4 h	85.6	5.2

As shown in Fig. 3A, RMA(1.8)-3 h consisted of cubic crystals ranging between 0.5 and 1.5 μm in length. Part of the crystals exhibited intergrowth, which is usually rationalized by a high concentration of nuclei [34]. Fig. 3B reveals that the largest crystals possessed chamfered edges, which is suitable for detergent grade zeolites. The zeolite crystals of the KFA(2.0)-4 sample showed similar characteristics, except for a slight increase in length to approximately 1–2 μm (Fig. 3C and D). Comparatively, the crystals in the commercial powder were found to measure between 1 and 7 μm in length (Fig. 3E) and to be relatively intergrown (Fig. 3F).

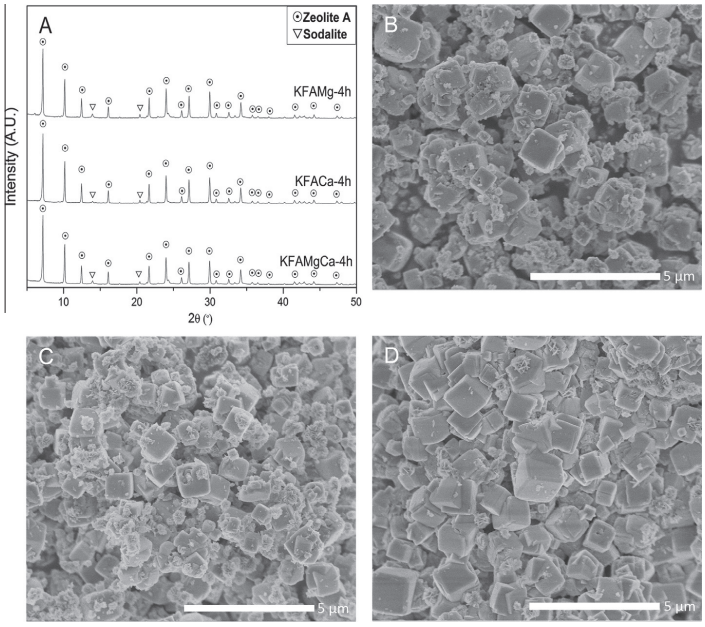

Fig. 4. (A) XRD diffractograms of the final products obtained from KFA after 4 h synthesis with addition of Ca, Mg and Ca–Mg and SEM micrographs showing: (B) KFA(2.0)Ca-4 h; (C) KFA(2.0)Mg4 h and (D) KFA(2.0)MgCa-4 h.

3.3. Brightness measurements

Table 3 shows the results of the brightness and yellowness measurements which were performed on RMA(1.8)-3 h, KFA(2.0)-4 h and the commercial powder. With 94.5% brightness and 3.0% yellowness, the sample obtained from Rio Mulatos clay after optimal synthesis time (RMA(1.8)-3 h) showed excellent optical properties. These values were superior to those of the commercial powder, which exhibited 92.6% brightness and 3.8% yellowness. In comparison, the sample produced from commercial kaolin was found to exhibit a slight orange color to the naked eye. This was confirmed by the poor brightness and relatively high yellowness values obtained for KFA(2.0)-4 h in Table 3, i.e. 76.4% and 14.4%, respectively. These values are typical of zeolite A powder synthesized from metakaolin. Therefore, the method to activate kaolin did not seem to influence the final color of the zeolite A powder.

3.4. Cation exchange capacity

As shown in Table 2, the commercial zeolite A and KFA(2.0)-4 h samples were completely in sodium form, as evidenced by the Na/Al ratios which were estimated to be 0.99 and 0.97, respectively. However, the as synthesized samples obtained by alkali fusion of Rio Mulatos clay were not completely in sodium form but also contained calcium ions that occupied approximately 11–12% of the sites. With regard to cation exchange capacity (CEC), 84% of the exchangeable sites of zeolite A can be compensated by Ca^{2+} cations at 294 K, which represents 592 meq Ca^{2+}/100 g anhydrous solid. Considering the final SiO_2/Al_2O_3 and 2Ca/Al ratios measured on the RMA(2.0)-3 h and RMA(1.8)-3 h samples by EDS, maximum CEC values of 480–487 meq Ca^{2+}/100 g anhydrous solid could be anticipated for these samples. As a matter of fact, loss-on-ignition and ICP-SFMS measurements on the calcium ion exchanged RMA(2.0)-3 h sample yielded a value of 487 meq Ca^{2+}/100 g anhydrous solid. The RMA(1.8)-3 h sample was ion exchanged with sodium nitrate to verify that the calcium ions were exchangeable. As shown in Table 2, the 2Ca/Al ratio was reduced from 0.12 to 0.03, which showed that this is the case.

It is noteworthy that all samples investigated in Table 2 showed (Na + 2Ca)/Al ratios very close to 1.0 in Table 2. This reflects the validity of the quantitative EDS method developed in this work. It was indeed found to be more reliable than ICP-SFMS because of the large error margin of the latter, which brought too much uncertainty on the elements present in large amounts.

4. Discussion

Usually, the poor brightness and yellowness of zeolite A powders synthesized from kaolin are attributed to formation of colored iron precipitates (e.g. iron(III) hydroxide) during the aging step and the crystallization process [35]. The iron content was found to be 0.44 and 0.54 wt.% by ICP-SFMS in the RMA(1.8)-3 h and KFA(2.0)-4 h samples, respectively. Although these amounts were similar and both samples were synthesized by the same method, the corresponding final zeolite products showed very different optical properties in terms of brightness and yellowness.

Referring to Table 1, the major compositional difference between the two raw materials investigated in this work was the high content in calcium and magnesium in Rio Mulatos clay. These elements were still present in appreciable amounts in the final products as shown by the EDS results in Table 2. Therefore, the difference in optical properties was first attributed to a positive effect of one of these (or both) elements. In order to test this hypothesis, amounts of calcium and magnesium similar to those present in

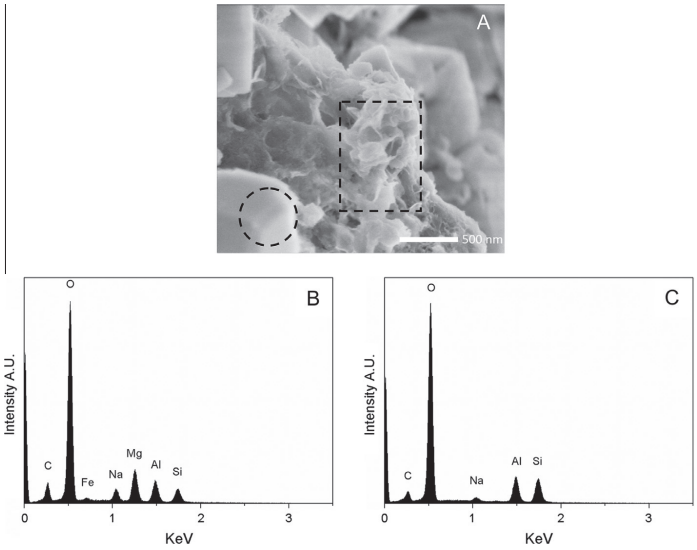

Fig. 5. (A) SEM micrograph of extraneous matter of RMA(1.8)-3 h; EDS analysis of (B) Extraneous matter (dotted square in A) and (C) Zeolite A crystal (dotted circle in A).

RMA clay were added to the synthesis mixture based on KFA clay before alkali fusion using nitrates. Three new products were obtained and denoted KFA(2.0)Ca-4 h, KFA(2.0)Mg-4 h and KFA(2.0)MgCa-4 h depending on whether only calcium or magnesium or both elements were added, respectively. According to the XRD patterns (Fig. 4A), these new products consisted of zeolite A with minor contents of sodalite (~5%). Based on the SEM results in Fig. 4B, C and D, these samples exhibited similar morphologies and consisted of cubic crystals with rounded edges ranging between 0.75 and 1.5 μm in length with a few intergrown crystals. The presence of small amounts of flower shaped crystals was attributed to sodalite. The results in Table 3 showed that the addition of solely calcium slightly improved yellowness. Interestingly, addition of magnesium to kaolin before alkali fusion remarkably enhanced the optical properties of the final powder, independently of whether calcium was added or not. The corresponding brightness and yellowness values were higher than those obtained by Chandrasekhar and colleagues [22] who employed a complex combination of chemical treatments to reduce the amount of Fe_2O_3 in the final zeolite product to 0.04 wt.%.

The results in Table 2 indicated that, in contrast to calcium, magnesium was not ion-exchanged by sodium when exposed to a solution of sodium nitrate, which was consistent with the fact that solvated magnesium ions can barely diffuse into zeolite A. In addition, the fact that all values of the (Na + 2Ca)/Al ratio were close to 1 strongly suggested that magnesium was not located inside zeolite A. As a matter of fact, Mg could not be detected by local EDS inside zeolite A crystals. This is illustrated by the EDS spectrum of Fig. 5B, which was obtained by point analysis in a zeolite A crystal, i.e. the encircled region in Fig. 5A. Instead, Mg and Fe were found to be concentrated in the extraneous material consisting of platelets and finely divided matter as revealed in the region delimited by the rectangle in Fig. 5A and the corresponding EDS spectrum in Fig. 5C. Consequently, our data strongly suggest that magnesium exerts a masking effect on iron by incorporating the latter inside magnesium aluminosilicate compounds with low coloration. This simple method appears as a promising alternative to complex and costly techniques developed in order to reduce the iron content in natural raw materials.

5. Conclusions

Zeolite A crystals were successfully synthesized from Bolivian montmorillonite type clay and commercial kaolinite using the alkali fusion method. The crystals had cubic habit with a length ranging between 0.5 and 2 μm and intergrown. Although Bolivian montmorillonite and commercial kaolinite contained similar concentration of iron, they radically differed in terms of optical properties. This was attributed to the magnesium present in the Bolivian raw material, which probably forced iron inside colorless extraneous magnesium aluminosilicate compounds. The effect was verified by addition of magnesium to kaolinite. This simple process appears very promising to prepare zeolite A with excellent optical properties from inexpensive natural raw materials.

Acknowledgments

The financial support by the Swedish Institute in the SIDA Program is acknowledged. Financial support from Bio4energy is also acknowledged. The authors also wish to thank The Knut and Alice Wallenberg Foundation for financial support with the Magellan SEM instrument.

References

[1] Josip Broni, Ana Pal, Boris Suboti, L. Itani, V. Valtchev, Influence of alkalinity of the starting system on size and morphology of the zeolite A crystals, Mater. Chem. Phys. 132 (2012) 973–976.
[2] A. de Lucas, M.A. Uguina, I. Covian, L. Rodriguez, Use of Spanish natural clays as additional silica sources to synthesize 13X zeolite from kaolin, Ind. Eng. Chem. Res. 32 (1993) 1645–1650.
[3] F.K. Sutili, N. Miotto, E. Rigoti, S.B.C. Pergher, F.G. Penha, Aplicação de zeólitas sintéticas como coadjuvante em formulação detergente, Quim. Nova 32 (2009) 879–883.
[4] C. Fruijtier-Pölloth, The safety of synthetic zeolites used in detergents, Arch. Toxicol. 83 (2009) 23–35.

[5] Z. Dragcevic, B. Subotic, J. Bronic, Effect of zeolites in detergents, Tekstil 42 (1993) 267–274.
[6] R.A. Llenado, Use of sodium type A zeolite in laundry detergents, in: D. Olson, A. Bisio (Eds.), Proceedings of the Sixth International Zeolite Conference, Butterworths, Reno, Usa, 1984, pp. 940–956.
[7] R.P. Denkewicz Jr., A. Monino, D. Russ, H. Sherry, Measurement and interpretation of zeolite NaA builder performance, J. Am. Oil Chem. Soc. 72 (1995) 31–35.
[8] T. Li, H. Liu, Y. Fan, P. Yuan, G. Shi, X.T. Bi, X. Bao, Synthesis of zeolite Y from natural aluminosilicate minerals for fluid catalytic cracking application, Green Chem. 14 (2012) 3255–3259.
[9] M. Mezni, A. Hamzaoui, N. Hamdi, E. Srasra, Synthesis of zeolites from the low-grade Tunisian natural illite by two different methods, Appl. Clay Sci. 52 (2011) 209–218.
[10] D. Boukadir, N. Bettahar, Z. Derriche, Etude de la synthese des zeolites 4A et HS a partir de produits naturels, Ann. Chim. – Sci. Mat. 27 (2002) 1–13.
[11] B. Ghosh, D.C. Agrawal, S. Bhatia, Synthesis of zeolite A from calcined diatomaceous clay: optimization studies, Ind. Eng. Chem. Res. 33 (1994) 2107–2110.
[12] A. Baccouche, E. Srasra, M. El Maaoui, Preparation of Na-P1 and sodalite octahydrate zeolites from interstratified illite and smectite, Appl. Clay Sci. 13 (1998) 255–273.
[13] K. Abdmeziem-Hamoudi, B. Siffert, Synthesis of molecular sieve zeolites from a smectite-type clay material, Appl. Clay Sci. 4 (1989) 1–9.
[14] A.G. San Cristóbal, R. Castelló, M.A. Martín Luengo, C. Vizcayno, Zeolites prepared from calcined and mechanically modified kaolins: a comparative study, Appl. Clay Sci. 49 (2010) 239–246.
[15] C.A. Ríos, C.D. Williams, M.A. Fullen, Nucleation and growth history of zeolite LTA synthesized from kaolinite by two different methods, Appl. Clay Sci. 42 (2009) 446–454.
[16] E.B.G. Johnson, S.E. Arshad, Hydrothermally synthesized zeolites based on kaolinite: a review, Appl. Clay Sci. 97–98 (2014) 215–221.
[17] C.A.R. Reyes, C.D. Williams, O.M. Alarcon, Synthesis of zeolite LTA from thermally treated kaolinite, Rev. Fac. Ing. Univ. Antiquia 53 (2010) 30–41.
[18] S. Chandrasekhar, Influence of metakaolinization temperature on the formation of zeolite 4A from kaolin, Clay Miner. 31 (1996) 253–261.
[19] C. Belviso, F. Cavalcante, A. Lettino, S. Fiore, A and X-type zeolites synthesised from kaolinite at low temperature, Appl. Clay Sci. 80–81 (2013) 162–168.
[20] S. Chandrasekhar, P.N. Pramada, Investigation on the Synthesis of Zeolite NaX from Kerala Kaolin, J. Porous Mater. 6 (1999) 283–297.
[21] E. Costa, A. De Lucas, M.A. Uguina, J.C. Ruiz, Synthesis of 4A zeolite from calcined kaolins for use in detergents, Ind. Eng. Chem. Res. 27 (1988) 1291–1296.
[22] S. Chandrasekhar, P. Raghavan, G. Sebastian, A.D. Damodaran, Brightness improvement studies on 'kaolin based' zeolite 4A, Appl. Clay Sci. 12 (1997) 221–231.
[23] R. Asmatutu, Removal of the discoloring contaminants of an east Georgia kaolin clay and its dewatering, Turkish J. Eng. Environ. Sci. 26 (2002) 447–453.
[24] R.J. Pruett, Advances in selective flocculation processes for the beneficiation of kaolin, Miner. Metall. Process 29 (2012) 27–35.
[25] C. Poole, H. Prijatama, N.M. Rice, Synthesis of zeolite adsorbents by hydrothermal treatment of PFA wastes: a comparative study, Miner. Eng. 13 (2000) 831–842.
[26] R.B. Scorzelli, L.C. Bertolino, A.B. Luz, M. Duttine, F.A.N.G. Silva, P. Munayco, Spectroscopic studies of kaolin from different Brazilian regions, Clay Miner. 43 (2008) 129–135.
[27] P. Sengupta, N.J. Saikia, D.J. Bharali, P.C. Saikia, P.C. Borthakur, ESR investigation of deferration treatment of iron-rich kaolinite clay from Deopani, Assam, India, Curr. Sci. India 91 (2006) 86–90.
[28] V.R. Ambikadevi, M. Lalithambika, Effect of organic acids on ferric iron removal from iron-stained kaolinite, Appl. Clay Sci. 16 (2000) 133–145.
[29] E.L. Basaldella, R.M.T. Sanchez, J.C. Tara, Iron influence in the aluminosilicate zeolites synthesis, Clays Clay Miner. 46 (1998) 481–486.
[30] V.S. Fajnor, K. Jesenak, Differential thermal analysis of montmorillonite, J. Therm. Anal. Calorim. 46 (1996) 489–493.
[31] M.P. Moisés, C.T.P. da Silva, J.G. Meneguin, E.M. Girotto, E. Radovanovic, Synthesis of zeolite NaA from sugarcane bagasse ash, Mater. Lett. 108 (2013) 243–246.
[32] J.S. Udhoji, A.K. Bansiwal, S.U. Meshram, S.S. Rayalu, Improvement in optical brightness of fly ash based zeolite-A for use as detergent builder, J. Sci. Ind. Res. 64 (2005) 367–371.
[33] H. Takeda, S. Hashimoto, S. Honda, Y. Iwamoto, The coloring of geopolymers by the addition of copper compounds, Ceram. Int. 40 (2014) 6503–6507.
[34] L. Gora, K. Streletzky, R.W. Thompson, G.D.J. Phillies, Study of the crystallization of zeolite NaA by quasi-elastic light-scattering spectroscopy and electron microscopy, Zeolites 18 (1997) 119–131.
[35] A. Zegeye, S. Yahaya, C.I. Fialips, M.L. White, N.D. Gray, D.A.C. Manning, Refinement of industrial kaolin by microbial removal of iron-bearing impurities, Appl. Clay Sci. 86 (2013) 47–53.

Paper II

Comparison between leached metakaolin and leached diatomaceous earth as raw materials for the synthesis of ZSM-5

Wilson Aguilar, Gustavo García, Johanne Mouzon, Jonas Hedlund

SpringerPlus 2014, 3:292

Aguilar-Mamani et al. SpringerPlus 2014, 3:292
http://www.springerplus.com/content/3/1/292

SpringerPlus
a SpringerOpen Journal

RESEARCH Open Access

Comparison between leached metakaolin and leached diatomaceous earth as raw materials for the synthesis of ZSM-5

Wilson Aguilar-Mamani[1,2*], Gustavo García[1,3], Jonas Hedlund[1] and Johanne Mouzon[1]

Abstract

Inexpensive raw materials have been used to prepare ZSM-5 zeolites with SiO_2/Al_2O_3 molar ratios in the range 20 – 40. Kaolin or Bolivian diatomaceous earth was used as aluminosilicate raw materials and sodium hydroxide and *n*-butylamine were used as mineralizing agents and template. Dealumination of the raw materials by acid leaching made it possible to reach appropriate SiO_2/Al_2O_3 ratios and to reduce the amount of iron and other impurities. After mixing the components and aging, hydrothermal treatment was carried out and the products were recovered The results clearly show for the first time that well-crystallized ZSM-5 can be directly prepared from leached metakaolin or leached diatomaceous earth using sodium hydroxide and *n*-butylamine as mineralizing agents and template under appropriate synthesis conditions. A longer induction time prior to crystallization was observed for reaction mixtures prepared from leached diatomaceous earth, probably due to slower digestion of the fossilized diatom skeletons as compared with that for microporous leached metakaolin. The use of leached diatomaceous earth allowed higher yield of ZSM-5 crystals within comparable synthesis times. However, low amounts of Mordenite formed, which was related to the high calcium content of diatomaceous earth. Another considerable advantage of diatomaceous earth over kaolin is that diatomaceous earth does not require heat treatment at high temperature for metakaolinization.

Keywords: Kaolin; Diatomaceous earth; n-butylamine; ZSM-5 zeolite

Introduction

The zeolite ZSM-5 (Zeolites Socony Mobil) is an aluminosilicate with high silica ratio with suitable properties for catalysis, adsorption and membrane applications (Jacobs 1981, Tavolaro and Drioli 1999, Weitkamp 2000). Researchers (Argauer and Landolt 1972) of Mobil Oil Corporation obtained the first patent on the synthesis of ZSM-5 zeolite, in which they described that this zeolite can be formed with molar ratios of SiO_2/Al_2O_3 varying between 20 and 120. Depending on this ratio, the acidity and surface properties of ZSM-5 vary and therefore it is important to carefully control this parameter in the final product (Armaroli et al. 2006, Shirazi et al. 2008).

Typical syntheses of ZSM-5 require sources of silicon and aluminium, a mineralizer (e.g. OH^- or F^-) and an organic molecule as templating agent. Quaternary ammonium compounds like tetrapropyl ammonium bromide (TPA-Br) (Padovan et al. 1984, Shirazi et al. 2008) and tetrapropyl ammonium hydroxide (TPA-OH) (Kotasthane and Shiralkar 1986) are mostly used for the synthesis of ZSM-5. Unfortunately, these quaternary ammonium compounds are rather expensive. The molecule *n*-butylamine was reported (Sang et al. 2004, Zhao 2005, Martins et al. 2006, Feng et al. 2009) as an alternative templating agent to replace TPA-Br and TPA-OH and is about 100 times less expensive on a molar basis. In the past two decades, efforts have also been undertaken to identify inexpensive Si and Al sources to synthesize ZSM-5(Chareonpanich et al. 2004, Sanhueza et al. 2004, Mignoni et al. 2007, Aliev et al. 2011) and it has been shown that kaolin clay and diatomaceous earth are two suitable and inexpensive sources of silica and alumina.

Kaolin clay contains kaolinite with a SiO_2/Al_2O_3 molar ratio close to 2 and therefore it is well suited for the preparation of low-silica zeolites such as zeolite A (Costa

* Correspondence: gonzalo316@gmail.com
[1]Chemical Technology, Luleå University of Technology, Luleå, Sweden
[2]Department of Chemistry, Faculty of Science and Technology, San Simon University, Cochabamba, Bolivia
Full list of author information is available at the end of the article

et al. 1988, Murat et al. 1992, Chandrasekhar et al. 1997, Sanhueza et al. 1999). To obtain this zeolite from kaolin, two steps are necessary: first, a thermal treatment of kaolin to obtain an amorphous and reactive material denoted metakaolin. The second step is a hydrothermal treatment to convert metakaolin to zeolite in an alkaline aqueous medium. Preparation of zeolites with higher SiO_2/Al_2O_3 molar ratios such as zeolites X (De Lucas et al. 1992, Caballero et al. 2007, Colina and Llorens 2007) and Y (Bosch et al. 1983, Atta et al. 2007) from kaolinite has also been reported. However, the syntheses of these zeolites require either an increase of the amount of silica or partial removal of aluminium. The first alternative implies using an additional source of silica with high solubility, e.g. sodium silicate. The second alternative, i.e. dealumination, consists in either leaching kaolin in a solution of an inorganic acid (HCl, H_2SO_4, HNO_3) (Ford 1992) or alternatively calcining the kaolin with an inorganic acid (H_2SO_4) (Colina et al. 2001, Colina et al. 2002)

The synthesis of ZSM-5 zeolite from kaolin with additional sources of silica has been reported in patent (Reid 1982) and research papers (Khatamian and Irani 2009, Kovo et al. 2009). Dealumination of metakaolinite to synthesize ZSM-5 has also been investigated (Madhusoodana et al. 2005); (Zhang et al. 2007); (Madhusoodana et al. 2001). In all these studies, expensive tetrapropylamine was used as template. The synthesis of ZSM-5 with a high SiO_2/Al_2O_3 molar ratio from metakaolin and silica sol and less expensive *n*-butylamine has been reported (Feng et al. 2009). However, to the best of our knowledge, a combination of dealumination of metakaolin by acid treatment together with the use of *n*-butylamine as a template has not yet been reported.

Diatomaceous earth is another inexpensive source of silica, which is a sedimentary rock comprised of fossilized skeletal remains of diatoms. It consists essentially of amorphous hydrated silica and a small amount of alumina and also impurities such as iron (Sanhueza et al. 2003). It can be used to produce mesoporous material such as MCM-41 (Sanhueza et al. 2006) and also both low and high silica zeolites such as A (Ghosh et al. 1994), P (Wajima et al. 2008) or NaP (Wajima et al. 2006), analcime (Chaisena and Rangsriwatananon 2005); (Rangsriwatananon et al. 2008), cancrinite (Chaisena and Rangsriwatananon 2005), hydroxisodalite (Chaisena and Rangsriwatananon 2005), NaY (Chi et al. 2011) and mordenite (Sanhueza et al. 2003). In most of these syntheses, the raw diatomaceous earth was acid treated to remove iron and other impurities. The conversion of diatomaceous earth to ZSM-5 was also studied in combination with other raw materials such as paper sludge ash (Wajima et al. 2008) or volcanic ash (Aliev et al. 2011). However, there are a few studies on the synthesis of ZSM-5 by using only diatomaceous earth as silica source. In these studies, diethanolamine(Sanhueza et al. 2004) and expensive tetrapropylammonium bromide (Shan et al. 2004) were used as templates and these synthesis required quite long crystallization times from 40 hours to 6 days at a quite high temperature of 180°C.

In the present work, we show for the first time that leached metakaolinite or diatomaceous earth in combination with sodium hydroxide and *n*-butylamine can be used as inexpensive raw materials for the synthesis of ZSM-5 without using an additional source of silica. However, both sources of alumino-silica are shown to behave differently during the course of synthesis and to lead to slightly different reaction products. In particular, we discuss these discrepancies in terms of composition, morphology, and porosity of the raw materials.

Experimental

Raw materials

Kaolin (Riedel de Haen, pro analysi), diatomaceous earth (Murmuntani zone in the locality of Llica, Potosi, Bolivia), sodium hydroxide (Sigma Aldrich, reagent grade, ≥98%, anhydrous pellets), *n*-butylamine (Sigma Aldrich, 99.5%) and hydrochloric acid (Merk, pro analysi 37%) were used as reagents.

Heat treatment

Kaolin was first calcined in a porcelain crucible that was placed in a furnace and heated at a rate of 8°C/min in air. When the temperature reached 750°C, this temperature was maintained for 2 h to obtain metakaolin and the temperature in the furnace was then reduced to room temperature. It was not necessary to carry out the heat treatment for the diatomaceous earth in order to obtain ZSM-5, and consequently, this material was not heat treated. On the other hand, if the heat treatment of kaolin was omitted, no zeolite formed.

Dealumination of raw materials

Metakaolin and diatomaceous earth were acid leached in a spherical glass container under reflux conditions in a thermostated oil bath maintained at 115°C. Metakaolin or diatomaceous earth was stirred in hydrochloric acid (3 M) for 150 minutes. The metakaolin or diatomaceous earth to acid weight ratio was 1:17. Subsequently, the suspension was quenched and the acid leached product was washed with distilled water. Finally, the product was separated by filtration and the filter cake was washed with distilled water until the pH reached a value close to 7.

Hydrothermal synthesis

The synthesis mixtures were prepared by mixing the aluminosilicate sources with distilled water, *n*-butylamine

(NBA) and sodium hydroxide. The molar ratios in the synthesis mixtures were: $Na_2O/SiO_2 = 0.18$; $SiO_2/Al_2O_3 = X$; $SiO_2/NBA = 7$; $H_2O/SiO_2 = 30$, where X = 33 and 44 for leached metakaolin and leached diatomaceous earth, respectively. The mixtures were aged under stirring for 24 hours at room temperature and were thereafter hydrothermally heated in Teflon lined stainless steel autoclaves kept for different times in an oil bath at 165°C. After hydrothermal treatment, the solids were recovered by filtration and washed with distilled water until the pH reached a value close to 7. The powders were dried at 100°C overnight and finally calcined at 550°C for 6 hours to remove the template.

Characterization of the products

The chemical compositions of kaolin, diatomaceous earth, leached aluminosilicates and the final products were determined using inductively coupled plasma-sector field mass spectrometry (ICP-SFMS). Samples of 0.1 g were fused with 0.4 g of $LiBO_2$ and dissolved in HNO_3. Crystallinity was examined by X-ray diffractometry (XRD) using a PANalytical Empyrean X-ray Diffractometer equipped with Cu LFF HR X-ray tube, a graphite monochromator, and a PIXcel3D detector. The X-ray tube was operated at 30 mA and 40 kV. The investigated 2θ range was from 5 to 50° with a step size of 0.026°. The degree of crystallinity was calculated by using the area of characteristic peaks of ZSM-5 between 22 and 25° after background removal following the equation by van Hooff (Vanhooff et al. 1991).

ZSM-5 crystals with an average length of 10 μm synthesized from silicic acid and TPAOH by following the method reported by Lechert and Kleinwort (Robson and Lillerud 2001) were used as standard.

The morphology of the ZSM-5 crystals was studied by scanning electron microscopy (SEM, Magellan 400, FEI Company) without coating. The chemical composition of individual crystals was determined by energy dispersive spectrometry (EDS, 80 mm^2 X-max detector, Oxford Instruments) at an accelerating voltage of 10 kV. Nitrogen adsorption-desorption data were recorded with an ASAP 2010 equipment from Micrometrics to determine the BET specific surface area, total pore volume and micropore volume of the raw materials and reaction products, as well as the reference crystals. The weight percentage of solid retentate after aging was determined by filtration through a 1 μm filter paper and gravimetric method, while the filtrates were analyzed by ICP-SFMS.

Results

Characterization of the starting materials

X-ray diffractograms of the raw aluminosilicates and dealuminated counterparts are shown in Figure 1. Kaolin of course contains mostly kaolinite (evidenced by reflections at $2\theta = 12.33$; 19.80; 20.40; 21.40. 24.81 and 35.11) but also traces of quartz ($2\theta = 20.85$; 26.66) and muscovite ($2\theta = 8.83$; 35.06). Kaolin after calcination and leaching was mostly an amorphous material with weak characteristic peaks of muscovite and quartz. On the other hand, raw diatomaceous earth shows the occurrence of halite NaCl ($2\theta = 27.41$; 31.76; 45.53), muscovite ($2\theta = 8.83$; 27.83; 35,06), albite ($2\theta = 22.03$; 23.70) and quartz ($2\theta = 20.85$; 26.66) in addition to amorphous material. After acid treatment and the subsequent washing, the amorphous material remained and NaCl was removed, but the other minor constituents were still present (muscovite, albite and quartz).

The chemical compositions of the raw and leached materials measured by ICP-SFMS are given in Table 1. Raw kaolin and diatomaceous earth had a SiO_2/Al_2O_3 molar ratio of 2.2 and 15, respectively. This ratio was successfully increased by acid leaching to 33 and 44 for kaolin and diatomaceous earth, respectively. Acid leaching also reduced significantly the concentration of impurities in both materials. Finally, the leached materials had comparable compositions in terms of magnesium, potassium and iron. However, leached diatomaceous earth was approximately 4 times richer in sodium and calcium, which can be understood from the presence of NaCl and calcium compounds in the raw diatomaceous earth originating from a region close the salt lake Uyuni.

Figure 2 shows the morphology of the raw materials and leached materials revealed by SEM. Kaolin is composed of stacks of platelets with hexagonal symmetry which is typical of natural kaolinites (Figure 2(a)). The leached metakaolin (Figure 2(b)) has very similar platelet morphology but the surface area increased from 12 to 288 m^2/g as presented in Table 2. This is not surprising since acid-leached metakolin is known to form microporous silica (Madhusoodana et al. 2001); (Zhang et al. 2007). Raw diatomaceous earth (Figure 2(d)) exhibited large particles with typical shapes of diatomaceous biogenic sediments. Some diatomaceous earth particles were partially broken in smaller pieces by the mechanical action of stirring during the acid treatment but their characteristic shapes could still be distinguished (Figure 2(e)). Leaching of diatomaceous earth only caused a slight increase in specific surface area (from 38 to 55 m^2/g; Table 2).

Hydrothermal synthesis

Hydrothermal synthesis in terms of composition of the synthesis mixture and synthesis time was first optimized to maximize the yield of ZSM-5 using leached metakaolin as a raw material. The composition used in this work was found to produce the highest yield of ZSM-5 crystals. Figure 3 shows the evolution of XRD crystallinity compared with a reference sample composed of 6–10 μm ZSM-5 crystals. It can be noticed in Figure 3(a) that samples prepared from leached metakaolin reached maximum crystallinity for synthesis times between 9

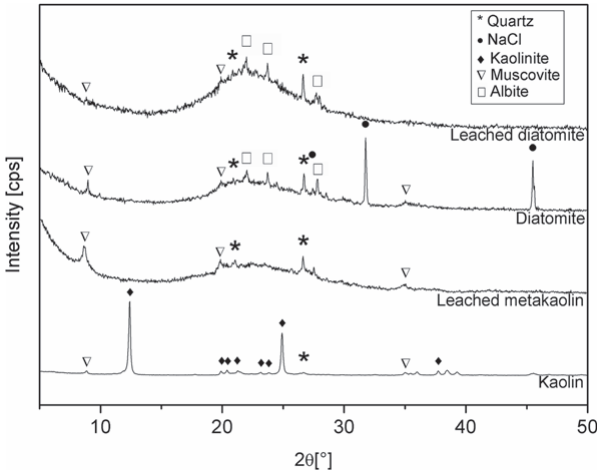

Figure 1 XRD diffractograms of the raw materials and acid-leached materials.

and 12 hours before decreasing for prolonged hydrothermal treatments. The reaction parameters of the dealumination and hydrothermal treatments obtained on kaolin were employed for diatomaceous earth. As shown in Figure 3(b), the best crystallinity for leached diatomaceous earth was obtained for 12 hours of synthesis.

Characterization of the crystalline products

The diffractograms of the final reaction products obtained from both types of raw materials after 12 h synthesis are presented in Figure 4. The main characteristic peaks correspond to the MFI structure ($2\theta = 7.9$; 8.7; 23.0 etc.) in good agreement with the reference pattern PDF-042-0024. The intensities of the main peak of quartz are similar in both samples and of the same order of magnitude as in the leached materials. Therefore, the quartz content is similar in both samples and originates from the raw materials. However, the reaction product obtained from diatomaceous earth contained traces of mordenite, approximately 5% of the intensity of the main peak of ZSM-5. The composition of the final products after 12 h synthesis was determined by ICP-SFMS analysis and the results were presented in Table 1. The average SiO_2/Al_2O_3 molar ratio was 23 and 40 for the reaction products obtained from leached metakaolin and diatomaceous earth, respectively. From these data, the reaction products could be considered as quite pure ZSM-5 with traces of mordenite formed during synthesis and of quartz remaining from the raw material.

The morphology of the reaction products was studied by SEM and typical images were presented in Figure 5. Synthesis from leached metakaolin resulted in the formation of flat tablet shaped ZSM-5 crystals with a diameter of 5–6 μm, but also some smaller particles, as shown in Figure 5(a). In contrast, the ZSM-5 crystals obtained from leached diatomaceous earth were rounded with average

Table 1 Compositions (in mole%) of kaolin, diatomaceous earth, leached metakaolin, leached diatomaceous earth and ZSM-5 products by ICP-SFMS

Composition	Kaolin	Leached metakaolin	ZSM-5 (K)	Diatomaceous earth	Leached diatomaceous earth	ZSM-5 (D)
SiO_2	67.7	95.9	94.0	78.8	96.4	96.0
Al_2O_3	30.1	2.92	4.15	5.22	2.17	2.40
CaO	0.15	0.12	0.10	4.44	0.49	0.63
Fe_2O_3	0.37	0.16	0.18	0.22	0.06	0.07
K_2O	1.13	0.60	0.65	1.29	0.33	0.30
MgO	0.59	0.19	0.22	3.30	0.19	0.23
Na_2O	0.16	0.08	0.65	6.78	0.35	0.37
Mol SiO_2/Al_2O_3	**2.2**	**33**	**23**	**15**	**44**	**40**

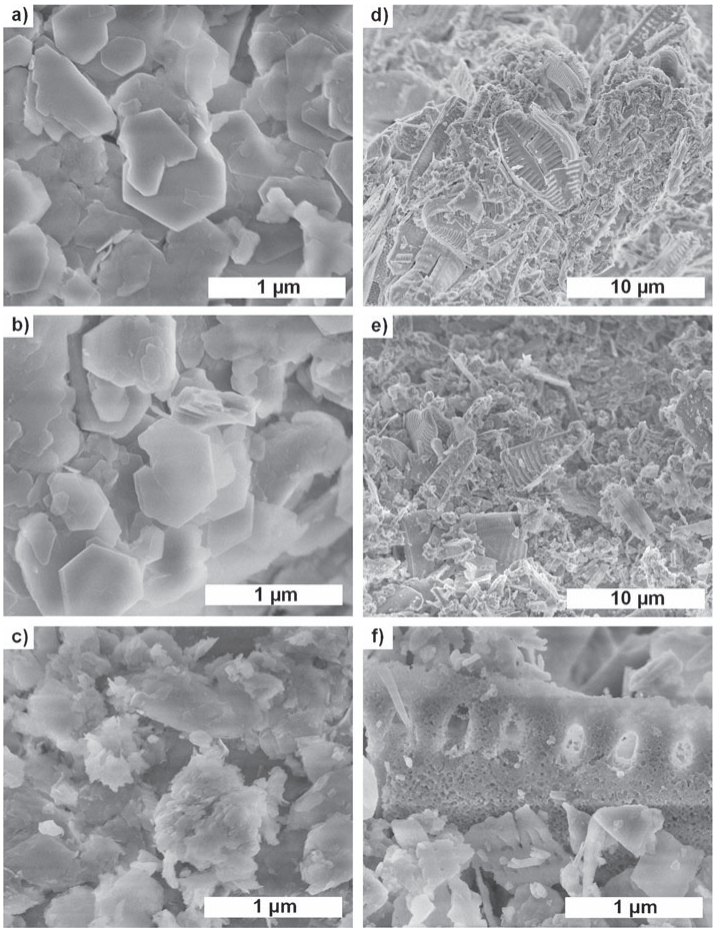

Figure 2 Morphology of the raw materials and leached materials. (a) Kaolin (50000x magnification). **(b)** Leached metakaolin (LMK) (50000x magnification). **(c)** Solid part of LMK after aging (50000x magnification). **(d)** Diatomaceous earth (5000x magnification). **(e)** Leached diatomaceous earth (LD) (50000x magnification). **(f)** Solid part of LD after aging (50000x magnification).

Table 2 Surface area and pore volumes derived from nitrogen adsorption data for the raw, leached materials, final products and standard sample

Sample	BET surface area (m^2/g)	Total pore volume (cm^3/g)	Micropore volume (cm^3/g)
Kaolin	12	0.058	0.004
Leached metakaolin	288	0.24	0.089
Diatomaceous earth	38	0.093	0.003
Leached diatomaceous earth	55	0.11	0.006
ZSM-5 (K)	255 (82%)	0.17	0.082 (68%)
ZSM-5 (D)	298 (96%)	0.15	0.098 (82%)
ZSM-5 standard	310	0.15	0.12

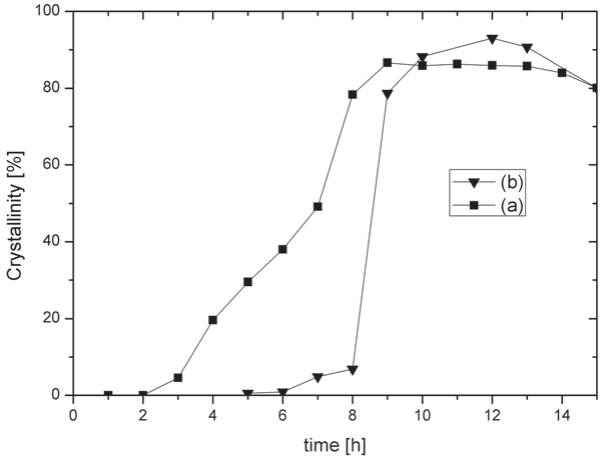

Figure 3 Crystallinity as a function of time of the reaction products prepared from acid leached materials. (a) Leached metakaolin. **(b)** Leached diatomaceous earth.

diameter around 7–8 μm and aspect ratio close to 1 (Figure 5(b)). This sample also contained smaller particles and particularly small slabs as those encircled in Figure 5(b), which were attributed to mordenite.

Discussion

As shown above, the combination of both sodium hydroxide and *n*-butylamine together with leached metakaolin or leached diatomaceous earth was efficient to produce micron-sized ZSM-5 crystals within similar synthesis times. However, the reaction mechanism seems to differ depending on which alumino-silica source was used. Figure 3(a) clearly shows that crystal growth is triggered after an induction period of 2 h and slowly progresses until maximum crystallinity is reached after 9 h when leached metakaolin was used. In contrast, the induction

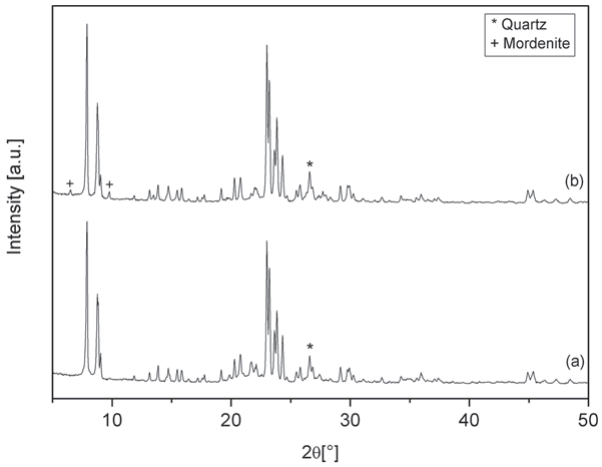

Figure 4 XRD diffractograms of the products obtained after 12 hours of synthesis from acid leached materials. (a) Leached metakaolin. **(b)** Leached diatomaceous earth.

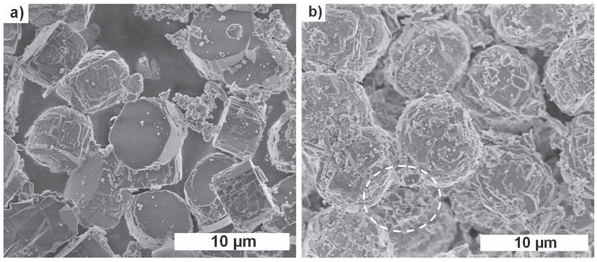

Figure 5 SEM images of ZSM-5 crystals from kaolin and diatomaceous earth. (a) Kaolin (5000x magnification). **(b)** Diatomaceous earth (5000x magnification).

period was extended to 6 h before a sudden burst of crystal growth occurred between 8 and 9 h, if leached diatomaceous earth was used as alumino-silica source (Figure 3(b)). The differences in growth rates are not yet understood. However, the difference in induction period between both synthesis mixtures may be related to the state of the synthesis mixtures after 24 h aging and before hydrothermal treatment. After filtration through a 1-μm filter paper, 26 and 80 wt.% of the original solid material remained from the aged synthesis mixtures prepared from leached metakaolin and leached diatomaceous earth, respectively. The filtrates were found to be silica-rich sols by ICP-SFMS (SiO_2/Al_2O_3 molar ratio ~ 400–800). As shown in Figure 2(c), the solid retentate of the aged synthesis mixture prepared from leached metakaolin consisted of poorly defined platelets with a SiO_2/Al_2O_3 molar ratio of 7.5, which probably stem from undigested muscovite or other materials that did not become microporous or possibly sintered upon calcination. On the other hand in Figure 2(f), particles with typical morphology of fossilized diatom still comprised the main constituent of the diatomaceous earth synthesis mixture after aging, even though further communition occurred by mechanical mixing during aging. Therefore, the longer induction time encountered for the leached diatomaceous earth system can be imparted to the heavily condensed state still present after aging in comparison to the silica-rich sol resulting from aging of the leached metakaolin mixture, the latter being more homogeneous and requiring less transformation for nucleation of zeolite crystals.

Although induction time was longer, the maximum crystallinity was slightly higher for samples prepared from diatomaceous earth than from kaolin and amounts to 93 and 87%, respectively, as shown in Figure 3. By a normalization of the BET specific surface area and total micropore volume with respect to the ZSM-5 standard sample also used for determining crystallinity by XRD, we show that the crystallinity of the reaction product obtained from kaolin is in good agreement with the values given in Table 2 with a specific surface area of 82%. The total micropore volume (68%) value indicates that the final product prepared from kaolin contains approximately 30% of non-microporous material in addition to the ZSM-5 crystals. The same values calculated from the BET specific surface area and total micropore volume for the diatomaceous earth-derived product, 96 and 82% respectively, are higher than that obtained by XRD (93%). This can be attributed to the presence of mordenite as a by-product in addition to non-microporous materials.

It was not possible to prevent the formation of mordenite by further optimization of the synthesis parameters. Instead, formation of mordenite occurred randomly, probably due to the variability of the diatomaceous earth raw material. Calcium was found to be concentrated in the mordenite crystals as revealed by the comparison of the EDS spectra between uncalcined ZSM-5 (Figure 6(a)) and mordenite (Figure 6(b)) crystals. Therefore, the higher calcium content in leached diatomaceous earth as compared to leached kaolin probably favored the formation of mordenite. The presence of *n*-butylamine as templating agent in the ZSM-5 crystals was also confirmed by EDS, as shown in Figure 6(a) with the characteristic peak of nitrogen and carbon, while that of sodium was quite weak.

The BET specific surface area obtained in this work for the sample prepared from leached diatomaceous earth (298 m^2/g) is comparable with that obtained in the study by Sang et al. [9] (294 m^2/g), who employed water glass and aluminum sulfate as Si and Al sources, respectively. Therefore, Bolivian diatomaceous earth appears as a competitive source of inexpensive raw materials for the synthesis of ZSM-5 crystals. In addition to the higher crystallinity and BET specific surface area achieved in this work compared with kaolin, diatomaceous earth does not require heat treatment at high temperature for metakaolinization.

Conclusions

The inexpensive raw materials: kaolin, Bolivian diatomaceous earth, sodium hydroxide and *n*-butylamine have

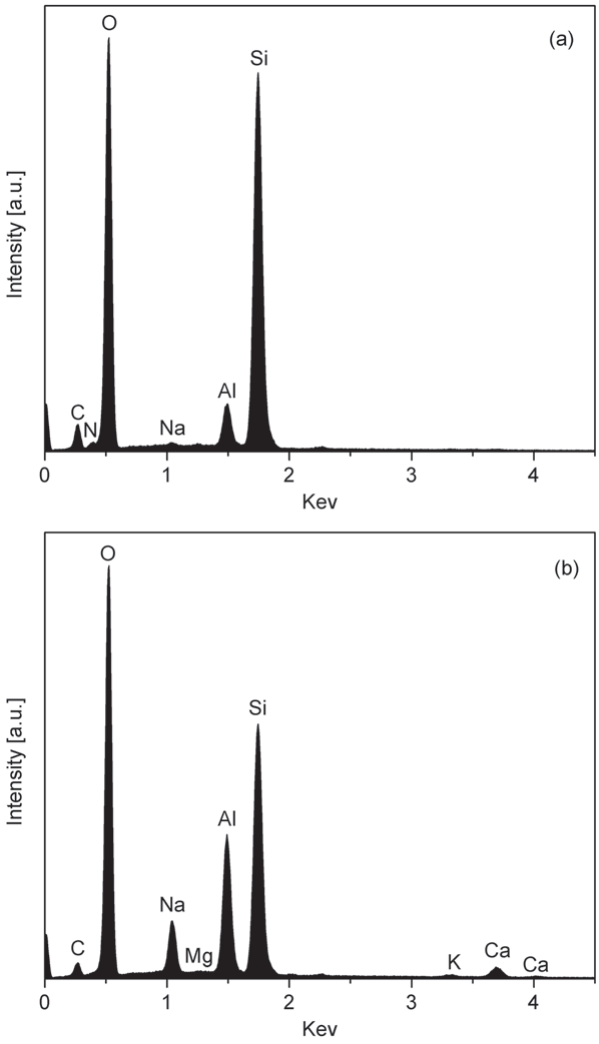

Figure 6 EDS spectra of the final product obtained from leached diatomaceous earth. (a) ZSM-5 crystal. **(b)** Mordenite crystal.

been used to prepare ZSM-5 zeolites with SiO_2/Al_2O_3 molar ratios in the range 20 – 40. Dealumination of the raw materials by acid leaching made it possible to reach appropriate SiO_2/Al_2O_3 molar ratios and to reduce the amount of iron and other impurities in the raw materials. After mixing and aging for 24 hours, synthesis by hydrothermal treatment was carried out at165°C either using leached metakaolin or leached diatomaceous earth as source of alumino-silica. The results clearly show for the first time that well-crystallized ZSM-5 can be directly prepared from both materials in combination with sodium hydroxide and *n*-butylamine under appropriate synthesis conditions. Reaction mixtures prepared from leached diatomaceous earth showed longer induction period due to the slower digestion of the fossilized diatom skeletons compared with microporous leached metakaolin. However, the use of leached diatomaceous earth allowed higher yield in ZSM-5 crystals within comparable synthesis times

despite the formation of low contents of mordenite, which was related to the high calcium content of diatomaceous earth. Another considerable advantage of diatomaceous earth over kaolin is that diatomaceous earth does not require heat treatment at high temperature for metakaolinization.

Competing interests
The authors declare that they have no competing interests.

Authors' contributions
WAM carried out the experiments and drafted the manuscript under the supervision of JM and JH. GG assisted in the analysis of the experiments. All authors read and approved the final manuscript.

Acknowledgements
Swedish International Development Cooperation Agency (SIDA) is acknowledged for supporting the work financially. The Knut and Alice Wallenberg foundation is acknowledged for financially supporting the Magellan SEM instrument.

Author details
[1]Chemical Technology, Luleå University of Technology, Luleå, Sweden. [2]Department of Chemistry, Faculty of Science and Technology, San Simon University, Cochabamba, Bolivia. [3]Solid State and Theoretical Chemistry, Chemistry Research Institute, San Andres Mayor University, University Campus, Cota Cota, 27 Street, La Paz, Bolivia.

Received: 10 April 2014 Accepted: 30 May 2014
Published: 10 June 2014

References

Aliev AM, Mamedova UA, Samedov KR, Sarydzhanov AA, Agaeva RY (2011) Synthesis and physicochemical study of ZSM-5 high-silica zeolite from natural raw materials. Russ J Phys Chem A 85:288–292
Argauer RJ, Landolt GR (1972) Crystalline Zeolite Zsm-5 and Method of Preparing the same., 886A, 14 Nov 1972
Armaroli T, Simon LJ, Digne M, Montanari T, Bevilacqua M, Valtchev V, Patarin J, Busca G (2006) Effects of crystal size and Si/Al ratio on the surface properties of H-ZSM-5 zeolites. Appl Catal A Gen 306:78–84
Atta A, Ajayi O, Adefila S (2007) Synthesis of faujasite zeolites from Kankara kaolin clay. J Appl Sci Res 3:1017–1021
Bosch P, Ortiz L, Schifter I (1983) Synthesis of faujasite type zeolites from calcined kaolins. Ind Eng Chem Prod Res Dev 22:401–406
Caballero I, Colina FG, Costa J (2007) Synthesis of X-type zeolite from dealuminated kaolin by reaction with sulfuric acid at high temperature. Ind Eng Chem Prod Res 46:1029–1038
Chaisena A, Rangsriwatananon K (2005) Synthesis of sodium zeolites from natural and modified diatomite. Mater Lett 59:1474–1479
Chandrasekhar S, Raghavan P, Sebastian G, Damodaran AD (1997) Brightness improvement studies on 'kaolin based' zeolite 4A. Appl Clay Sci 12:221–231
Chareonpanich M, Namto T, Kongkachuichay P, Limtrakul J (2004) Synthesis of ZSM-5 zeolite from lignite fly ash and rice husk ash. Fuel Process Technol 85:1623–1634
Chi ZQ, Li JH, Chen HF (2011) Synthesis of NaY zeolite molecular sieves from calcined diatomite. Adv Mater Res 236:362–368
Colina FG, Llorens J (2007) Study of the dissolution of dealuminated kaolin in sodium–potassium hydroxide during the gel formation step in zeolite X synthesis. Microporous Mesoporous Mater 100:302–311
Colina FG, Esplugas S, Costa J (2001) High temperature reaction of kaolin with inorganic acids. Brit Ceram Trans 100:203–206
Colina FG, Esplugas S, Costa J (2002) High-temperature reaction of kaolin with sulfuric acid. Ind Eng Chem Res 41:4168–4173
Costa E, De Lucas A, Uguina MA, Ruiz JC (1988) Synthesis of 4A zeolite from calcined kaolins for use in detergents. Ind Eng Chem Res 27:1291–1296
De Lucas A, Uguina MA, Covian I, Rodriguez L (1992) Synthesis of 13X zeolite from calcined kaolins and sodium silicate for use in detergents. Ind Eng Chem Res 31:2134–2140
Feng H, Li C, Shan H (2009) In-situ synthesis and catalytic activity of ZSM-5 zeolite. Appl Clay Sci 42:439–445
Ford KJR (1992) Leaching of fine and pelletised Natal kaolin using sulphuric acid. Hydrometallurgy 29:109–130
Ghosh B, Agrawal DC, Bhatia S (1994) Synthesis of Zeolite A from Calcined Diatomaceous Clay: Optimization Studies. Ind Eng Chem Res 33:2107–2110
Jacobs PA (1981) Properties of the end members in the Pentasil-family of zeolites: characterization as adsorbents. Zeolites 1:161–168
Khatamian M, Irani M (2009) Preparation and characterization of nanosized ZSM-5 zeolite using kaolin and investigation of kaolin content, crystallization time and temperature changes on the size and crystallinity of products. J Iran Chem Soc 6:187–194
Kotasthane AN, Shiralkar VP (1986) Thermoanalytical studies of high silica ZSM-5 zeolites containing organic templateS. Thermochimica Acta 102:37–45
Kovo AS, Hernandez O, Holmes SM (2009) Synthesis and characterization of zeolite Y and ZSM-5 from Nigerian Ahoko Kaolin using a novel, lower temperature, metakaolinization technique. J Mater Chem 19:6207–6212
Madhusoodana CD, Kameshima Y, Yasumori A, Okada K (2001) Fast formation of ZSM-5 zeolite using microporous silica obtained from selective leaching of metakaolinite. Clay Sci 11:369–380
Madhusoodana C, Das R, Kameshima Y, Okada K (2005) Preparation of ZSM-5 zeolite honeycomb monoliths using microporous silica obtained from metakaolinite. J Porous Mat 12:273–280
Martins L, Peguin RPS, Urquiet-González EA (2006) Cu and Co exchanged ZSM-5 zeolites: activity towards no reduction and hydrocarbon oxidation. Quimica Nova 29:223–229
Mignoni ML, Detoni C, Pergher SBC (2007) Estudo da síntese da zeólita ZSM-5 a partir de argilas naturais. Quimica Nova 30:45–48
Murat M, Amokrane A, Bastide J, Montanaro L (1992) Synthesis of zeolites from thermally activated kaolinite. Some observations on nucleation and growth. Clay Min 27:119–130
Padovan M, Leofanti G, Solari M, Moretti E (1984) Studies on the ZSM—5 zeolite formation. Zeolites 4:295–299
Rangsriwatananon K, Chaisena A, Thongkasam C (2008) Thermal and acid treatment on natural raw diatomite influencing in synthesis of sodium zeolites. J Porous Mater 15:499–505
Reid (1982) Manufacture of zeolites. European Patent Office :68817, 24 June 1982
Robson H, Lillerud KP (2001) In Chapter 62 - MFI High-Alumina ZSM-5 Si(93), Al(7). Vol. pp. Elsevier Science, Amsterdam
Sang S, Chang F, Liu Z, He C, He Y, XU L (2004) Difference of ZSM-5 zeolites synthesized with various templates. Catal Today 93–95:729–734
Sanhueza V, Kelm U, Cid R (1999) Synthesis of molecular sieves from Chilean kaolinites: 1. Synthesis of NaA type zeolites. J Chem Technol Biotechnol 74:358–363
Sanhueza V, Kelm U, Cid R (2003) Synthesis of mordenite from diatomite: a case of zeolite synthesis from natural material. J Chem Technol Biotechnol 78:485–488
Sanhueza V, Kelm U, Cid R, López-Escobar L (2004) Synthesis of ZSM-5 from diatomite: a case of zeolite synthesis from a natural material. J Chem Technol Biotechnol 79:686–690
Sanhueza V, López-Escobar L, Kelm U, Cid R (2006) Synthesis of a mesoporous material from two natural sources. J Chem Technol Biotechnol 81:614–617
Shan W, Zhang Y, Wang Y, Xia J, Tang Y (2004) Synthesis of Meso-/Macroporous Zeolite (Fe, Al)-ZSM-5 Microspheres from Diatomite. Chem Lett 33:270–271
Shirazi L, Jamshidi E, Ghasemi MR (2008) The effect of Si/Al ratio of ZSM-5 zeolite on its morphology, acidity and crystal size. Cryst Res Technol 43:1300–1306
Tavolaro A, Drioli E (1999) Zeolite membranes. Adv Mater 11:975–996
Van Hooff JHC, Roelofsen JW (1991) Chapter 7 Techniques of Zeolite Characterization. In: van Bekkum EMF H, Jansen JC (eds) In Studies in Surface Science and Catalysis, Vol. 58. Elsevier, pp 241–283
Wajima T, Haga M, Kuzawa K, Ishimoto H, Tamada O, Ito K, Nishiyama T, Downs RT, Rakovan JF (2006) Zeolite synthesis from paper sludge ash at low temperature (90°C) with addition of diatomite. J Hazard Mater 132:244–252
Wajima T, Shimizu T, Ikegami Y (2008) Zeolite synthesis from paper sludge ash with addition of diatomite. J Chem Technol Biotechnol 83:921–927
Weitkamp J (2000) Zeolites and catalysis. Solid State Ionics 131:175–188

Zhang Y, Gao W, Cui L (2007) In-situ Growth of ZSM-5 Zeolite on Acid-Activated Metakaolin. In: Ruren Xu ZGJC, Wenfu Y (eds) Studies in Surface Science and Catalysis, Volume 17. Elsevier, pp 426–431

Zhao H (2005) The difference between ZSM-5 zeolites manufactured from various synthesis systems and their catalytic performances. J China Petroleum Petrochem Technology 3:49–55

doi:10.1186/2193-1801-3-292
Cite this article as: Aguilar-Mamani *et al.*: **Comparison between leached metakaolin and leached diatomaceous earth as raw materials for the synthesis of ZSM-5.** *SpringerPlus* 2014 **3**:292.

Paper III

Synthesis of zeolite Y from diatomite as silica source

Gustavo García, Saúl Cabrera, Jonas Hedlund, Johanne Mouzon

Microporous and Mesoporous Materials 219 (2016) 29 – 37

Microporous and Mesoporous Materials 219 (2016) 29–37

Contents lists available at ScienceDirect

Microporous and Mesoporous Materials

journal homepage: www.elsevier.com/locate/micromeso

Synthesis of zeolite Y from diatomite as silica source

Gustavo Garcia [a, b, *], Edgar Cardenas [a, b], Saúl Cabrera [b], Jonas Hedlund [a], Johanne Mouzon [a]

[a] Chemical Technology, Luleå University of Technology, 971 87 Luleå, Sweden
[b] Chemistry Research Institute, San Andres Mayor University, UMSA, La Paz, Bolivia

ARTICLE INFO

Article history:
Received 6 May 2015
Received in revised form
30 June 2015
Accepted 17 July 2015
Available online 26 July 2015

Keywords:
Faujasite
Zeolite P
Diatomite

ABSTRACT

Bolivian diatomite was successfully used as a silica source for the synthesis of zeolite Y. Prior to synthesis, the diatomite was leached with sulfuric acid to remove impurities and aluminum sulfate was used as an aluminum source. The raw materials were reacted hydrothermally at 100 °C in water with sodium hydroxide and different Na_2O/SiO_2 ratios were investigated. The final products were characterized by scanning electron microscopy, X-ray diffraction, gas adsorption and inductively coupled plasma-atomic emission spectroscopy. Diatomites originating from different locations and therefore containing different types and amounts of minerals and clays as impurities were investigated. After optimization of synthesis time, zeolite Y with low SiO_2/Al_2O_3 ratio (3.0–3.9) was obtained at a high yield for high alkalinity conditions ($Na_2O/SiO_2 = 0.85–2.0$). Lower Na_2O/SiO_2 ratios resulted in incomplete dissolution of diatomite and lower yield. Nevertheless, decreasing alkalinity resulted in a steady increase of the SiO_2/Al_2O_3 ratio in zeolite Y. Consequently, it was possible to synthesize almost pure zeolite Y with a SiO_2/Al_2O_3 ratio of 5.3 for a Na_2O/SiO_2 ratio of 0.6, albeit at a low yield. In this respect, diatomite enables the synthesis of high silica zeolite Y and behaves similarly to colloidal silica in traditional syntheses, with both sources of silica having in common a high degree of polymerization. Interestingly, the presence of minerals and clays in the starting diatomite had marginal effects on the outcome of the synthesis. However, their dissolution resulted in presence of calcium and magnesium in the zeolite Y crystals. Finally, overrun of all investigated compositions resulted in the formation of zeolite P nucleating and growing onto dissolving zeolite Y crystals, which was shown to be triggered when aluminum was completely depleted at high alkalinity.

1. Introduction

Zeolites are crystalline aluminosilicate molecular sieves with unique properties. These compounds are comprised of a three-dimensional network of silicon and aluminum oxide tetrahedrons (SiO_4 and AlO_4^-) linked by shared oxygen atoms and containing charge-compensating cations. The resulting structures form porous frameworks with micropores in the range of ~2–10 Å [1], which confer them molecular sieving properties. Zeolites also possess very high surface areas due to this microporosity and exhibit variable acidic properties depending on composition. Because of these special properties, they can be used in a wide range of applications such as ion exchange, adsorption, catalysis and membrane separation [2].

Two zeolites of particular interest are zeolite X and zeolite Y. These are faujasite type zeolites (FAU), defined by a SiO_2/Al_2O_3 ratio between 2 and 3 for zeolite X and greater than 3 for zeolite Y [3]. The basic structural units for this type of zeolite are sodalite cages which form supercages able to accommodate spheres up to 1.2 nm in diameter. The openings to these large cavities are 12-membered oxygen rings with a free diameter of 7.4 Å [4]. Zeolite X can be employed as an adsorbent for CO_2 capture [5], but it is mostly used in the detergent industry to compliment or substitute zeolite A due to its high capacity for the removal of Mg^{2+} ions in hard water [6]. Zeolite Y is the most widely employed zeolite catalyst due to its use in fluid catalytic cracking (FCC) for conversion of heavy petroleum molecules into gasoline-range hydrocarbons because of its high size selectivity, high concentration of active acid sites, and thermal stability [7–9].

* Corresponding author. Chemical Technology, Luleå University of Technology, 971 87 Luleå, Sweden. Tel.: +46 0920 49 25 02; fax: +46 0920 49 13 99.
E-mail addresses: gustavo.garcia@ltu.se, gusygarmen@hotmail.com (G. Garcia).

http://dx.doi.org/10.1016/j.micromeso.2015.07.015
1387-1811/

Traditional methods for synthesizing FAU-type zeolites typically involve chemical grade reagents as starting materials and crystallization from a gel or clear solution under hydrothermal conditions. Typical synthesis mixtures are usually composed of sodium silicates, sodium aluminate, aluminum salts or colloidal silica in a strong alkaline media. Other processes also include seeding to obtain the desired zeolite [10]. However, synthesis of zeolites from low cost raw materials has also been investigated, since chemical grade reagents are expensive. Until now, the use of materials such as kaolin [11], high silica bauxite [12], halloysite [13], interstratified illite-smectite [14], montmorillonite [15], bentonite [16], and incinerated ash [17] has been reported. Of these raw materials, kaolin has been the most extensively studied, since its composition in terms of SiO_2/Al_2O_3 ratio corresponds to that of zeolite A. Consequently, an additional source of silica is required in order to increase the SiO_2/Al_2O_3 ratio for the synthesis of FAU-type zeolites from kaolin.

Diatomite, a type of siliceous biologic sedimentary rock, is an attractive raw material with high silica content. It contains mainly amorphous silicon oxide derived from biogenic siliceous sediments (unicellular algae skeletons, frustules) and is available in bulk quantities at low cost [18]. Being amorphous and silica rich, diatomite does not require any additional heat treatment or silica source for use in the synthesis of FAU-type zeolites, both of which represent additional costs [19]. However, the occurrence of $CaCO_3$ and Fe as impurities is quite common in diatomite type materials [20] and adequate treatments must be employed for purification [21]. Moreover, potassium, which is known to promote the formation of zeolite P [22], is also common in this kind of raw material meaning that a reduction in potassium content is required.

A number of groups have reported the use of diatomite as raw material for zeolite synthesis [23–26]. However, to the best of our knowledge, there are very few reports about the synthesis of FAU-type zeolites using diatomites as the silicate source. This is probably due to the difficulty of synthesizing a highly crystalline product consisting of FAU-type zeolites without contamination from zeolite P, which is often grown as a main secondary product [27]. Li et al. reported the use of diatomite to form pure zeolite Y [28]. However, a technique based on fusion and seeding was used to obtain pure zeolite Y and prevent the formation of zeolite P. Synthesis of zeolite Y with suitable properties for use in FCC was also reported Li et al. using a combination of specially treated kaolin and diatomite with a special seeding technique but without the involvement of external Al–or Si– containing chemicals [29].

In the present work, we report on the synthesis of FAU-type zeolite with different SiO_2/Al_2O_3 ratios from diatomite with high crystallinity and yield. The effect of varying the Na_2O/SiO_2 ratio and synthesis time at constant SiO_2/Al_2O_3 and H_2O/Na_2O ratios in the $SiO_2–Al_2O_3–Na_2O–H_2O$ system is discussed, as well as the influence of the diatomite purity on the final products. No energy consuming fusion and no (costly) seeds are needed in the method presented here.

2. Experimental

2.1. Materials

Diatomite originating from the Murmuntani zone, near Llica in the Potosi region of Bolivia, was used as aluminosilicate source. Three different sampling locations were investigated. The corresponding diatomite samples are herein referred to as diatomite 1 (D1), diatomite 2 (D2) and diatomite 3 (D3). Aluminum sulfate octadecahydrate in powder form $(Al_2(SO_4)_3 * 18H_2O$, Riedel-de Haën, p.a., >99%) was employed to adjust the SiO_2/Al_2O_3 ratio to that of typical syntheses of zeolite Y. The alkalinity of the synthesis mixture was regulated with sodium hydroxide (NaOH, Sigma Aldrich, p.a., ≥98%). Silicon (Merck, p.a., >99) was used to calibrate the peak position during XRD experiments. The unit cell dimension was determined from the data and used to estimate the SiO_2/Al_2O_3 ratio in the crystals. A commercial powder of zeolite Y (Akzo Nobel, CBV100L-T) was used as reference sample for comparison of the results obtained by nitrogen gas adsorption and X-ray diffraction.

2.2. Synthesis procedure

The raw diatomites were crushed and treated with 6M H_2SO_4 at 373 K for 24 h in an autoclave under hydrothermal conditions, rinsed with distilled water until pH 7 and dried overnight [19]. During filtration, a dark sediment formed at the bottom of the glass beaker. This layer, which was found to consist of large particles of plagioclase and quartz by SEM and XRD, was discarded and only the rest of the materials having a white aspect were utilized in the next steps of processing. Acid treated diatomite (aD1, aD2 or aD3) as well as a suitable amount of $Al_2(SO_4)_3$ to adjust the SiO_2/Al_2O_3 molar ratio were added to NaOH solutions of different concentrations whilst stirring. The molar ratios of the synthesis mixtures were: $Na_2O/SiO_2 = 0.4–2.0$; $SiO_2/Al_2O_3 = 11$; $H_2O/Na_2O = 40$. These solutions were aged with stirring at room temperature in glass beakers for 24 h. At the end of the aging period, the reaction mixture was transferred to Teflon-lined autoclaves. The autoclaves were placed in an oven kept at 373 K for different periods of time. At the end of the hydrothermal treatment, the autoclaves were quenched in cold water. The solid product was separated from the reaction mixture by suction filtering using filter paper (Munktell, grade 00H). The solid product was repeatedly filtered and dispersed in distilled water until the pH of the filtrate liquid was less than 9. The final solid product was dried in an oven at 373 K overnight and weighed in order to estimate the yield.

2.3. Characterization

To determine the chemical composition of the diatomite, acid treated diatomite and final products, inductively coupled plasma-atomic emission spectroscopy (ICP-AES) was performed: 0.1 g sample was digested with 0.375 g of $LiBO_2$ and dissolved in HNO_3. Loss on ignition (LOI) was determined by heating the sample to 1273 K. The mineralogical composition of the raw materials and final products were determined by X-ray diffraction (XRD) using a PANalytical Empyrean X-ray diffractometer, equipped with a PixCel3D detector and a graphite monochromator. CuKα1 radiation with $\lambda = 1.540598$ Å at 45 kV and 40 mA was used and 2θ was varied in the range 5–50° at a scanning speed of 0.026°/s. The peaks observed in the diffractograms were compared with the powder diffraction files (PDF) database. The SiO_2/Al_2O_3 ratio of the FAU zeolites was calculated by determining the lattice parameter from the (555) reflection of faujasite and using the empirical relationship proposed by Rüscher et al. [30]. Crystallinity was determined by calculating the area under the peaks in the $2\theta = 31.0–32.5°$ region after background removal and comparing it to that obtained for a commercial zeolite Y powder. The morphology of the raw materials, intermediate products and final products were studied by extreme high resolution-scanning electron microscopy using an XHR-SEM Magellan 400 instrument supplied by the FEI Company. The samples were investigated using a low accelerating voltage and no conductive coating was used. Energy dispersive spectroscopy (EDS, X-max detector 50 mm^2, Oxford Instruments) was also performed to establish the overall composition of the final products and to gain compositional information about individual zeolite Y crystals and extraneous phases. EDS analysis was carried out at 10 kV on a SEM equipped with a

microinjector (Merlin SEM, Carl Zeiss) in order to mitigate charging by blowing nitrogen gas close to the surface of samples, repeating the same methodology that was previously shown to be successful to estimate the amount of exchanged ions in zeolite A [31]. The apparent Si/Al ratios were slightly overestimated and therefore corrected by plotting the values measured by EDS on commercial powders of zeolite A, X and Y as a function of the corresponding Si/Al ratios obtained by XRD. A relationship following a straight line with a coefficient of determination R^2 of 1 was obtained and used for calibration. Nitrogen adsorption at 77 K was recorded using a Micromeritics ASAP 2010 instrument. Specific surface area was determined using the Brunauer–Emmett–Teller (BET) method. The micropore volume and the external surface area of the final products were determined by the *t*-plot method using the formula:

$$t = [13.9900/(0.0340 - \log(P/P_o))]\hat{0}.5000$$

Yield was also determined from the micropore volume of the samples by comparing their micropore volumes with the value of the commercial powder of zeolite Y.

3. Results

3.1. Starting materials

The XRD diffractograms of the raw diatomites are shown in Fig. 1(A). Depending on the sampling location, different amounts of halite (NaCl, PDF: 01-071-4661), calcite ($CaCO_3$, PDF: 01-078-4614), quartz (SiO_2, PDF: 01-085-0457), muscovite ($KAl_2(Si,Al)_4O_{10}(OH)_2$, PDF: 00-058-2034), montmorillonite ($Ca_{0.5}((Al_2Si_4O_{11})(OH))$, PDF: 01-076-8291), chlorite (chamosite $Fe_3Si_2O_5(OH)_4$, PDF: 00-010-0404), plagioclase ($Na_{0.499}Ca_{0.491}(Al_{1.488}Si_{2.506}O_8)$, PDF: 01-079-1149) and gypsum ($Ca(SO_4)(H_2O)_2$, PDF: 01-070-0982) were found to be present in addition to the amorphous background related to the amorphous silica structure of diatomite. The identified secondary compounds are typical of diatomites of this type [32]. The presence of halite was expected, since the raw material originated from Llica, a region near the Uyuni salt lake. The composition of the original diatomites and corresponding acid leached diatomites was obtained by ICP-AES and the results are given in Table 1. The main elements in the raw diatomites D1, D2 and D3 were silicon and aluminum with SiO_2/Al_2O_3 ratios ranging between 15.1 and 20.1. However, Fe, Na, Ca, K, S and Mg were also present as impurities with variable contents depending on the sampling location. In accordance with XRD results, the high iron content in D1 (i.e. 1.49 wt% Fe_2O_3) seems to be related to the high content in the iron-rich member of the chlorite group, chamosite, while the presence of other clays (e.g. muscovite, montmorillonite) results in potassium and magnesium contents which are comparatively similar and within the same order of magnitude (i.e. close to 2 wt% for K_2O and MgO) in the three diatomites investigated in this work. The high concentration in calcium in sample D2 (i.e. 4 wt% CaO) is undoubtedly due to the presence of calcium carbonate in addition to the plagioclase corresponding to calcian albite and consisting approximately of a 50-50 at% solid solution of sodium and calcium. The latter was also identified in the other diatomites D1 and D3. However, the diatomite D3 was the purest raw material containing comparatively less amounts of quartz, plagioclase and muscovite. It is noteworthy that sulfur was present in the original diatomite and particularly in sample D3 (i.e. 1.68 wt% SO_3). This was found to be related to the presence of gypsum (calcium sulfate dihydrate) crystals as identified by XRD.

Comparison between the XRD (Fig. 1) and ICP-AES results (Table 1) of the original materials and the acid treated counterparts (aD) shows that sodium chloride and calcium carbonate were removed by rinsing and dissolution by the acid, respectively. The acid leaching step was also successful in decreasing the iron and magnesium contents five to ten fold. Sulfur was almost completely washed away by the acid treatment in sample aD3, which can be attributed to the dissolution of the gypsum crystals [33]. The fact that the SO_3 content remained unchanged in aD1 and even increased almost five fold in aD2 can most probably be related to insufficient washing to strip the sulfate ions originated from the sulfuric acid away.

The first filtration step during washing served as a purification step, as the dark sedimented layer containing large particles of quartz and plagioclase was discarded. Accordingly, the CaO content was decreased approximately two fold in all samples. Despite this improvement, considerable amounts of quartz and plagioclase remained. As a result, calcium represented the main impurity after acid leaching of the three diatomites with aD2 containing as much as 2 wt% CaO, whereas aD1 and aD3 only contained 0.79 and 0.40 wt% CaO (Fig. 1B).

Another direct consequence of the acid treatment was that the SiO_2/Al_2O_3 ratio was increased to values ranging between 42.9 and 52.8. Therefore, aluminum sulfate, an inexpensive salt, was added to the synthesis mixture in order to adjust the SiO_2/Al_2O_3 ratio to suitable levels.

3.2. Synthesis optimization

In order to optimize the synthesis of zeolite Y, different compositions were investigated at fixed aging, synthesis temperature and synthesis time (see Table 2) using aD2 as aluminosilica source.

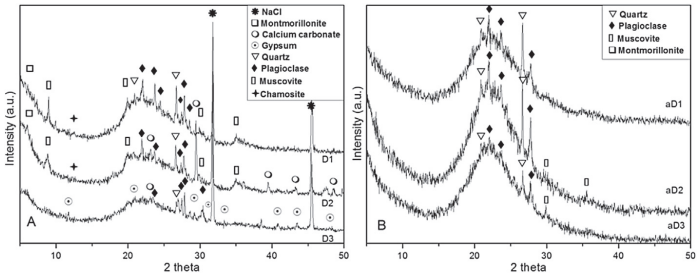

Fig. 1. XRD diffractograms of the different diatomites before and after acid leaching: (A) D1 (plagioclase-rich), D2 (calcium carbonate-rich) and D3 (calcium sulfate-rich) before acid treatment; (B) acid treated diatomites aD1, aD2 and aD3.

Table 1
Chemical composition of the raw diatomites (D1, D2 and D3) and the corresponding acid treated diatomites (aD1, aD2 and aD3) determined by ICP-AES.

Material	Weight (%)								Ratio
	SiO_2	Al_2O_3	Fe_2O_3	Na_2O	CaO	K_2O	MgO	SO_3	SiO_2/Al_2O_3
D1	77.30	8.01	1.49	7.17	1.84	1.64	1.72	0.35	16.4
aD1	94.07	3.73	0.11	0.31	0.79	0.48	0.16	0.34	42.9
D2	75.83	8.54	0.56	6.74	3.99	1.94	2.12	0.29	15.1
aD2	92.27	3.43	0.09	0.30	1.97	0.42	0.15	1.37	45.7
D3	75.66	6.39	0.77	10.34	0.98	1.73	2.45	1.68	20.1
aD3	95.51	3.08	0.12	0.32	0.40	0.38	0.18	0.01	52.8

Table 2
Composition and synthesis conditions for sample aD2-S0.4 to aD2-S2.0.

Sample	Molar composition			Ageing		Heating		Main product (secondary product within brackets)
	SiO_2/Al_2O_3	Na_2O/SiO_2	H_2O/Na_2O	Time (h)	Temperature (K)	Time (h)	Temperature (K)	
aD2-S2.0	11.6	2.0	40	24	298	48	373	P
aD2-S1.2	11.1	1.2	40	24	298	48	373	P
aD2-S0.9	11.1	0.9	40	24	298	48	373	FAU, (P)
aD2-S0.8	11.1	0.8	40	24	298	48	373	FAU, (P)
aD2-S0.7	11.1	0.7	40	24	298	48	373	FAU, (P)
aD2-S0.6	11.6	0.6	40	24	298	48	373	FAU, (P)
aD2-S0.5	11.6	0.5	40	24	298	48	373	Amorphous
aD2-S0.4	11.5	0.4	40	24	298	48	373	Amorphous

FAU = zeolite Y, P = zeolite P.

As shown in the $SiO_2 - Al_2O_3 - Na_2O$ phase diagram in Fig. 2, the Na_2O/SiO_2 ratio in the present work was varied in the range 0.4–2.0 in order to move along a straight line through the pure zeolite Y regions reported by Breck and Flanigen [3]. In fact, two different compositional regions were identified by these authors depending on whether sodium silicate or colloidal silica was used as silica source. Using aD2 as starting material in our system, only amorphous material was obtained as a product for Na_2O/SiO_2 ratios <0.6 (aD2-S0.4 and aD2-S0.5 in Table 2 and Fig. 2), while mixtures consisting of zeolite FAU and P were obtained when the Na_2O/SiO_2 ratio was varied between 0.6 and 0.9. By further increasing the Na_2O/SiO_2 ratio, zeolite P was the only product in samples aD2-S1.0, aD2-S1.2 and aD2-S2.0. It was possible to reproduce these results by using aD1. Unexpectedly, the purest diatomite aD3 did not permit to obtain faujasite for Na_2O/SiO_2 ratios below 0.7.

As shown in Fig. 3, scanning electron microscopy revealed evident signs of overrun (i.e. zeolite P) in sample aD2-S0.6 after 48 h of synthesis time. Well-defined tetragonal crystals attributed to zeolite P appear to grow on dissolving FAU zeolite crystals. Both zeolites showed comparable SiO_2/Al_2O_3 ratios, namely 4.36 for FAU and 4.30 for P as determined by XRD and EDS, respectively. This fits with the fact that the XRD pattern of zeolite P is very close to that reported by Hansen et al. for high silica tetragonal NaP with a SiO_2/Al_2O_3 ratio of 6.9 (PDF 40–1464) [34]. Such nucleation and growth of zeolite P on dissolving faujasite has already been observed by scanning and transmission electron microscopy [35,36]. It is well-known that zeolite P is a more stable phase than zeolite FAU and that the former can nucleate before complete formation of the latter [37]. Therefore, to maximize the yield of the FAU zeolite and to limit the formation of zeolite P, synthesis time was reduced

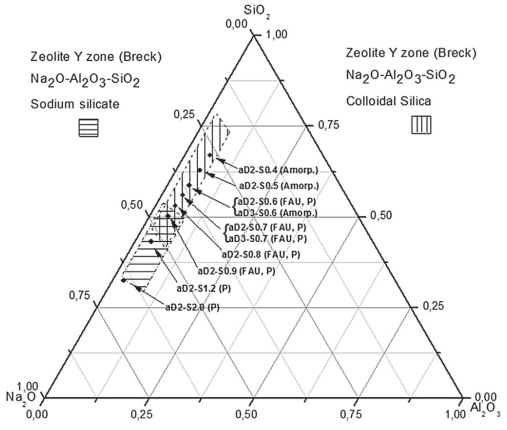

Fig. 2. $SiO_2 - Al_2O_3 - Na_2O$ phase diagram showing the distribution of the samples synthesized at different Na_2O/SiO_2 ratios (see ref. 3 for more information related to the two highlighted regions).

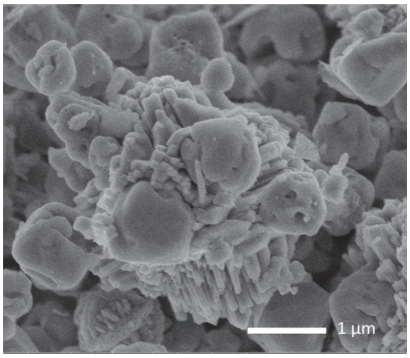

Fig. 3. SEM of aD2-S0.6 at 48 h.

below 48 h for Na_2O/SiO_2 ratios comprised between 0.6 and 2.0 using aD1 as starting material.

As shown in Fig. 4(A), zeolite P was found to be absent by XRD as synthesis time was reduced to 30 h for a Na_2O/SiO_2 ratio of 0.6. However, the XRD results also indicated the presence of appreciable amounts of amorphous material. Hence, it was not possible to obtain well-crystallized FAU zeolite for this composition. The same behavior was observed for a Na_2O/SiO_2 ratio of 0.7 (Fig. 4(B)), for which 28 h was the optimal time to avoid the presence of zeolite P. FAU zeolite, nearly free from zeolite P was obtained when synthesis time was lowered to 15 h for a Na_2O/SiO_2 ratio of 0.8 (Fig. 4(C)), but the background indicated the presence of a few amount of amorphous material. Reducing time to 13, 6 and 6h for Na_2O/SiO_2 ratios of 0.9, 1.2 and 2.0, respectively, prevented the formation of zeolite P and resulted in FAU-type zeolite with high crystallinity as the only product, as shown in Fig. 4(D), (E) and (F), respectively.

Interestingly, although no faujasite could be synthesized for Na_2O/SiO_2 ratios below 0.7 when aD3 was used, a well-crystallized faujasite product was obtained when this ratio was set to 0.85 and synthesis time adjusted to 13 h (see XRD results for aD3-S0.85–13h in Fig. 5).

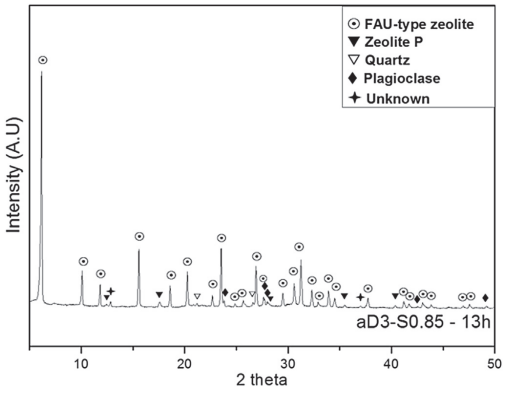

Fig. 5. XRD diffractogram of the sample aD3-S0.85-13h.

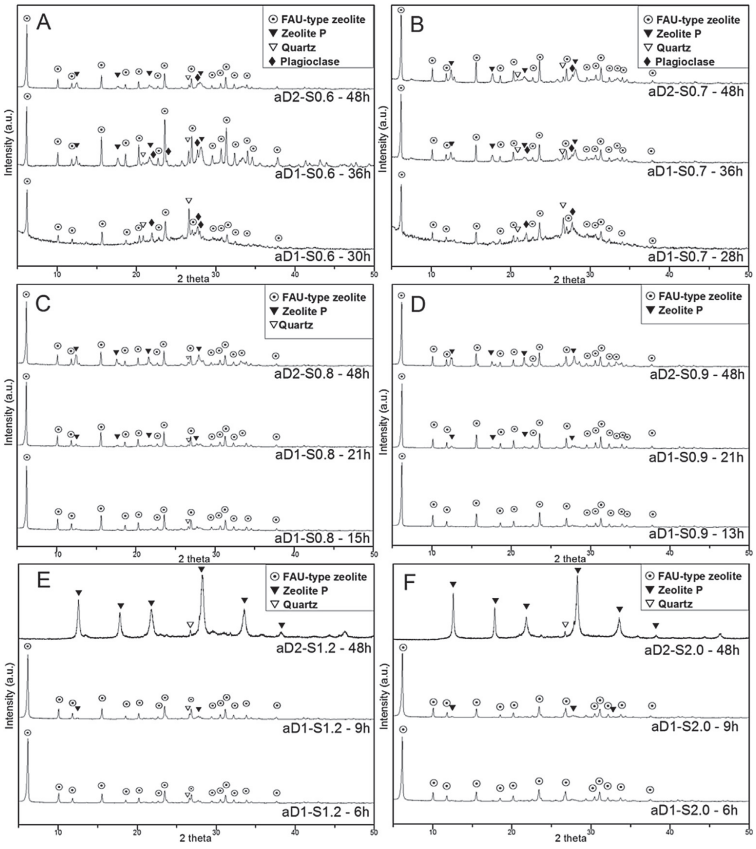

Fig. 4. XRD diffractograms of the solid products obtained after different synthesis times for Na_2O/SiO_2 ratios of: (A) 0.6; (B) 0.7; (C) 0.8; (D) 0.9; (E) 1.2; and (F) 2.0.

3.3. Characteristics of the final product

Table 3 gives the SiO_2/Al_2O_3 ratio in the FAU crystals determined by X-ray diffraction for the different Na_2O/SiO_2 ratios of the synthesis mixture, as a function of synthesis time and of which raw material was used. For each Na_2O/SiO_2 ratio except 0.6, the observed values are constant within deviations of ±0.2, which was found to be the precision of the method or caused by the variability in the final product by reproducing the same synthesis several times. As shown above, after passing an optimal synthesis time, zeolite P appeared in all cases and the FAU particles started to dissolve. Therefore, the nucleation of zeolite P and subsequent dissolution of FAU-zeolite resulted in a rather constant measured SiO_2/Al_2O_3 ratio in the dissolving FAU crystals, except for a Na_2O/SiO_2 ratio of 0.6 which showed a strong decrease of this parameter along with dissolution of the FAU crystals. This suggests that the shell of the FAU crystals is Si-rich and the core Al-rich in aD2-S0.6. This has already been observed experimentally on large FAU-crystals by energy dispersive spectroscopy [38] or on Ce^{3+} exchanged zeolite Y by X-ray photoelectron spectroscopy [39].

Fig. 6 shows scanning electron micrographs of all samples obtained after optimal synthesis time. All samples contained euhedral particles consisting of more or less intergrown crystals with octahedral symmetry. Particle size clearly increased as alkalinity was decreased by lowering the Na_2O/SiO_2 ratio from 2.0 to 0.7 (Fig. 6(A)–(E)), specifically from 0.5 μm for aD1-S2.0-6h to 2.3 μm for aD1-S0.7-28h. The degree of intergrowth also clearly diminishes with lowering the Na_2O/SiO_2 ratio in the same range. The crystals in aD1-S2.0-6h are irregular due to strong intergrowth, while increasingly more well-defined crystals with octahedral symmetry formed as the Na_2O/SiO_2 ratio was progressively decreased. However, particle size was found to decrease and the degree of intergrowth to increase again for aD1-S0.6-30h (Fig. 6(F)), which corresponds to the lowest investigated Na_2O/SiO_2 ratio that led to the formation of FAU zeolite. For Na_2O/SiO_2 ratios less than or equal to 0.8, the presence of unreacted materials becomes obvious (Fig. 6(D)–(F)). Large non-reacted diatomite skeletons were still present in aD1-S0.6 after 30h of synthesis, as shown in Fig. 7(A).

Although the reactivity process window with respect to alkalinity was narrower on the low alkalinity side for aD3 in comparison with the other leached diatomites, the well-crystallized final product obtained for aD3-S0.85-13h exhibited particles with morphology and size consistent with aD1-S0.8 and aD1-S0.9, as it can be observed in Fig. 7(B).

4. Discussion

The amount of zeolite produced in the system investigated herein depends strongly on alkalinity. The amount of FAU zeolite produced can be roughly estimated from the measured microporosity yield and X-ray crystallinity, which are reported in comparison to the values obtained for a commercial zeolite Y powder in Table 4 (for selected samples free of zeolite P). High values of the microporosity yield and X-ray crystallinity were obtained for Na_2O/SiO_2 ratios in the range 0.85–2.0, which shows that FAU crystals could be produced from diatomite at a high yield. The remaining unreacted extraneous minerals (e.g. quartz and plagioclase identified by XRD in Fig. 4) and clays most likely limited the highest values of the microporosity yield that could be achieved. The increase of the crystallinity values as the Na2O/SiO2 ratio was decreased from 2.0 to 0.85 was attributed to textural effects due to particle size. However, the microporosity yield and X-ray crystallinity values dropped dramatically as alkalinity was decreased for Na_2O/SiO_2 ratios below 0.85. As shown above, fragments of diatomite were still present in the aD1-S0.6-30h sample, which clearly indicates that alkalinity was insufficient to digest the entire raw materials and cause complete reaction for Na_2O/SiO_2 ratios below 0.85.

Table 4 also shows the yield in terms of aluminum (η_{Al}) calculated from gravimetric measurements and ICP-AES. Interestingly, this value oscillates around 1, between 0.87 and 1.36. Since yield values cannot be higher than 1, this strongly indicates that all aluminum introduced in the synthesis mixture is present in the final solid product, since the variations around 1 are within the margin of error of ICP-AES. Considering that high microporosity yield and X-ray crystallinity values were obtained for Na_2O/SiO_2 ratios in the range 0.85–2.0 and that these results corresponded to the longest allowed synthesis time for obtaining FAU zeolite as the sole product, it can be concluded that it is the depletion in aluminum that triggered the formation of zeolite P in these samples. It is well known that aluminum is preferentially consumed over silicon in the beginning of the growth of FAU zeolites and that growth ceases as aluminum is depleted, which renders the synthesis of high silica faujasite difficult. This is usually assigned to the fact that aluminate ions are necessary for the formation of sodalite cages, which are part of the FAU structure [40]. However, although highly suspected and despite several attempts [41], a clear relationship between the growth rate of FAU crystals and the concentration of aluminate ions has never been established.

The SiO_2/Al_2O_3 ratio in the zeolite (R_{XRD} in Table 4) increased steadily as alkalinity decreased in our system using diatomite as silica source reaching values of 3.9 or higher for Na_2O/SiO_2 ratios ≤ 0.85. In fact, it is well-known that low alkalinity conditions are required to synthesize high silica faujasite, since it has been shown by different research groups that the SiO_2/Al_2O_3 ratio increases in various zeolites as the excess alkalinity decreases [42,43]. However, the synthesis of high silica faujasite usually requires the use of colloidal silica as silica source, since FAU crystals with SiO_2/Al_2O_3 ratios larger than 3.9 cannot be obtained in the SiO_2–Al_2O_3–Na_2O–H_2O system by utilizing sodium silicate [3]. The use of diatomite also allowed SiO_2/Al_2O_3 ratios larger than or equal to 3.9 to be reached in the compositional field identified for colloidal silica by Breck and Flanigen (see Fig. 2). Both silica sources are similar, in that they both have a higher degree of polymerization of

Table 3
SiO_2/Al_2O_3 composition determined by XRD of the FAU products from optimal synthesis time and further on.

Starting material	Na_2O/SiO_2	SiO_2/Al_2O_3										
		6h	9h	12h	13h	14h	15h	28h	30h	33h	36h	48h
aD1, aD2	0.6								5.3	4.8	4.7	4.6
	0.7							4.7			4.6	4.7
	0.8						4.1					4.0
	0.9			3.9	3.6							3.7
	1.2	3.0	3.2	3.4								
	2.0	3.4	3.0	3.2								
aD3	0.85				3.9	3.9	4.0					

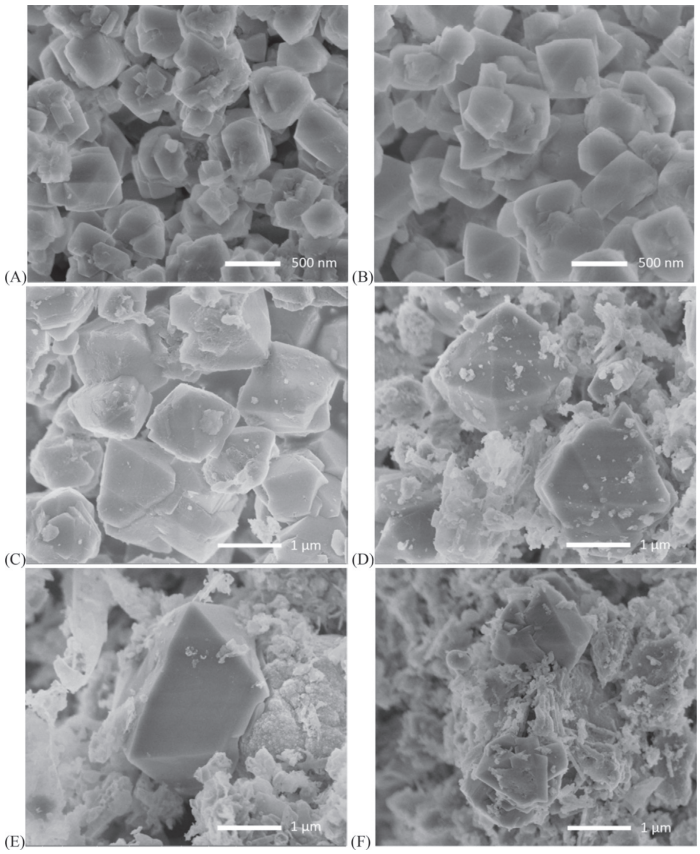

Fig. 6. Scanning electron micrographs of (A) aD1-S2.0-6h; (B) aD1-S1.2-6h; (C) aD1-S0.9-13h; (D) aD1-S0.8-15h; (E) aD1-S0.7-28h; (F) aD1-S0.6-30h.

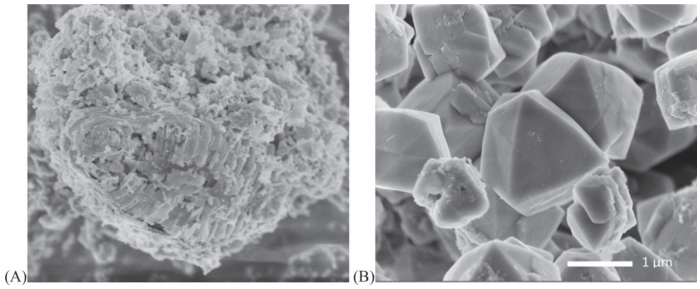

Fig. 7. Scanning electron micrographs showing: (A) a large fragment of diatomite remaining in aD1-S0.6 after 30 h of synthesis; (B) aD3-S0.85-13h.

silica than sodium silicates. Hence, our results suggest that the higher polymerized state of silica in colloidal silica and diatomite seems to play a role in the formation of high silica faujasite. It might be due to the release of larger silica species [42] or by further decrease of alkalinity during depolymerization of the starting silica source [44], or a mixture thereof. However, diatomite was too bulky to be completely consumed under the investigated synthesis conditions. Further investigation of our system with diatomite is under

Table 4
Yield, SiO_2/Al_2O_3 ratios and porous properties of the final products of the optimized syntheses.

Sample	Yield in terms of Al (η_{Al})	EDS SiO_2/Al_2O_3 ratio (R_{EDS})	XRD SiO_2/Al_2O_3 ratio (R_{XRD})	X-ray crystallinity	Surface area BET (m^2/g)	External surface area (m^2/g)	Micropore volume (cm^3/g)	Microporous yield
aD1-S0.6-30h	0.97	4.6	5.3	0.18	94.4	29.61	0.030	0.10
aD1-S0.7-28h	0.92	4.4	4.7	0.22	107.7	44.88	0.029	0.09
aD1-S0.8-15h	0.99	4.0	4.1	0.48	466.6	44.55	0.197	0.63
aD3-S0.85-13h	0.99	4.1	3.9	0.94	584.5	35.84	0.255	0.82
aD1-S0.9-13h	0.87	3.8	3.6	0.81	618.4	51.76	0.264	0.85
aD1-S1.2-6h	1.13	3.2	3.1	0.73	611.0	60.51	0.256	0.83
aD1-S2.0-6h	1.36	3.5	3.4	0.69	646.2	56.57	0.276	0.89
zY com	–	5.2	5.2	1.00	717.1	51.21	0.311	1.00

way in order to understand the formation and growth of silica-rich FAU crystals. This knowledge is required if new strategies for the synthesis of high silica faujasite without the use of expensive colloidal silica or organic compounds such as tetraethylammonium hydroxide [45] or crown ethers [44] are to be found.

According to Breck and Flanigen's definition, zeolite X is formed when the faujasite structure contains aluminum such as the SiO_2/Al_2O_3 ratio is below 3 [3]. This definition was confirmed by Rüscher et al. who argued that both domains of zeolite X and Y exist above this ratio and that pure zeolite Y can only be claimed if ratio is greater than or equal to 5.4 [39]. This delimitation was based on the resistance against amorphization during dealumination by steaming. In light of these definitions, all final products obtained in this work can be denominated zeolite Y. However, syntheses aD1-S2.0-6h and aD1-S1.2-6h produced FAU crystals with SiO_2/Al_2O_3 ratios close to 3 (see Table 4), which therefore can be said to mainly consist of zeolite X with very few zeolite Y domains. Lowering the Na_2O/SiO_2 ratio was not sufficient to produce pure zeolite Y, since synthesis aD1-S0.6-30h produced crystals with an average SiO_2/Al_2O_3 ratio of 5.3 (Table 4), but with an aluminum gradient (Table 3) and in low yield. However, both Breck and Flanigen's and Rüscher's studies showed that crystals with a SiO_2/Al_2O_3 ratio higher than 3.8 possessed hydrothermal stability only inferior by approximately 10% to that obtained for high-silica zeolite Y after steaming at 410 °C for 3 h or 500 °C for 5 h, respectively. Therefore, the product of synthesis aD3-S0.85-13h, which showed a SiO_2/Al_2O_3 ratio of 3.9 and high crystallinity, may be a stable and inexpensive alternative for FCC catalysts. In this regard, the porous properties of aD3-S0.85-13h in terms of BET specific surface area and micropore volume were comparable to the best samples prepared from aD1 for Na_2O/SiO_2 ratios ranging between 0.9 and 2.0 and therefore only limited by the unreacted extraneous minerals and clays that were initially present in the diatomite. In this regard, the zeolite Y products with highest crystallinity prepared in this study exhibit values for external surface area ranging between 51.76 and 60.51 m^2/g for samples prepared from aD1, whereas a lower value of 35.84 was obtained for aD3-S0.85-13h. The series of values for aD1 does not show any trend with respect to crystal size and the order of magnitude of these values is rather high compared with other works, in which zeolite Y crystals have been synthesized from chemical grade reagents [46]. The high values obtained for the external surface area are most likely also related to the unreacted minerals and clays remaining in the samples, since the difference in magnitude noticed between the products with high crystallinity prepared from aD1 and aD3 compares favorably with that found between the values directly measured after leaching on aD1 and aD3, i.e. 34.84 and 15.97 m^2/g, respectively.

With regard to the influence of the impurities contained in the starting diatomites, the ions released in solution during dissolution of the minerals and clays were not found to affect particularly the course of reaction. The only reproducibility issue observed was the impossibility to obtain FAU crystals for a Na_2O/SiO_2 ratio of 0.6 with the leached diatomite aD3. Considering the concentrations of the different elements present in the three leached diatomites given in Table 1, the only observation that can be made is that calcium and sulfate ions might favor the nucleation of FAU crystals under low alkalinity conditions. However, certain elements were incorporated as exchangeable cations inside the zeolites. In fact, magnesium and calcium were found to be located inside the FAU crystals by local EDS measurements, which was not the case of potassium with reservation related to diffusion of this element under high dose irradiation by the electron beam in the SEM. The level of occupation of the ion-exchangeable sites inside the FAU zeolites for Na, Ca and Mg was determined by the EDS method that we previously developed by the authors [31]. Interestingly, the two-fold difference in CaO content between the leached diatomites aD1 and aD3 (i.e. 0.79 and 0.40 wt% CaO, respectively, in Table 1) resulted in twice as less uptake of calcium inside sample aD3-S0.85-13h as compared with FAU zeolites prepared from aD1, as indicated by the Ca/Al ratios of 0.05 and 0.09 given in Table 5 for aD3-S0.85-13h and the average value of the aD1 samples, respectively. Furthermore, comparable content in MgO in both leached diatomites (i.e. 0.16 and 0.18 wt% MgO for aD1 and aD3, respectively, in Table 1) caused comparable uptake of magnesium in the corresponding FAU crystals independently of which of these two leached diatomites was used. These observations underpin the fact that improved methods must be developed to purify diatomite in order to use the latter as aluminosilica source for producing FCC-grade zeolite Y.

5. Conclusions

In this study, it was shown that Bolivian diatomite from the Potosi region could be used as silica-rich source for the synthesis of zeolite Y. Diatomites originating from different locations and therefore containing different types and amounts of minerals and clays as impurities were investigated. After optimization of synthesis time, zeolite Y with low SiO_2/Al_2O_3 ratio (3.0-3.9) was obtained at a high yield for high alkalinity conditions (Na_2O/SiO_2 = 0.85-2.0). Lower Na_2O/SiO_2 ratios resulted in incomplete dissolution of diatomite and lower yield. Nevertheless, decreasing alkalinity resulted in a steady increase of the SiO_2/Al_2O_3 ratio in

Table 5
Relative equivalents with respect to aluminum of the cations located in the zeolite of the final products. The values were determined by EDS.

Sample	Na/Al	2Ca/Al	2Mg/Al	(Na+2Ca+2Mg)/Al
zY com	1.00	n.d.	n.d.	1.00
aD1 samples[a]	0.90	0.09	0.02	1.00
aD3-S0.85-13h	0.97	0.05	0.03	1.05

n. d. (non-detected).
[a] Average values for aD1-S2.0-6h, aD1-S1.2-6h and aD1-S0.9-13h.

zeolite Y. Consequently, it was possible to synthesize almost pure zeolite Y with a SiO_2/Al_2O_3 ratio of 5.3 for a Na_2O/SiO_2 ratio of 0.6, but at a low yield. In this respect, diatomite enables the synthesis of high silica zeolite Y and behaves similarly to colloidal silica in traditional syntheses, with both sources of silica having in common a high degree of polymerization. Interestingly, the presence of minerals and clays in the starting diatomite had marginal effects on the outcome of the synthesis. However, their dissolution resulted in presence of calcium and magnesium in the zeolite Y crystals. Finally, overrun of all investigated compositions resulted in the formation of zeolite P nucleating and growing onto dissolving zeolite Y crystals, which was shown to be triggered when aluminum was completely depleted at high alkalinity.

Acknowledgments

The financial support by the Swedish Institute in the SIDA Program is acknowledged. Financial support from Bio4energy is also acknowledged. The authors also wish to thank The Knut and Alice Wallenberg Foundation for financial support with the Magellan SEM instrument.

References

[1] C.A. Ríos, C.D. Williams, M.A. Fullen, Appl. Clay Sci. 42 (2009) 446–454.
[2] S.C. Larsen, J. Phys. Chem. C 111 (2007) 18464–18474.
[3] D.W. Breck, Synthesis and properties of union carbide zeolites L, X and Y, in: Conference at University of London, 1967, pp. 47–61.
[4] S. Bhatia, Zeolite Catalysis: Principles and Applications, CRC Press, Florida, 1990.
[5] S.M. Auerbach, Handbook of Zeolite Science and Technology, Marcel Dekker, New York, 2003.
[6] A. De Lucas, M.A. Uguina, I. Covián, L. Rodríguez, Ind. Eng. Chem. Res. 32 (1993) 1645–1650.
[7] G. García, M. Falco, P. Crespo, S. Cabrera, U. Sedran, Catal. Today 166 (2011) 60–66.
[8] Q. Tan, X. Bao, T. Song, Y. Fan, G. Shi, B. Shen, C. Liu, X. Gao, J. Catal. 251 (2007) 69–79.
[9] W. Song, G. Li, V.H. Grassian, S.C. Larsen, Environ. Sci. Technol. 39 (2005) 1214–1220.
[10] M. Lassinantti, J. Hedlund, J. Sterte, Microporous Mesoporous Mater 38 (2000) 25–34.
[11] D. Boukadir, N. Bettahar, Z. Derriche, Ann. de Chimie Sci. des Mater. 27 (2002) 1–13.
[12] E.B. Drag, A. Miecznikowski, F. Abo-Lemon, M. Rutkowski, Stud. Surf. Sci. Catal. 24 (1985) 147–154.
[13] A.F. Gualtieri, Phys. Chem. Min. 28 (2001) 719–728.
[14] A. Baccouche, E. Srasra, M. El Maaoui, Appl. Clay Sci. 13 (1998) 255–273.
[15] Z. Lounis, F. Djafri, A.E.K. Bengueddach, Ann. de Chimie Sci. des Mater. 31 (2006) 439–447.
[16] R. Ruiz, C. Blanco, C. Pesquera, F. González, I. Benito, J.L. López, Appl. Clay Sci. 12 (1997) 73–83.
[17] X. Querol, N. Moreno, J.C. Umaa, A. Alastuey, E. Hernández, A. López-Soler, F. Plana, Int. J. Coal Geol. 50 (2002) 413–423.
[18] S.É. Ivanov, A.V. Belyakov, Glass Ceram. Engl. Transl. Steklo i Keramika 65 (2008) 48–51.
[19] K. Rangsriwatananon, A. Chaisena, C. Thongkasam, J. Porous Mater 15 (2008) 499–505.
[20] S. Martinovic, M. Vlahovic, T. Boljanac, L. Pavlovic, Int. J. Min. Process 80 (2006) 255–260.
[21] X. Liu, C. Yang, Y. Wang, Y. Guo, Y. Guo, G. Lu, Chem. Eng. J. 243 (2014) 192–196.
[22] M. Murat, A. Amokrane, J.P. Bastide, L. Montanaro, Clay Miner. 27 (1992) 119–130.
[23] A. Chaisena, K. Rangsriwatananon, Mater. Lett. 59 (2005) 1474–1479.
[24] Y. Du, S. Shi, H. Dai, Particuology 9 (2011) 174–178.
[25] B. Ghosh, D.C. Agrawal, S. Bhatia, Ind. Eng. Chem. Res. 33 (1994) 2107–2110.
[26] Y. Jia, W. Han, G. Xiong, W. Yang, Mater. Lett. 62 (2008) 2400–2403.
[27] H. Faghihian, N. Godazandeha, J. Porous Mater 16 (2009) 331–335.
[28] J.H. Li, Z.Q. Chi, H.F. Chen, Adv. Mater. Res. 236–238 (2011) 362–368.
[29] T. Li, H. Liu, Y. Fan, P. Yuan, G. Shi, X.T. Bi, X. Bao, Green Chem. 14 (2012) 3255–3259.
[30] C.H. Rüscher, J. -Chr Buhl, W. Lutz, in: A. Galarneau, F.D. Renzo, F. Fajula, J. Vedrine (Eds.), Zeolites and Mesoporous Materials at the Dawn of the 21st Century, Stud. Surf. Sci. Cat., vol. 135, Elsevier, Amsterdam, 2001, p. 1, 13-P15.
[31] G. García, W. Aguilar-Mamani, I. Carabante, S. Cabrera, J. Hedlund, J. Mouzon, J. Alloys Compd. 619 (2015) 771–777.
[32] S. Mendioroz, M.J. Belzunce, J.A. Pajares, J. Therm. Anal. 35 (1989) 2097–2104.
[33] X. Wang, L. Yang, X. Zhu, J. Yang, Particuology 17 (2014) 42–48.
[34] S. Hansen, U. Håkansson, A.R. Landa-Canovas, L. Falth, Zeolites 13 (1993) 276–280.
[35] F.G. Dwyer, P. Chu, J. Catal. 59 (1979) 263–271.
[36] H.W. Zandbergen, D. van Dyck, The Use of High Resolution Electron Microscopy in Fundamental Zeolite Research, vol. 49, 1989, pp. 599–608.
[37] R.M. Barrer, Hydrothermal Chemistry of Zeolites, 1982. London.
[38] T.J. Weeks Jr., D.E. Passoja, Clays Clay Min. 25 (1977) 211–213.
[39] J.F. Tempere, D. Delafosse, J.P. Contour, Chem. Phys. Lett. 33 (1975) 95–98.
[40] C.H. Rüscher, N. Salman, J.C. Buhl, W. Lutz, Microporous Mesoporous Mater 92 (2006) 309–311.
[41] T. Lindner, H. Lechert, Zeolites 14 (1994) 582–587.
[42] S.P. Zhdanov, Molecular Sieves, Society of Chemical Industry, 1968. London.
[43] H. Lechert, H. Kacirek, H. Weyda, Molecular Sieves, Van-Nostrand Reinhold, New York, 1992.
[44] F. Delprato, L. Delmotte, J.L. Guth, L. Huve, Zeolites 10 (1990) 546–552.
[45] J.M. Newsam, M.M.J. Treacy, D.E.W. Vaughan, K.G. Strohmaier, W.J. Mortier, J. Chem. Soc. Chem. Commun. (1989) 493–495.
[46] Y. Zhao, Z. Liu, W. Li, Y. Zhao, H. Pan, Y. Liu, M. Li, L. Kong, M. He, Microporous Mesoporous Mater 167 (2013) 102–108.

Paper IV

Influence of NaCl in the synthesis of FAU-type zeolites

Gustavo García, Saúl Cabrera, Jonas Hedlund, Johanne Mouzon

Submitted to Journal of Crystal Growth

Selective synthesis of FAU-type zeolites

Gustavo Garcia[a, b*], Saúl Cabrera[b], Jonas Hedlund[a], Johanne Mouzon [a]

[a] Chemical Technology, Luleå University of Technology, 971 87 Luleå, Sweden

gustavo.garcia@ltu.se,

Telephone: +46 0920 49 25 02, **Fax:** + 46 0920 49 13 99

[b] Solid State and Theoretical Chemistry, Chemistry Research Institute, San Andres Mayor University, University Campus, CotaCota, 27 Street, La Paz, Bolivia.

*Corresponding author

Abstract

In the present work, parameters influencing the selectivity of the synthesis of FAU-zeolites from diatomite were studied. The final products after varying synthesis time were characterized by scanning electron microscopy, energy dispersive spectroscopy, X-ray diffraction and gas adsorption. It was found that high concentrations of NaCl could completely inhibit the formation of zeolite P, which otherwise usually forms as soon as maximum FAU crystallinity is reached. In the presence of NaCl, the FAU crystals were stable for extended time after completed crystallization of FAU before onset of Ostwald ripening and formation of sodalite. It was also found that addition of NaCl barely changed the crystallization kinetics of FAU zeolite and only reduced the final FAU particle size and SiO_2/Al_2O_3 ratio slightly. Other salts containing either Na or Cl were also investigated. Our results suggest that there is a synergistic effect between Na^+ that promotes formation of sodalite cages and Cl^- that seems to retard the crystallization process of zeolite P and analcime. This new finding may be used to increase the selectivity of syntheses leading to FAU-zeolites and avoid the formation of undesirable by-products, especially if impure natural sources of aluminosilica are used.

Keywords

Faujasite, Sodium Chloride, zeolite P, mineralizer.

Introduction

The crystallization of zeolites is affected by numerous synthesis parameters, such as SiO_2/Al_2O_3 initial ratio, alkalinity, aging time, synthesis time and temperature, nature of the reagents, etc. These parameters have to be controlled if pure zeolite phases are desired as small variations may result in the formation of unwanted secondary phases [1].

FAU zeolite family comprised by Faujasite, X and Y, the latter with the general formula $Na_{1.88}Al_2Si_{4.8}O_{13.54}$* $9H_2O$ [2]. FAU-type zeolites have important applications in the industry such as separation processes, based mainly on zeolite X, and catalytic conversions, based mainly on zeolite Y [3]. This type of zeolite is synthesized in the Na_2O-SiO_2-Al_2O_3 system. However, zeolite P, with the formula $Na_8Al_8Si_8O_{32}$*$14H_2O$ [4], is often an undesired by-product, which may form during synthesis of FAU-type zeolite [5]. Several studies have identified the use of pure chemical reagents [1], organic structure directing agents [6] and seeding [7, 8] as key factors for selectively synthesizing FAU-type zeolites without the formation of zeolite P. Impure natural sources of aluminosilica such as clays and diatomites require additional treatments (e.g. thermal activation, acid treatment) in order to make the material reactive or avoid zeolite P formation. Another important parameter that may influence the selectivity is the presence and quantity of foreign inorganic ions.

Inorganic ions (cations and anions) are known to favor the formation of determined zeolites and thereby to behave as structure directing agents or mineralizers. Two widely used mineralizers are OH^- and F^- ions [9]. The role of alkali cations is primarily to balance the negative charge caused by the introduction of aluminum as $[AlO_4]^{-5}$ in the zeolite framework. However, the participation of alkali cations has also been shown to be fundamental to determine the final zeolite product [10]. Na^+ ions play as structure directing agent by interacting first with water molecules and subsequently with silica and alumina species directing the final structure of the zeolite product. Dewaele et al. [10] studied the effect of different alkali chloride salts added to the synthesis mixture to obtain pure FAU-type zeolites. The main findings were that the different alkali ions (Na^+, K^+, Li^+, Rb^+, Cs^+, NH_4^+) added as chlorides mainly influenced the type of zeolite that formed, but also strongly affected the morphology,

composition and size of the crystals. Na^+ ions promote the formation of zeolites LTA, FAU and SOD (sodalite, $Na_6[Al_6Si_6O_{24}]*2NaCl{\cdot}6H_2O$) [11], which are composed of sodalite cages. However, FAU and LTA will eventually transform to the more thermodynamically stable zeolite P after the optimal synthesis time has been exceeded. On the other hand, K^+, Rb^+ and Cs^+ have been shown to favor the formation of more compact zeolite frameworks such as P, M and analcime [12]. Zhan et al. [13] have reported that NaCl at low concentration (down to Na/Si= 0.001) favors FAU over LTA and reduces particle size. Liu et al. [14] also observed a diminishment of particle size in the synthesis of super-fine zeolite Y by adding NaCl to the synthesis mixture, which was explained by a strong electrolyte effect in the solution.

In the present work, we report on another effect of NaCl on the synthesis of pure FAU-type zeolite from diatomite, namely the inhibition of the formation of undesired zeolite P as secondary phase. Moreover, we studied the effect of NaCl on the crystallization rate, yield, crystal size and Si/Al ratio as well as the influence of the addition of various salts containing either Na^+ or Cl^- on the final as-synthesized zeolite product. We found that NaCl can be used to increase the selectivity of syntheses leading to FAU type zeolite.

Experimental design

Synthesis procedure

Sampling and treatment of the Bolivian diatomite used as raw material are described elsewhere [15]. The acid treated diatomite aD1 was used. It was added to a NaOH solution whilst stirring together with a suitable amount of $Al_2(SO_4)_3$ to arrive at the desired SiO_2/Al_2O_3 molar ratio. NaCl was added to the mixture to adjust the composition to the following ratios: Na_2O/SiO_2 = 1.2; SiO_2/Al_2O_3 = 11; H_2O/Na_2O = 40 and $NaCl/Al_2O_3 = x$, where x = 0, 1 and 40 (corresponding to 0, 4 and 152% increase in Na_2O, respectively). After aging for 24h, the mixtures were transferred to Teflon lined autoclaves and placed in an oven kept at 373 K. After hydrothermal treatment for a certain time, the autoclave was quenched and the solid product was repeatedly filtered and dispersed in distilled water until the

pH of the filtrate liquid was less than 9. The final solid product was dried in an oven at 373 K overnight and weighed in order to estimate the yield.

Finally, different salts were evaluated in addition to NaCl. In this case the molar composition of the synthesis mixture was: Na_2O/SiO_2 = 1.0; SiO_2/Al_2O_3 = 11; H_2O/Na_2O = 40 and X/Al_2O_3 = 40, where *X* = NaCl, $NaNO_3$, NaF, Na_2SO_4, KCl, NH_4Cl or NH_4OH.

Characterization

Powder XRD data of the zeolite products were recorded by a PANalytical Empyrean X-ray diffractometer equipped with a PixCel3D detector and a graphite monochromator. CuKα1 radiation was used and 2θ was varied in the range 5-50°.

The SiO_2/Al_2O_3 ratio of the FAU zeolites was calculated using the empirical relationship proposed by Rüscher et al. [16] by determining the lattice parameter from the (555) reflection of faujasite by using silicon as an internal standard. Faujasite crystallinity was determined by calculating the area under the peaks in the 2θ region 30.0-31.8° after background removal and comparing it to that obtained for a commercial zeolite Y powder with a SiO_2/Al_2O_3 ratio of 5.16.

The morphology of the raw materials, intermediate products and final products were studied by scanning electron microscopy (SEM) using a Magellan 400 instrument supplied by the FEI Company. The samples were investigated using a low accelerating voltage and no conductive coating. Also, crystal size distribution was estimated by measuring a population of 100 crystals for each sample.

Energy dispersive spectroscopy (EDS, X-max detector 50 mm^2, Oxford Instruments) was also performed to establish the overall composition of the final solid products and the dried liquid phase. EDS analysis was performed at 10 kV on a SEM equipped with a microinjector (Merlin SEM, Carl Zeiss) in order to mitigate charging by feeding nitrogen gas close to the surface of samples, repeating the same methodology that was previously shown to be successful to estimate the amount of exchanged ions in zeolite A [17]. The partition of silicon in the final solid products was estimated from the silicon content measured by EDS in the liquid and solid phases. The sum of the calculated

quantities for Si in the solid and liquid phases was found to be in good agreement with the quantity that was originally introduced in the mixture.

Nitrogen adsorption at 77 K was recorded using a Micromeritics ASAP 2010 instrument. Specific surface area was determined using the Brunauer–Emmett–Teller (BET) method. The micropore volume and the external surface area of the final products were determined by the *t*-plot method using the formula:

$t = [13.9900 / (0.0340 - \log (P/P_0))] \text{ ^ } 0.5000$ (1)

The microporous yield was also determined from the micropore volume of the samples by comparison with the micropore volume of the commercial powder of zeolite Y.

Results

The composition with a Na_2O/SiO_2 ratio of 1.2 and $x = 0$ was studied as a function of synthesis time. This series is hereafter referred to as S1.2-0NaCl. Figure 1 shows that FAU zeolite starts to crystallize after 1 h and that maximum crystallinity is reached between 4 and 6h of synthesis time. Longer synthesis times (>6h) lead to a decrease of XRD crystallinity due to dissolution of FAU crystals. Instead, the more thermodynamically stable zeolite P forms (Figure 1B). SEM micrographs of S1.2-0NaCl at different synthesis times are shown in Figure 2. After 5h (Figure 2A), the sample consists mainly of FAU-type crystals with octahedral shape and a high degree of intergrowth. Extending synthesis time causes the FAU zeolite crystals to be completely replaced by tetragonal crystals of zeolite P after 48h (Figure 2B).

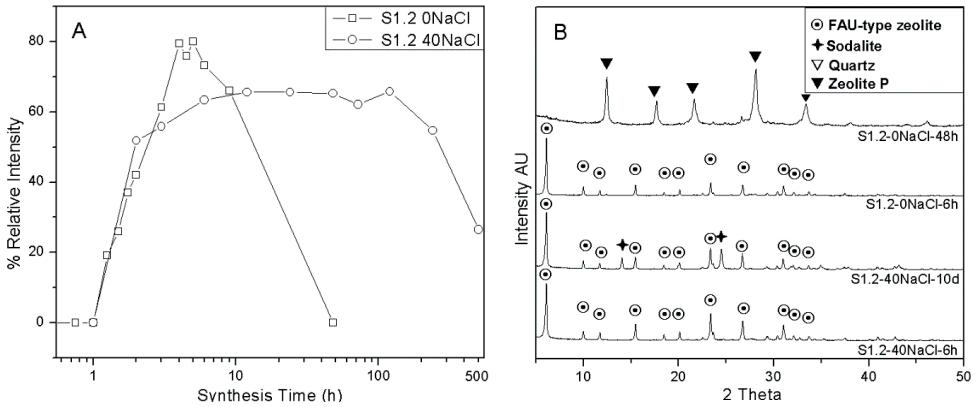

Figure 1. (A) Relative XRD crystallinity for the S1.2 system with $x = 0$ and 40 as a function of synthesis time. (B) XRD diffractograms for selected samples showing either maximum faujasite crystallinity or high degree of overrun.

The addition of a large amount of NaCl ($x = 40$, i.e. S1.2-40NaCl) barely changes the crystallization rate as shown in Figure 1A by the relative faujasite XRD crystallinity curve. Crystallization also starts after 1h and crystallization rate is similar until 2 h before slowing down during the following four hours to reach maximum crystallinity after approximately 6 h. This time to reach maximum crystallinity is comparable with that obtained without the addition of NaCl. However, the presence of NaCl causes crystallinity to remain constant over a longer period of time, the faujasite XRD crystallinity decreases only after 120 h of synthesis. As a matter of fact, the formation of zeolite P was completely inhibited and instead another secondary product was identified after 240 h of synthesis, namely sodalite (Figure 1B).

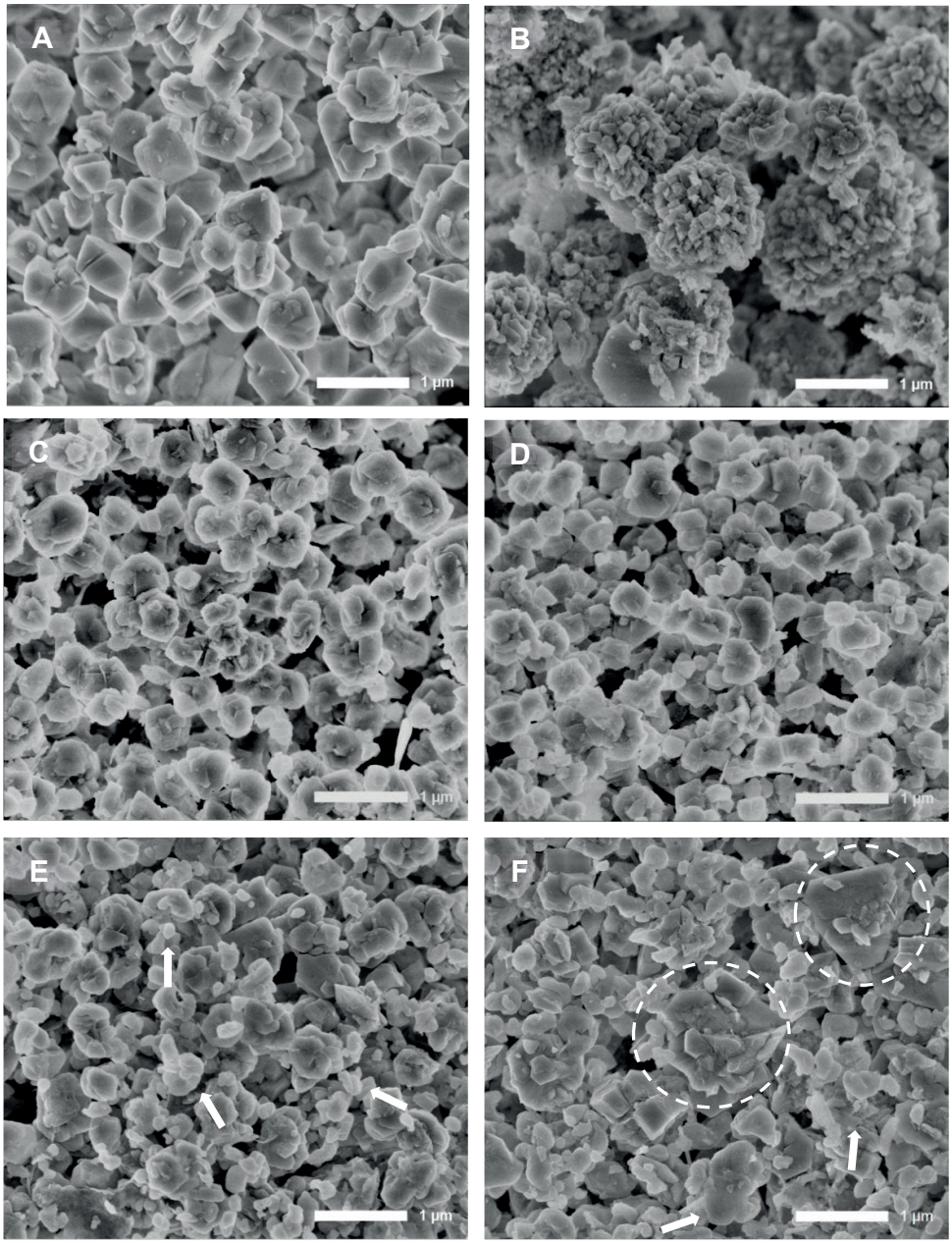

Figure 2. SEM micrographs showing: S1.2-0NaCl after (A) 5 h and (B) 48h of synthesis time; and S1.2-40NaCl after different synthesis times: (C) 6h, (D) 120h, (E) 240 h and (F) 504h.

These results for S1.2-40NaCl were confirmed by SEM observations. It is evident by comparing Figure 2C and Figure 2D that no morphological changes occur to the faujasite crystals between 6 and 120 h. After 240 h (Figure 2E), the apparition of rounded shaped crystals (white arrows) that are attributed to sodalite can be noticed as well as an increase in size of FAU-type crystals. This trend is more remarkable after 504 h of synthesis time in Figure 2F, while the population of sodalite crystals further developed (white arrows), it can be also appreciated the occurrence of FAU-type crystals with sizes around 1 μm, probably by Ostwald ripening (white circles); during ripening the subcritical FAU-type clusters are considered to dissolve spontaneously, so that their mass is released to contribute to further growth of remaining clusters, giving as a result larger FAU-type crystals [18].

Table 1. Data on silicon partition, relative XRD crystallinity, SiO_2/Al_2O_3 ratio, microporous yield and external surface area.

Sample	**Si in final solid** (% of all Si)	**Relative XRD Crystallinity** (%)	**XRD SiO_2/Al_2O_3**	**Microporous yield** (%)	**External surface area** (m^2/g)
S1.2-0NaCl-5h	50	87.7	2.91	79	42.5
S1.2-40NaCl-6h	52	63.3	2.71	93	65.0
S1.2-40NaCl-120h (5d)	48	65.8	2.66	92	81.2
S1.2-40NaCl-240h (10d)	-	54.9	2.66	68	43.5
Commercial zeolite Y	-	100	5.16	100	49.5

Although the relative XRD crystallinity was lower for S1.2-40NaCl-6h than for S1.2-0NaCl-5h with 63.3 and 87.7%, respectively, the sample with NaCl addition showed a higher crystallinity from microporous yield, i.e. 93% to be compared with 79% in the absence of NaCl (see Table 1). Interestingly, both samples consisted mostly of faujasite crystals according to XRD and were produced at comparable yield as indicated by the partition of silicon between the liquid and the final product for the corresponding syntheses, i.e. 50 and 52% of the total silicon present in the final solid product in S1.2-0NaCl-5h and S1.2-40NaCl-6h, respectively. In fact, the discrepancies between relative XRD crystallinity and microporous yield might be explained in terms of crystal size in both samples. As

shown in Fig. 2(A) and Fig.2(C), the sample synthesized in the presence of sodium chloride consisted of smaller crystals. This was confirmed by measuring crystal size in SEM micrographs on a large number of crystals. Figure 3 shows the corresponding size distribution for both samples. A median size of 600 nm was measured on S1.2-0NaCl-5h. The 10% decrease in size for S1.2-40NaCl-6h, i.e. 540 nm, might have caused a decrease in intensity of the diffracted peaks used for calculating crystallinity, while it contributed to expose more external surface area for probing the microporous volume, as shown in Table 1 by the higher value of the specific external surface area for S1.2-40NaCl-6h compared with S1.2-0NaCl-5h.

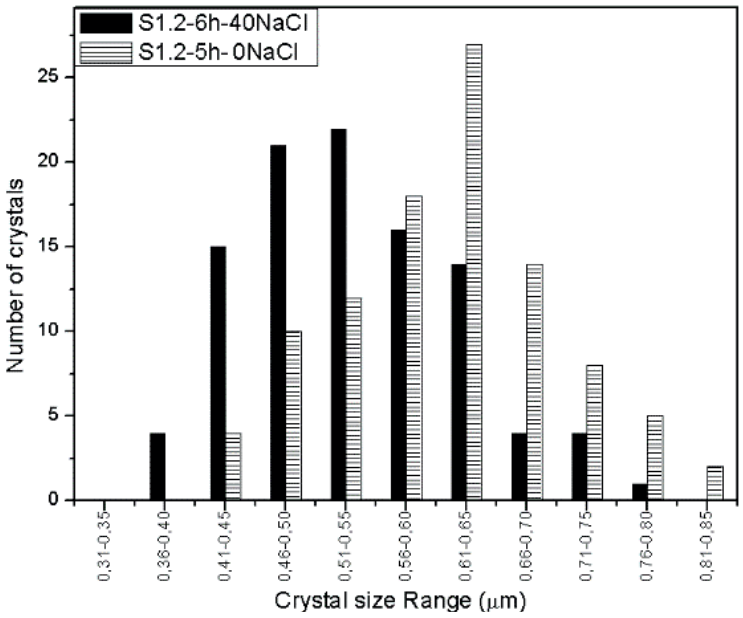

Figure 3. Crystal size distribution in S1.2-40NaCl-6h (black) and S1.2-0NaCl-5h (dense).

Discussion

Table 1 also gives the SiO_2/Al_2O_3 ratio in the FAU crystals determined by X-ray diffraction for the samples with $x = 0$ or 40 for different synthesis times. It is evident that the samples synthesized in the presence of a large amount of NaCl exhibit a lower SiO_2/Al_2O_3 ratio of approximately 2.7 to be compared with 2.9 without NaCl addition. In our previous work [15], we showed that all the

aluminum was present in the final solid product. Therefore, the addition of NaCl must have promoted incorporation of Al from plagioclase or an intermediate product into the framework of the zeolite [15], which might also be responsible for the higher microporous yield of the S1.2-40NaCl samples (93 and 92% for 6 and 120 h, respectively) compared with S1.2-0NaCl (79% for 5 h). This effect is most probably due to the higher concentration of Na^+ ions, as the same trend was evidenced in our previous work, in which higher Na_2O/SiO_2 ratios by addition of NaOH led to lower SiO_2/Al_2O_3 ratios in the FAU-type zeolite [15]. A higher incorporation of aluminium in the zeolite framework is of course expected in the case of high concentration and availability of charge balancing Na^+ cations.

Another similarity between the addition of NaOH and NaCl is the smaller crystal size obtained by increasing the Na_2O/SiO_2 ratio. Since the S1.2-0NaCl-5h and S1.2-40NaCl-6h samples reached maximum crystallinity with similar yields according to the final partition of silicon (Table 1), NaCl clearly influenced nucleation, probably be increasing the number of nuclei, resulting in smaller final crystals. This is usually interpreted as an increase of supersaturation in classical crystallization theories [19]. Recently, Liu *et al*. [14] reached a similar conclusion based on inorganic salts that were introduced to the synthesis mixture under controlled synthesis factors, such as alkalinity and crystallizing temperature. The results showed that the particle size of zeolite Y could be apparently decreased by introduction of NaCl. Besides, Zhan *et al*. [13] showed that particle size is reduced by the addition of NaCl at low concentration (down to Na/Si= 0.001). Zhan et al. also showed that the formation of FAU zeolite is favored over LTA in these conditions. The authors proposed that NaCl promotes the formation of more building units of 6 membered rings (6R and D6R) over 4 membered rings (4R and 4DR), the latter being the precursors for zeolite A and zeolite P (only 4R). This seems to be caused by the transformation of 4R and D4R to 6R and D6R. As a result, there probably exists a higher number of 6 membered rings for the connection of sodalite cages to form FAU-type zeolite crystals than 4-membered rings for connection of sodalite cages in the configuration leading to LTA-type crystals [20]. This may be also the reason explaining the facts that formation of zeolite P is inhibited and that FAU-type zeolite directly forms sodalite (composed by sodalite cages) at very long synthesis time in the presence of large amounts of NaCl.

Furthermore, it might be tempting to impart the key role of these observations to sodium ions, since it is known as a "structure-directing agent" of sodalite cages. However, considering the findings of Zhang et al. [13], Cl^- was demonstrated to strongly promote the formation of FAU-type zeolites. To challenge this hypothesis, NaCl was substituted with different salts in the aD1-S1.0-40NaCl-120h system. The ratio x = salt/Al_2O_3 was set to 40 with respect to Na^+, Cl^- or NH_4^+ contained in the salt. The X-ray diffractograms of the resulting products are presented in Figure 4. As discussed earlier, the addition of NaCl results in pure FAU even after 120 h of synthesis. Interestingly, the addition of $NaNO_3$ resulted in almost pure sodalite. The formation of sodalite at higher Na_2O/SiO_2 ratio is similar to the addition of NaOH as in our previous work [15], apart from being triggered earlier herein. However, other anions were also found to play an important role on the outcome of the syntheses. As a matter of fact, addition of NaF or Na_2SO_4 did not prevent the formation of zeolite P, but resulted in a mixture of zeolite P and analcime. As analcime is known to be an overrun product of zeolite P [21], the reaction kinetics seems to have been increased by these salts. This can be understood by the fact that fluorine ions F^- are known to act as mineralizer as OH^-. Our results suggest that it might also be the case of sulfate ions. To investigate the effect of chlorine ions, both KCl and NH_4Cl were evaluated. The former resulted in the formation of almost exclusively zeolite P, which can be related to potassium ions known to favor nucleation of this phase [12]. Surprisingly, zeolite crystallization was completely inhibited by NH_4Cl. Quartz was originally present inside the diatomite Addition of NH_4OH resulted in the formation of montmorillonite-type clay. Therefore, our results suggest that chlorine ions inhibits crystallization of zeolite P and analcime and that the beneficial effect of NaCl addition on the synthesis of faujasite zeolite is due to a synergic effect of Na^+ and Cl^- ions.

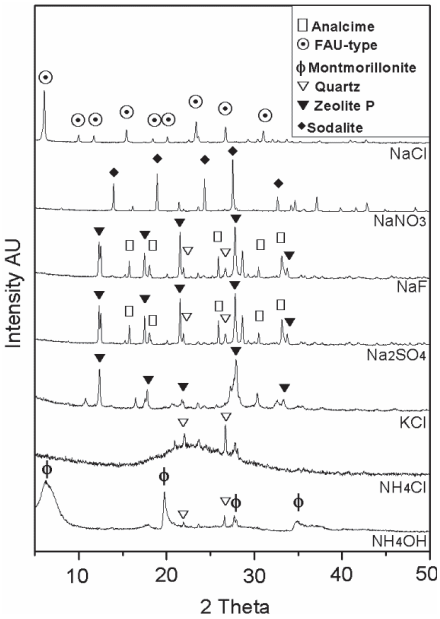

Figure 4. XRD diffractograms of S1.0-40X-120h, where X = NaCl, $NaNO_3$, NaF, Na_2SO_4, KCl, NH_4Cl or NH_4OH.

Finally, in order to determine the necessary quantity of NaCl, the amount of added NaCl was reduced to $x = 1$. Figure 5 shows the XRD results of samples S1.2-0NaCl-12h and S1.2-1NaCl-12h. Obviously, this lower amount of NaCl was still successful in inhibiting the formation of zeolite P until at least 12 h of synthesis.

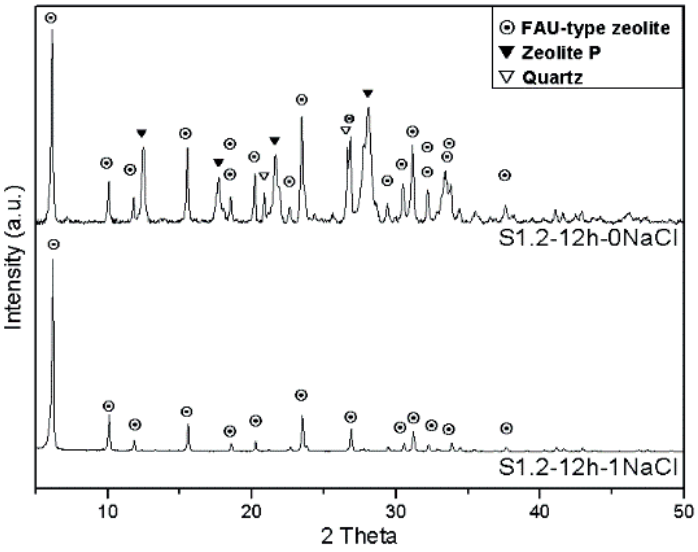

Figure 5. XRD diffractograms of S1.2-0NaCl-12h and S1.2-1NaCl-12h.

5. Conclusion

In the present work, the effect of NaCl on the selective synthesis of FAU-zeolites from diatomite was studied. A high amount of this salt (i.e. 152% increase in Na_2O) was found to inhibit the formation of zeolite P. In the presence of NaCl, the FAU crystals were stable for extended synthesis times before onset of Ostwald ripening and formation of sodalite as a new product. Inhibition of zeolite P was still effective for a smaller addition of NaCl (i.e. 4% increase in Na_2O). Besides, the addition of NaCl barely changed the crystallization kinetics of FAU but reduced particle size by 10% and the SiO_2/Al_2O_3 ratio from 2.91 to 2.71. Other salts containing either Na or Cl were also tested in order to investigate the role of NaCl. Our results suggest that there is a synergistic effect between Na^+ that promotes formation of sodalite cages and Cl^- that retards the crystallization process of zeolite P and Analcime. This new finding may be used in order to increase the selectivity of FAU-zeolites and avoid the formation of undesirable by-products, especially if impure natural sources of aluminosilica are used.

6. Acknowledgments

The financial support by the Swedish Institute in the SIDA Program is acknowledged. Financial support from Bio4energy is also acknowledged. The authors also wish to thank The Knut and Alice Wallenberg Foundation for financial support with the Magellan SEM instrument.

References

[1] K.E. Hamilton, E.N. Coker, A. Sacco Jr, A.G. Dixon, R.W. Thompson, Zeolites 13 (1993) 645-653.
[2] D.W. Breck, Synthesis and Properties of Union Carbide Zeolites L, X and Y, in: Conference at University of London, 1967, pp. 47-61.
[3] H. Awala, J.P. Gilson, R. Retoux, P. Boullay, J.M. Goupil, V. Valtchev, S. Mintova, Nature Materials 14 (2015) 447-451.
[4] S. Hansen, U. Håkansson, A.R. Landa-Canovas, L. Falth, Zeolites 13 (1993) 276-280.
[5] H. Faghihian, N. Godazandeha, Journal of Porous Materials 16 (2009) 331-335.
[6] J.F. Charnell, Journal of Crystal Growth 8 (1971) 291-294.
[7] J.H. Li, Z.Q. Chi, H.F. Chen, Synthesis of NaY zeolite molecular sieves from calcined diatomite, in: Advanced Materials Research, vol 236-238, 2011, pp. 362-368.
[8] X.S. Zhao, G.Q. Lu, H.Y. Zhu, Journal of Porous Materials 4 (1997) 245-251.
[9] T. Lindner, H. Lechert, Zeolites 14 (1994) 582-587.
[10] N. Dewaele, P. Bodart, Z. Gabelica, J.B. Nagy, SYNTHESIS AND CHARACTERIZATION OF FAUJASITE-TYPE ZEOLITES II. THE ROLE OF ALKALI CHLORIDES, in: Studies in Surface Science and Catalysis, 1985, pp. 119-128.
[11] B. Xu, P. Smith, C. Wingate, L. De Silva, Hydrometallurgy 105 (2010) 75-81.
[12] M. Murat, A. Amokrane, J.P. Bastide, L. Montanaro, Clay Minerals 27 (1992) 119-130.
[13] Y. Zhan, X. Li, Y. Zhang, L. Han, Y. Chen, Ceramics International 39 (2013) 5997-6003.
[14] X. Liu, L. Li, T. Yang, Z. Yan, Shiyou Xuebao, Shiyou Jiagong/Acta Petrolei Sinica (Petroleum Processing Section) 28 (2012) 555-560.
[15] G. Garcia, E. Cardenas, S. Cabrera, J. Hedlund, J. Mouzon, Microporous and Mesoporous Materials 219 (2016) 29-37.
[16] C.H. Rüscher, J. -Chr. Buhl, W. Lutz, in: A. Galarneau, F.D. Renzo, F. Fajula, J. Vedrine (Eds.), Zeolites and Mesoporous Materials at the Dawn of the 21 st Century, Stud. Surf. Sci. Cat., vol 135, Elsevier, Amsterdam, 2001, pp. 1, 13-P15.
[17] G. García, W. Aguilar-Mamani, I. Carabante, S. Cabrera, J. Hedlund, J. Mouzon, Journal of Alloys and Compounds 619 (2015) 771-777.

[18] G. Madras, B.J. McCoy, Chemical Engineering Science 57 (2002) 3809-3818.

[19] B. Subotic, J. Bronic, R.v. Ballmoos, J.B. Higgins, M.M.J., in: Proc. 9th Int. Zeolite Conf., Butterworth-Heinemann, Treacy (Eds.), 1993, p. 321.

[20] M. Ogura, Y. Kawazu, H. Takahashi, T. Okubo, Chemistry of Materials 15 (2003) 2661-2667.

[21] S.N. Azizi, A. Alavi Daghigh, M. Abrishamkar, Journal of Spectroscopy 2013 (2013) 5.

Paper V

Zeolite coated steel monoliths for carbon dioxide separation

J. Mouzon, G. García, R.S. Luciano, E. Potapova, M. Grahn, D. Korelskiy, and J. Hedlund

To be submitted

Zeolite coated steel monoliths for carbon dioxide separation

J. Mouzon, G. Garcia, R.S. Luciano, E. Potapova, M. Grahn, D. Korelskiy, and J. Hedlund*

Chemical Technology, Luleå University of Technology, SE-971 87 Luleå, Sweden

*To whom correspondence should be addressed: jonas.hedlund@ltu.se; tel.: +46 920 492105; fax: +46 920 491199.

Abstract

Steel monoliths with nonporous walls and high cell density were coated with 3 μm or 11 μm thick zeolite films. The sample very characterized by SEM, EDS and XRD and the CO_2 adsorption performance was evaluated by break through experiments. The films very well defined with even thickness and comprised pure zeolite NaX. The adsorbents displayed very sharp breakthrough fronts with good CO_2 adsorption capacity. This makes zeolite NaX coated steel monoliths promising alternatives to traditional adsorbents in processes with short cycle times.

Keywords

Carbon dioxide, adsorption, structured adsorbent, zeolite X

Introduction

Zeolites are crystalline aluminosilicates of natural or synthetic origin with a three-dimensional framework structure with micropores. Faujasite (FAU) type zeolites have a cubic unit cell and a framework comprising so-called 12-ring pores running in the <111> directions of the crystals. The diameter of the ring is about 7.4 Å, but the effective pore diameter is dependent of the type of counter ions in the zeolite. The zeolites X and Y both have an FAU framework, and the Si/Al ratio is per definition between 1-1.5 for zeolite X and greater than 1.5 for zeolite Y [1].

These zeolites adsorb CO_2 and high adsorption capacity of zeolite NaX pellets has been reported in several works. At the experimental conditions used in the present study, i.e. a partial CO_2 pressure corresponding to 10% of atmospheric and room temperature, Rodrigues et al. [2] report a capacity of 2.5 mol CO_2/kg zeolite. However, Myers et al. [3] report an even higher capacity of 3.6 CO_2/kg zeolite at 31.4 °C for zeolite NaX powder. As the CO_2 adsorption capacity is high, pellets of zeolite X are used in cyclic gas separation processes, such as pressure swing adsorption (PSA) and temperature swing adsorption (TSA) processes for CO_2 separation.

These processes may be intensified by reduction of cycle time, however currently used adsorbents in the form of packed beds of beads or extrudates suffer from high internal mass transfer resistance in the beads or extrudates and pressure drop in the bed at the high gas velocities that occur at short cycle times. These resistances impose limitations for the PSA/TSA adsorption processes in terms of cycle time, energy demand, and overall system efficiency. It is possible to reduce these limitations by using non-particulate adsorbent structures, i.e. structured adsorbents such as monoliths, laminates, foams and fabric structures [4].

The main advantages of monolithic adsorbents as compared to pellets are the lower resistance to mass transfer due to the shorter diffusion path, and the lower pressure drop resulting from a higher void volume and the straight channels in monoliths. Although adsorbent loading usually is significantly lower in monoliths as compared to pellets, this could be compensated for by reduced cycle time and increased cycle frequency to increase throughput, while keeping the pressure drop low.

We have explored zeolite coated monoliths for carbon dioxide separation[2] and showed that zeolite NaX coated cordierite monoliths displayed much sharper breakthrough fronts and lower pressure drop than zeolite pellets. A model showed that at very short cycle times, structured adsorbents could even reach higher productivity than pellets although the

adsorption capacity was lower [5]. It was also demonstrated by experiments and numerical modeling that the high porosity of the walls in cordierite monoliths had an adverse effect on the breakthrough front. The pores in the monolith result in dispersion by pore filling with carbon dioxide gas, not adsorption [6]. Therefore, the work indicated that dense supports may improve the process performance of coated monolith adsorbents. To maximize adsorption capacity, the film thickness should be as large as possible and numerical modelling of nonpourous monoliths coated with films of varying thickness was carried out [7]. It was shown that a film thickness of 20 or 30 μm resulted in broadening of the CO_2 breakthrough front, but films with 10 μm thickness or low displayed sharp fronts. Consequently, the work indicated that an ideal CO_2 adsorbent is a non-porous monolith with high cell density coated with an about 10 μm thick zeolite NaX film.

The scope of the present work was to prepare such adsorbents and evaluate CO_2 separation performance by breakthrough experiments.

Materials and Methods

Cylindrical nonporous steel monoliths (Metalit, Emitec, Germany) with a high cell density of 1600 cpsi were used as carriers for the structured adsorbents. The outer steel shell of the monoliths had a length of 15.2 cm and an outer diameter of 3.0 cm, while the length of the (nonporous) honeycomb structure in the shell was 14.9 cm with a diameter of 2.8 cm, corresponding to a volume of 92 ml, see Figure 1. The surface area of the steel in these monoliths is 7332 cm^2 per monolith according to the supplier. The weight of each steel monolith used for deposition of zeolite films was recorded prior to growth of zeolite films.

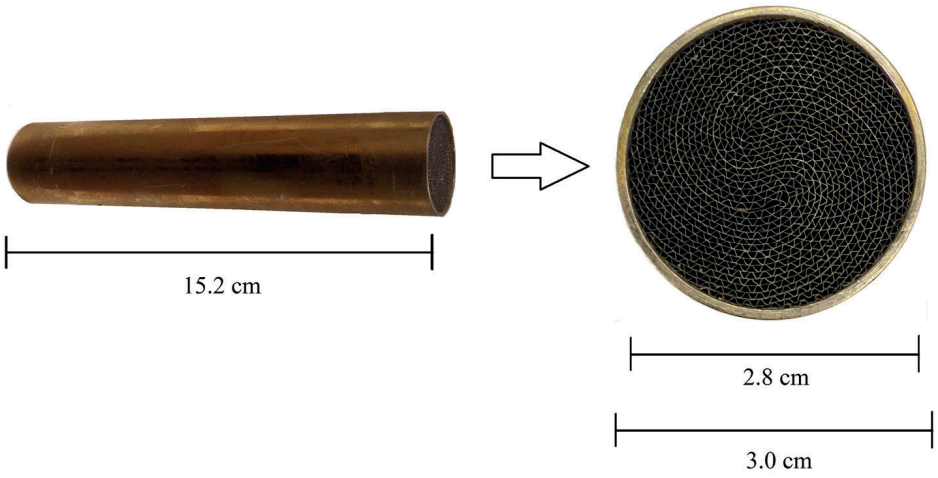

Figure 1. Photographs of steel monoliths used as carrier material for the structured adsorbent.

A zeolite NaX film was grown on the carrier material using a similar method as described before [5]. In brief, the monolith was first rinsed with a 0.1 M aqueous ammonia solution and then treated with a 0.4 wt % aqueous solution of a cationic polymer at pH 8 to render the surface positively charged. A 1 wt % aqueous dispersion of zeolite NaX crystals with a diameter of 80 nm was used for seeding. The monolith was treated with the dispersion for 1 h to adsorb a monolayer of the crystals on the surface. The excess of seeds was removed by rinsing with a 0.1 M aqueous ammonia solution. After seeding, zeolite NaX films were grown on the monoliths by hydrothermal treatment in a clear synthesis solution with the molar composition: $73Na_2O:Al_2O_3:8SiO_2:4547H_2O$. The synthesis was performed in a glass reactor immersed in an oil bath kept at 90°C and connected to a reflux condenser. The synthesis was performed in 21 or 70 steps of 65 min each to reach a film thickness of about 3 and 10 µm, respectively. After each step, the monolith was rinsed with a 0.1 M aqueous ammonia solution. After synthesis, the samples were rinsed and dried at 350 °C in room air, cooled in vacuum and vented with dry nitrogen gas before the weights of the zeolite coated monoliths were recorded. The weights of the zeolite films were estimated from the difference of the weight after synthesis and the weight of the carrier material recorded before synthesis.

The morphology of the structured adsorbent was investigated using a Zeiss Merlin field emission scanning electron microscope. Cross sections of the samples were prepared by cooling the sample in liquid nitrogen and fracturing. Energy dispersive spectroscopy (EDS, X-max detector 50 mm^2, Oxford Instruments) The analysis was performed at 10 kV at low

magnification (100 times) using a microinjector in order to mitigate charging by blowing nitrogen gas close to the surface of samples and thereby preventing diffusion of Na. The method was calibrated using a sample of zeolite A powder with known composition as a reference.

X-ray diffraction data was recorded with a step size of 0.026° 2θ using a PANalytical Empyrean X-ray diffractometer equipped with a PIXcel 3D detector and a Cu LFF HR X-ray tube.

Breakthrough experiments were carried out using several experimental configurations as illustrated in Figure 2. For breakthrough experiments, two steel monoliths were mounted in series in a steel column with an inner diameter of 3.2 cm. Graphite tape (Aesseal, Sweden) was wrapped around the column to seal the gap between the monolith and the column. Glass beads were placed in the bottom of the column, to reduce the dead volume of the conical column entrance. Prior to the experiment, the column was kept at a temperature of 300°C for three hours, with a nitrogen (Linde Gas, 99.99%) flow of 0.2 dm^3/min. After cooling, CO_2 breakthrough experiments were conducted at atmospheric pressure and room temperature. For this purpose, a feed comprised of 10% CO_2 in nitrogen (AGA Gas AB, 99.990% CO_2/99.9990% N_2) with a flow rate of 1.00, 0.50 or 0.25 dm^3/min was used. The carbon dioxide concentration in the effluent from the column was measured by an IR 1507 fast response carbon dioxide infrared transducer (CA-10 Carbon Dioxide Analyzer - Sable Systems International, response time 0.5 s). Regeneration of the adsorbent between the adsorption steps was carried by heating the column to 120°C, with a nitrogen flow of 0.2 dm^3/min. Heating rates during activation and regeneration of the adsorbent were 2°C/min and the cooling rates were lower (self-cooling).

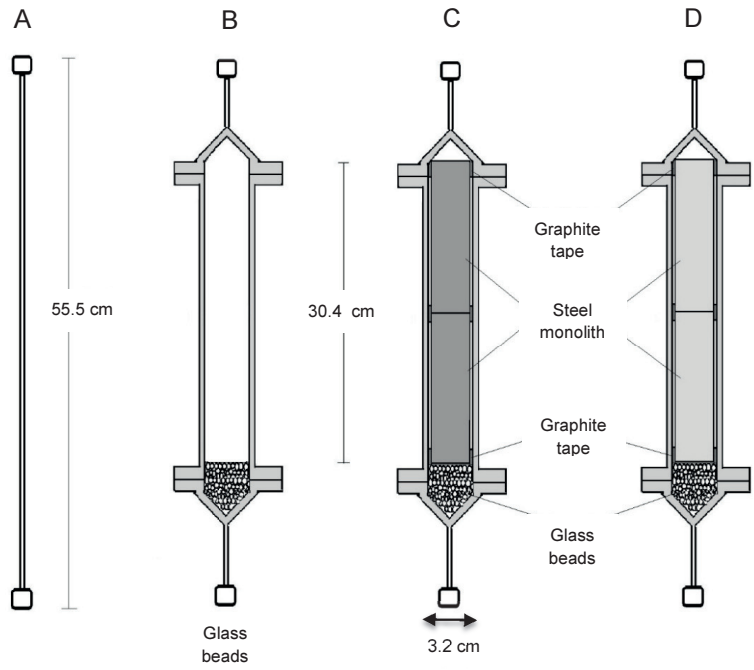

Figure 2. Schematic illustrations of the different experimental configurations evaluated for breakthrough experiments: (A) Tube (ID 1.5 mm) with a total length of 555 mm connected to the breakthrough apparatus, (B) column (ID 3.2 cm) with glass beads, (C) column with 2 steel monoliths, graphite tape and glass beads and (D) column with 2 zeolite coated steel monoliths, graphite tape and glass beads.

The CO_2 adsorption capacity q of the zeolite on the monoliths was estimated from the breakthrough data from the time t to reach C/C_0=0.5 for the coated monoliths and the time t to reach C/C_0=0.5 for the uncoated monoliths using the simple equation:

$$q = \frac{p_{CO_2} F \left(t^{coated}_{C/C_0=0.5} - t^{uncoated}_{C/C_0=0.5} \right)}{R\, T\, m} \quad (1)$$

In this relation, p_{CO_2} is the partial pressure of CO_2, F is the flow rate, R is the ideal gas constant, T is the temperature of the gas and m is the mass of zeolite on the monolith in the break through experiment.

Results and Discussion

Figure 3 shows representative SEM images of the structured adsorbents prepared in the present work. The images of the cross sections illustrate that walls of the steel monolith were smooth and nonporous, as opposed to the cordierite monoliths used in earlier work[2b]. The plan view images show that the crystals in the film have typical FAU morphology and no other crystals with other morphologies, i.e. zeolite crystals of other phases are observed. Also the films are quite clean and free from any sediments of crystals deposited from the synthesis mixture as observed in earlier work[2b]. Furthermore, the zeolite film was continuous, even, and appeared to be comprised of well-intergrown crystals. As illustrated in the Figure, the film thickness was about 3 μm for the sample grown in 21 steps and 11 μm for the sample grown in 70 steps, see Table 1. Consequently, the film thickness is almost linearly proportional to the number of growth steps, as expected, and increased with about 0.15 μm per step. For the sake of simplicity, the samples are hereafter referred to as the 3 μm and 11 μm films, respectively.

Table 1. Film thickness, Si/Al and Na/Al ratios determined by EDS and zeolite mass for the adsorbents.

Number of growth steps	Film thickness (μm)	Molar Si/Al ratio	Molar Na/Al ratio	Zeolite mass (g)
21	3	1.09	0.97	5.6
70	11	1.10	0.98	19.8

The results of the EDS analysis of the 3 and 11 μm films are given in Table 1. The Si/Al and Na/Al ratios are in the range 1.09-1.10 and 0.97-0.98, respectively. This shows that the FAU crystals in the films are the sodium form of zeolite X. The weights of the zeolite films, determined from the difference in weight before and after film growth on the two monoliths used for breakthrough experiments were 5.6 g and 19.8 g for the 3 μm and 11 μm films, respectively. The weight of the films is linearly proportional to the film thickness as expected.

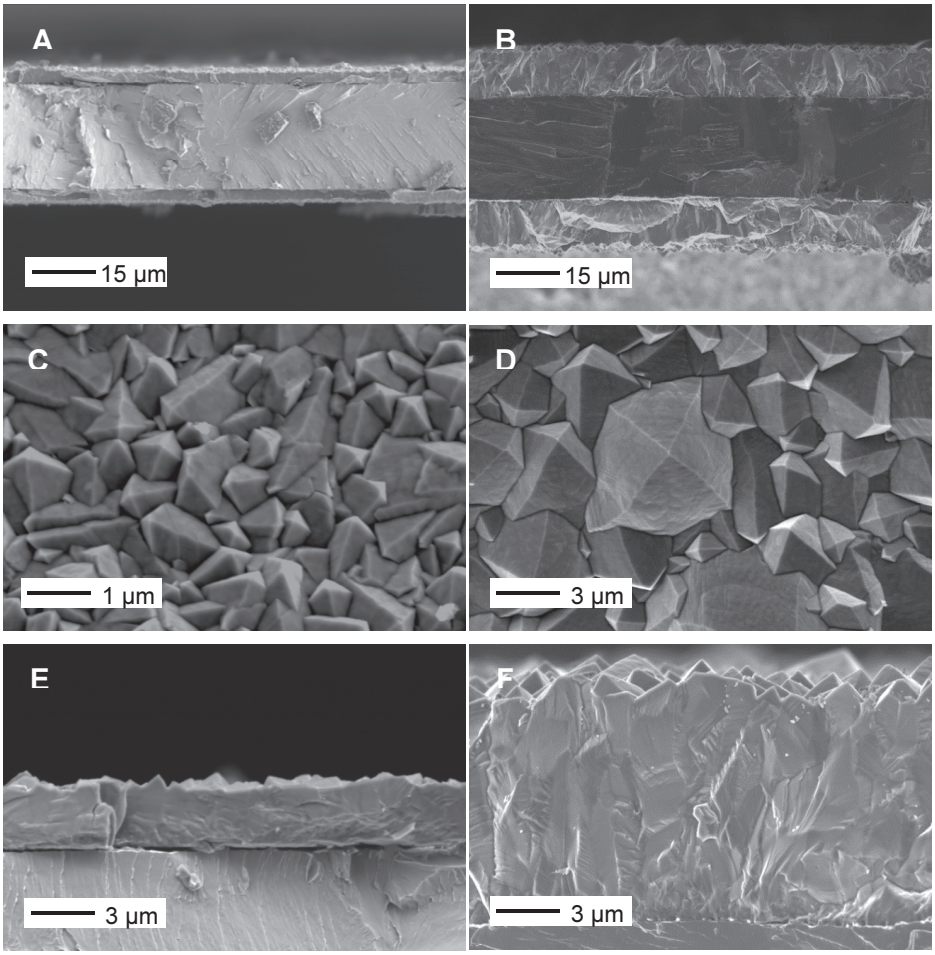

Figure 3. SEM images of the structured adsorbent, 3 µm (left) and 11 µm films (right).

Figure 4 shows XRD data recorded for a piece cut from the structured adsorbent with the 3 µm film after removal of the background signal. The vertical bars represent the ICDD reference pattern 01-070-2168 for randomly oriented zeolite NaX crystals. No other reflections apart from those typical zeolite NaX and stainless steel were observed for the sample. In addition, the intensities of the measured reflections agree well with those of the database pattern for randomly oriented crystals. This shows that the film is comprised of randomly oriented zeolite NaX crystals in concert with SEM and EDS observations.

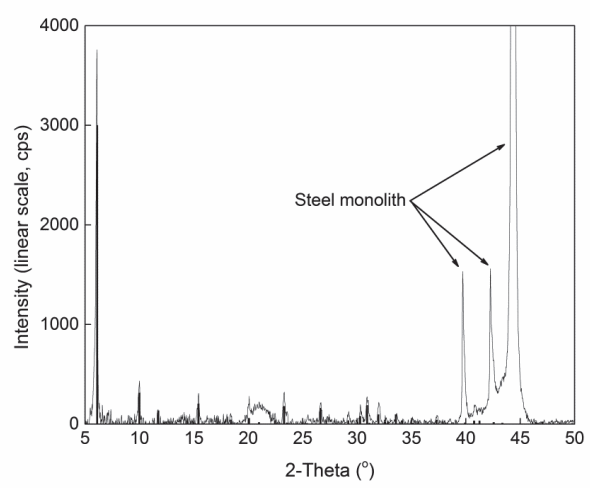

Figure 4. XRD pattern of steel monolith coated with a 3 μm zeolite film. The vertical bars represent the ICDD reference pattern 01-070-2168 for randomly oriented zeolite NaX crystals. Reflections originating from steel are indicated with arrows.

Carbon dioxide breakthrough experiments

Figure 5 shows breakthrough data recorded for a steel tube (illustrated in Figure 2 a) connected to the breakthrough apparatus for a flow rate of 1.00 dm^3/min. The volume of the steel tube is as small as about 4 ml, corresponding to a delay of only 0.2 s at this flow rate. Consequently, this experiment measures the response time and dispersion created by the breakthrough apparatus and the CO_2 analyser. Breakthrough of CO_2 (i.e. $C/C_0 > 0.05$) is detected after less than 1 s, which illustrates that the response time of the system is very low. A concentration of about 10% CO_2, i.e. $C/C_0 \approx 1$ is reached after about 10 seconds and this time corresponds to the dispersion created by the system.

The breakthrough data recorded for the column with glass beads (illustrated in Figure 2 b) connected to the breakthrough apparatus for a flow rate of 1.00 dm^3/min is also shown in Figure 5. Due to the much larger void volume of the column with glass beads (251 ml) as compared to the steel tube (4 ml), the breakthrough front is now shifted about 17 seconds in time, this shift match very well with the expected delay of 15 seconds due to filling of the larger volume. However, the dispersion of the breakthrough front for the column is quite similar to that for the tube, and consequently, the observed dispersion is only an effect of dispersion in the break through apparatus and not in the column itself.

Figure 5 also shows the breakthrough curve recorded when the column was loaded with two steel monoliths (as illustrated in Figure 2 c) for a flow rate of 1.00 dm^3/min. In this case, the breakthrough front is shifted 4 s earlier in time, which precisely matches the expected shift due to the reduced dead volume of the system by introduction of a volume of nonporous steel monoliths (4.5 s). Again, the dispersion of the breakthrough front is about 10 s, as a result of dispersion in the breakthrough apparatus. The time t to reach C/C_0=0.5 for the uncoated monoliths is 13 seconds at this flow rate (average for 5 runs), see Table 2.

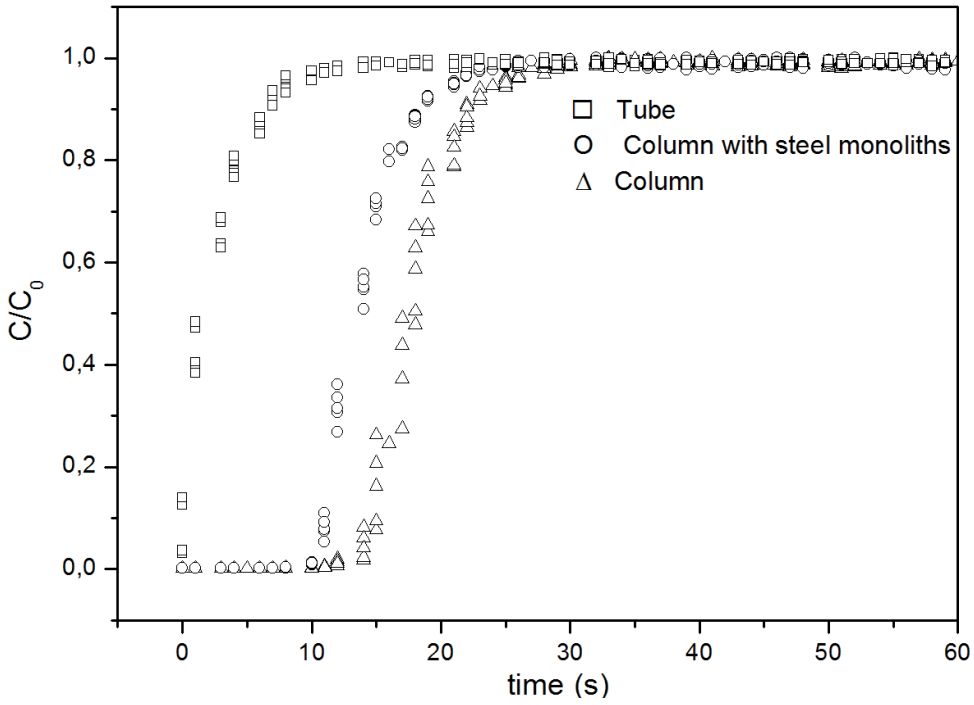

Figure 5. Experimental breakthrough profiles (points) for a flow rate of 1.00 dm^3/min recorded for steel tube (ID 1.5 mm), column (ID 3.2 cm) with glass beads and column with steel monoliths, graphite tape and glass beads as illustrated in Figure 2 a-c, respectively.

Breakthrough data for the steel monoliths coated with a 3 μm zeolite film are illustrated in Figure 6. Sharp and overlapping breakthrough profiles were obtained after regeneration of the adsorbent at 120°C. The breakthrough front is still quite sharp, but is broadened slightly as compared to the front recorded for the column with steel monoliths without zeolite. The

times t to reach $C/C_0=0.5$ (average for 5 breakthrough experiments) and the CO_2 adsorption capacity q estimated using equation 1 for the different flowrates are given in Table 2. The average adsorption capacity q is 2.7 mol CO_2/kg zeolite for the 3 µm zeolite film. The standard deviation is as small as 0.1 mol CO_2/kg zeolite, which indicates good precision of the breakthrough experiments.

Table 2. Breakthrough data and estimated CO_2 adsorption capacities for the 3 and 11 µm zeolite films for the flowrates of 0.25, 0.50 and 1.00 dm^3/min.

Structured Adsorbent	**Flow rate (dm^3/min)**		
	0.25	**0.50**	**1.00**
	time t to reach $C/C_0=0.5$		
Uncoated monolith	52.7	25.2	13.0
3 µm zeolite film	876	445	238
11 µm zeolite film	3659	1639	723
	CO_2 adsorption capacity q (mol CO_2/kg zeolite)		
3 µm zeolite film	2.6	2.7	2.9
11 µm zeolite film	3.1	2.8	2.5

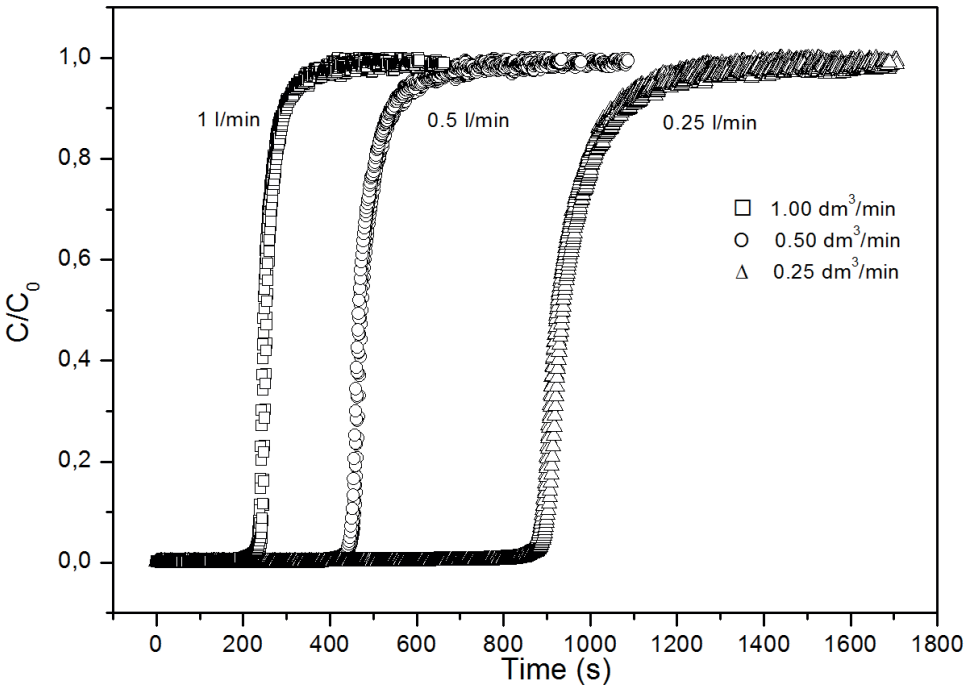

Figure 6. Experimental carbon dioxide breakthrough profiles for steel monolith coated with a 3 μm zeolite film for flow rates of 1.00, 0.50 and 0.25 dm^3/min. Each breakthrough experiment is carried out 5 times and the adsorbent is regenerated at 120°C between the adsorption cycles.

Breakthrough data for the steel monoliths coated with an 11 μm zeolite film are illustrated in Figure 7. Again, where sharp and overlapping breakthrough profiles were obtained, but in this case, breakthrough of carbon dioxide occurs much later due to much higher adsorption capacity of the much thicker zeolite film. The times t to reach C/C_0=0.5 and the CO_2 adsorption capacity q estimated using equation 1 for the steel monoliths coated with a 11 μm zeolite film are given in Table 2. The average adsorption capacity q is 2.8 mol CO_2/kg zeolite, i.e. very similar to that observed for the monoliths coated with a 3.0 μm zeolite film. However, in this case the standard deviation is slightly larger 0.3 mol CO_2/kg zeolite.

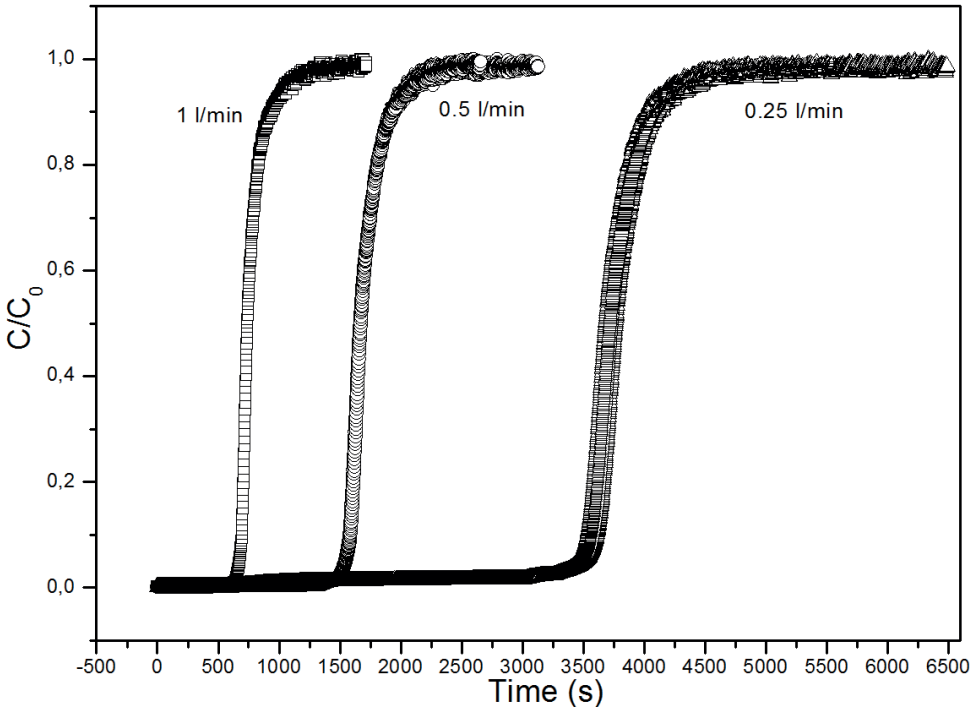

Figure 7. Experimental carbon dioxide breakthrough profiles (points) for steel monolith coated with an 11 µm zeolite film for flow rates of 1.00, 0.50 and 0.25 dm^3/min. Each breakthrough experiment is carried out 5 times and the adsorbent is regenerated at 120°C between the adsorption cycles.

The average adsorption capacity for the 3 and the 11 µm monoliths estimated using equation 1 is 2.8 mol CO_2/kg zeolite with a standard deviation of 0.2 mol CO_2/kg zeolite. This adsorption capacity is in-between the values of 2.5 and 3.6 reported by Rodrigues et al.[3] and Myers et al.[4], respectively. Furthermore, the adsorption capacity 2.8 mol CO_2/kg zeolite corresponds to 0.3 mmol CO_2/cm^3 adsorbent for the 11 µm monolith. This can be compared to the adsorption capacity for zeolite NaX beads, which is about 2.3 mmol CO_2/cm^3 adsorbent[2b], i.e. about 8 times larger. Consequently, an 8 times larger column with an 11 µm monolith will have the same adsorption capacity as a column filled with beads. Alternatively, an 8 times shorter cycle time may be used to separate the same amount of CO_2 per time.

Conclusions

The structured adsorbents comprised of nonporous steel monoliths coated with a 3 μm or 11 μm thick zeolite NaX film prepared in the present work showed good adsorption performance. The adsorbents displayed very sharp breakthrough fronts with good CO_2 adsorption. The average adsorption capacity amounted to 2.8 mol CO_2/kg zeolite which is close to that reported for zeolite beads at similar conditions. The monolith coated with an 11 μm thick zeolite film displayed an adsorption capacity 0.3 mmol CO_2/cm^3 adsorbent which is only about 8 times lower than that for a bed of packed adsorbent beads. This makes zeolite NaX coated steel monoliths promising alternatives to traditional adsorbents in processes with short cycle times.

Acknowledgements

The Swedish International Development Cooperation Agency (SIDA), Ångpanneföreningens forskningsstiftelse (ÅForsk) and Bio4energy are gratefully acknowledged for financial support of this work.

References

1. Breck, D. W., Synthesis and Properties of Union Carbide Zeolites L, X and Y. In *Conference at University of London*, 1967; pp 47-61.

2. Cavenati, S.; Grande, C. A.; Rodrigues, A. E., Adsorption equilibrium of methane, carbon dioxide, and nitrogen on zeolite 13X at high pressures. *J. Chem. Eng. Data* **2004,** *49* (4), 1095-1101.

3. Dunne, J. A.; Rao, M.; Sircar, S.; Gorte, R. J.; Myers, A. L., Calorimetric heats of adsorption and adsorption isotherms .2. O-2, N-2, Ar, CO2, CH4, C2H6, and SF6 on NaX, H-ZSM-5, and Na-ZSM-5 zeolites. *Langmuir* **1996,** *12* (24), 5896-5904.

4. Mosca, A.; Hedlund, J.; Webley, P. A.; Grahn, M.; Rezaei, F., Structured zeolite NaX coatings on ceramic cordierite monolith supports for PSA applications. *Microporous and mesoporous materials* **2010,** *130* (1-3), 38-48.

5. Rezaei, F.; Mosca, A.; Hedlund, J.; Webley, P. A.; Grahn, M.; Mouzon, J., The effect of wall porosity and zeolite film thickness on the dynamic behavior of adsorbents in the form of coated monoliths. *Separation and Purification Technology* **2011,** *81* (2), 191-199.

6. Rezaei, F.; Mosca, A.; Webley, P.; Hedlund, J.; Xiao, P., Comparison of traditional and structured adsorbents for co2 separation by vacuum-swing adsorption. *Ind. Eng. Chem. Res.* **2010,** *49* (10), 4832-4841.